ขั้นตอนวิธีการไม่ประสานเวลาเลียนแบบหลักการทางฟิสิกส์โดยปราศจากความรู้ทางเวลาแบบครอบคลุมสำหรับเครือข่ายตัวรับรู้ไร้สาย

นายศุภเสฏฐ์ ชูชัยศรี

วิทยานิพนธ์นี้เป็นส่วนหนึ่งของการศึกษาตามหลักสูตรวิศวกรรมศาสตรดุษฎีบัณฑิต
สาขาวิชาวิศวกรรมคอมพิวเตอร์ ภาควิชาวิศวกรรมคอมพิวเตอร์
คณะวิศวกรรมศาสตร์ จุฬาลงกรณ์มหาวิทยาลัย
ปีการศึกษา 2554

A PHYSICOMIMETICS DESYNCHRONIZATION ALGORITHM WITHOUT GLOBAL TIME KNOWLEDGE FOR WIRELESS SENSOR NETWORKS

Mr.Supasate Choochaisri

A Dissertation Submitted in Partial Fulfillment of the Requirements

for the Degree of Doctor of Philosophy Program in Computer Engineering

Department of Computer Engineering

Faculty of Engineering

Chulalongkorn University

Academic Year 2011

Thesis Title	A PHYSICOMIMETICS DESYNCHRONIZATION ALGORITHM WITHOUT GLOBAL TIME KNOWLEDGE FOR WIRELESS SENSOR NETWORKS
By	Mr.Supasate Choochaisri
Field of Study	Computer Engineering
Thesis Advisor	Assistant Professor Chalermek Intanagonwiwat, Ph.D.

Accepted by the Faculty of Engineering, Chulalongkorn University in Partial Fulfillment of the Requirements for the Doctoral Degree

..... Dean of the Faculty of Engineering
(Associate Professor Boonsom Lerdhirunwong, Dr.Ing.)

THESIS COMMITTEE

..... Chairman
(Professor Prabhas Chongstitvatana, Ph.D.)

..... Thesis Advisor
(Assistant Professor Chalermek Intanagonwiwat, Ph.D.)

..... Examiner
(Professor Boonserm Kijsirikul, Ph.D.)

..... Examiner
(Assistant Professor Kultida Rojviboonchai, Ph.D.)

..... External Examiner
(Associate Professor Anan Phonphoem, Ph.D.)

ศุภเสฏฐ์ ชูชัยศรี: ขั้นตอนวิธีการไม่ประสานเวลาเลียนแบบหลักการทางฟิสิกส์โดยปราศจากความรู้ทาง เวลาแบบครอบคลุมสำหรับเครือข่ายตัวรับรู้ไร้สาย. (A PHYSICOMIMETICS DESYNCHRONIZATION ALGORITHM WITHOUT GLOBAL TIME KNOWLEDGE FOR WIRELESS SENSOR NETWORKS) อ.ที่ปรึกษาวิทยานิพนธ์หลัก : ผศ. ดร. เฉลิมเอก อินทนากรวิวัฒน์, 120 หน้า.

การไม่ประสานเวลามีประโยชน์ในการจัดการให้โหนดในเครือข่ายทำงานที่เวลาต่างกันซึ่งเป็นคุณสมบัติที่ต้องการสำหรับการจัดสรรทรัพยากร การจัดลำดับการเข้าถึงสื่อกลางแบบแบ่งตามเวลา และการหลีกเลี่ยงการส่งข้อมูลชนกัน อย่างไรก็ตามเป็นการยากที่จะทำให้โหนดในเครือข่ายตัวรับรู้ไร้สายไม่ประสานเวลากันเนื่องจากมีข้อจำกัดหลายประการ ในวิทยานิพนธ์นี้ผู้วิจัยมุ่งเน้นไปที่การไม่ประสานเวลาสำหรับเครือข่ายตัวรับรู้ไร้สายซึ่งมีทรัพยากรจำกัดที่ปราศจากความรู้ทางเวลาแบบครอบคลุม (นาฬิกาของโหนดไม่มีการประสานเวลา) ผู้วิจัยได้นำเสนอขั้นตอนวิธีการใหม่สำหรับการไม่ประสานเวลาโดยเลียนแบบหลักการทางฟิสิกส์เพื่อจัดระเบียบการเข้าถึงทรัพยากรที่ใช้ร่วมกันอย่างเท่าเทียมกันและเพื่อลดการชนกันของการส่งสัญญาณไร้สาย ขั้นตอนวิธีการที่นำเสนอทำการสร้างสนามแรงประดิษฐ์สำหรับโหนดตัวรับรู้ไร้สายซึ่งได้รับแรงบันดาลใจจากการจัดรูปแบบวงกลมในวิทยาการหุ่นยนต์และหลักการทางฟิสิกส์ โหนดแต่ละตัวในเครือข่ายจะส่งแรงประดิษฐ์ไปผลักโหนดอื่นให้ทำงานที่เฟสเวลาแตกต่างกัน คู่โหนดที่อยู่ในเฟสเวลาใกล้กันจะมีแรงกระทำต่อกันมากเพื่อผลักคู่โหนดให้ห่างออกจากกันในโดเมนทางเวลา แต่ละโหนดปรับเฟสเวลาเป็นสัดส่วนตามแรงรวมที่ได้รับ เมื่อแรงรวมที่ได้รับสมดุลแล้วโหนดต่างๆจะอยู่ในสภาวะไม่ประสานเวลา ผู้วิจัยทำการประเมินผลการทดลองของขั้นตอนวิธีการไม่ประสานเวลาที่นำเสนอบนทอซซิมซึ่งเป็นเครื่องจำลองสำหรับเครือข่ายตัวรับรู้ไร้สาย และได้ทำการทดลองกับอุปกรณ์จริงซึ่งทำงานด้วยระบบปฏิบัติการไทนี่โอเอส ผลจากการทดลองแสดงให้เห็นว่าขั้นตอนวิธีการไม่ประสานเวลาเลียนแบบหลักการทางฟิสิกส์ที่นำเสนอนั้นมีเสถียรภาพในการทำงาน รองรับการปรับขนาดของเครือข่ายดีกว่าวิธีการอื่นมาก และก่อให้เกิดความผิดพลาดในการไม่ประสานเวลาน้อยกว่าวิธีการอื่นอย่างมีนัยสำคัญ

ภาควิชา ..วิศวกรรมคอมพิวเตอร์.. ลายมือชื่อนิสิต .....

สาขาวิชา ..วิศวกรรมคอมพิวเตอร์.. ลายมือชื่ออ.ที่ปรึกษาวิทยานิพนธ์หลัก .....

ปีการศึกษา .....2554.....

5271867021: MAJOR COMPUTER ENGINEERING
KEYWORDS: DESYNCHRONIZATION / PHYSICOMIMETICS/ ARTIFICIAL FORCE FIELD / WIRELESS SENSOR NETWORK / WIRELESS NETWORK

SUPASATE CHOOCHAISRI : A PHYSICOMIMETICS DESYNCHRONIZATION ALGORITHM WITHOUT GLOBAL TIME KNOWLEDGE FOR WIRELESS SENSOR NETWORKS. ADVISOR : ASST. PROF. CHALERMEK INTANAGONWIWAT, PH.D., 120 pp.

Desynchronization is useful for scheduling nodes to perform tasks at different time. This property is desirable for resource sharing, Time Division Multiple Access (TDMA) scheduling, and data transmission collision avoiding. However, to desynchronize nodes in wireless sensor networks is difficult due to several limitations. In this dissertation, we focus on desynchronization for resource-limited wireless sensor networks that resource-limited sensor nodes lack global time knowledge (*i.e.*, clocks are not synchronized). We propose a novel physicomimetics desynchronization algorithm to organize all accesses to a shared resource to be collision-free and even equitable. Inspired by robotic circular formation and Physics principle, the proposed algorithm creates an artificial force field for wireless sensor nodes. Each neighboring node has artificial forces to repel other nodes to perform tasks at different time phases. Nodes with closer time phases have stronger forces to repel each other in the time domain. Each node adjusts its time phase proportionally to total received forces. Once the total received forces are balanced, nodes are desynchronized. We evaluate our desynchronization algorithm on TOSSIM, a simulator for wireless sensor networks and evaluate on real hardware devices running TinyOS. The evaluation results indicate that the proposed algorithm is stable, scales much better than existing approaches, and incurs significantly lower desynchronization error.

Department : ... Computer Engineering ... Student's Signature .....
Field of Study : .. Computer Engineering .. Advisor's Signature .....
Academic Year : ..... 2011 .....

Acknowledgements

First and foremost, I would like to express my deep and sincere gratitude to my great supervisor Asst. Prof. Dr. Chalermek Intanagontwiwat, for his guidance, patience, and support. He has advised me for almost seven years since my senior project at the undergraduate level, then, my master thesis, and finally my Ph.D. dissertation. He has inspired me in so many ways. I am proud that I was under his supervision.

I greatly appreciate Prof. Dr. Prabhas Chongstitvatana, Prof. Dr. Boonserm Kijsirikul, Assoc. Prof. Dr. Anan Phonphoem, and Asst. Prof. Dr. Kultida Rojviboonchai, for being my dissertation committee and giving several useful comments and suggestions to improve this dissertation. I also acknowledge Rawin Youngnoi, Assoc. Prof. Dr. Paisan Nakmahachalasint, and Asst. Prof. Dr. Manop Wongsaisuwan who gave me a pointer in the mathematical analysis of this dissertation.

I appreciate the CP CU Academic Excellence Scholarship (Ad-cha-ri-ya-kuen-rang Scholarship) from Department of Computer Engineering, Faculty of Engineering, Chulalongkorn University that supports all tuition fee during my Ph.D. program.

I thank all UbiNET research group members during my Ph.D. program for their discussion and contribution to research works and DMDE research group members for the great time we lived together within the same research room (see the full list at Appendix).

I am grateful to my family for their endless support and I sincerely thank my dearest Wichearee Thitayarasa who always stands by my side and always understands me.

Last but not least, I would like to thank Department of Computer Engineering for meaningful experience. During my time at this department, I have learned three important lessons:

- *Passion is more important than intelligence.*
- *The more we contribute the more we gain.*
- *No matter how hard a problem is, if we do not give it up, we will surpass it eventually.*

Contents

Chapter Page

List of Tables

List of Figures

Figure Page

Figure Page

CHAPTER I

INTRODUCTION

Wireless Sensor Networks (WSNs) have been rapidly growing and enabling several new approaches to collect environmental data such as works of Mainwaring et al. (2002), Gui and Mohapatra (2004), Xu et al. (2004), He et al. (2004), and Choochaisri et al. (2010). Such data, in particular event data, often associate with timestamps used for sequencing chronological order of events. Therefore, many WSN systems usually require sensor nodes to cooperate to have a common notion of time in order to accomplish tasks with consistent results. Several protocols have been proposed to distributedly synchronize the notion of time among sensor nodes in the systems (*e.g.*, TPSN (Ganeriwal et al. (2003)), FTSP (Maróti et al. (2004)), GTSP (Sommer and Wattenhofer (2009)), and EGTSP (Apicharttrisorn et al. (2010))).

However, some systems simply require nodes to work at the same time without a global notion of time; for example, a system that nodes only wake up at the same time to relay packets, a system that nodes only sample data at the same time to take snapshots of an environment. Inspired by firefly synchronicity, RFA (Werner-Allen et al. (2005)) is the first protocol designed to achieve this requirement. Conversely, some systems require nodes *not* to work at the same time without a global notion of time (*i.e.*, to *desynchronize*). *Desynchronization* organizes all accesses to a shared resource to be collision-free and even equitable. A concrete example is a system using a Time Division Multiple Access (TDMA) protocol. Nodes access the shared medium only in their time slots to send messages with no collision. In addition, desynchronization schedules duty cycles to improve overall performance. For instance, in the sensing coverage problem, only some nodes wake up to sense and their sensing ranges cover the overall region. Meanwhile, other nodes that their sensing ranges are redundant can stay in idle or sleep mode to reduce their energy consumption and prolong the network lifetime. These two sets of nodes can periodically swap their tasks to preserve overall sensing coverage. Other potential applications are techniques to increase a sampling rate in multiple analog-to-digital converters, to schedule resource in multi-core processors, and to control traffic at intersections (Patel et al. (2007)).

To design an algorithm to solve the desynchronization problem, several challenges are inevitable. First, in most of WSNs, there is no central control. If there is a central master node, the master node can assign different starting points of time to different nodes in a network to avoid the collision. Therefore, the problem becomes easier to solve. However, without such a central master node, a desynchronization algorithm has to process in a distributed manner to reach the global consensus.

Second, the problem becomes harder when there is no global time or a common notion of time available in a network. Due to the nature of clock oscillators, the clock skew and clock drift normally occurs; nodes perceive different local times and clocks run at different speed (Apicharttrisorn et al. (2010)). With a time synchronization protocol, it is able to divide a time period into the exact number of slots. Nodes can also cooperatively determine the exact beginning of time slots to access the shared medium. However, many WSN systems do not assume time synchronization for achieving the global time. Even some systems assume time synchronization, the process to synchronize the time incurs overhead and takes time.

Third, for multi-hop WSNs, the hidden terminal problem leads to packet collision. A node cannot determine whether its second-hop neighbor is transmitting a packet to the same receiver. If the node senses the wireless medium and does not aware of any transmission while its second-hop neighbor is actually transmitting, their transmitted packets can collide at the receiver. The RTS-CTS scheme proposed in the 802.11 standard can avoid the problem. However, the RTS-CTS scheme incurs overhead and delay, and reduces the overall throughput. Additionally, many manufacturers disable the RTS-CTS function by default (Gollakota and Katabi (2008)).

Additionally, due to the characteristic of WSNs, most WSN devices are resource limited. For example, TelosB, which is one of well-known WSN devices, provides 8 MHz CPU, 10KB RAM, 1 MB external flash storage, and works on two AA-batteries. With limited computational power, the algorithm should be simple. With limited memory, only small data buffer is provided. With limited storage, a node should store data only if necessary. With limited energy, the control overhead should be minimized.

Furthermore, the desynchronization problem is similar to the distributed graph coloring problem (Motskin et al. (2009)). The graph coloring problem is known to be

an NP-Hard problem. Additionally, the distributed graph coloring problem in a network with uncertain environment is much harder.

Last but not least, a system running a desynchronization algorithm should converge to the desynchrony state. The simulation and testbed evaluation can show the convergence property of an algorithm for some specific scenarios. However, to mathematically prove the convergence of the system is not trivial.

In this dissertation, we propose a novel physicomimetics desynchronization algorithm for wireless sensor networks to solve such challenges. A physicomimetics algorithm is the method that imitates the science of Physics. Herein, we imitate the idea of a force field in a spatial domain from Physics and adapt this idea to be a technique for desynchronization in a temporal domain. To the best of our knowledge, this dissertation is the first that studies and applies physicomimetics to address the desynchronization problem. Our high-level goal is to develop a physicomimetics desynchronization algorithm that solves the mentioned challenges. A network system that applies the developed algorithm will achieve the stability with the lower desynchronization error compared to previous works on desynchronization.

1.1 Design Goals for a Physicomimetics Desynchroniation Algorithm

To develop a physicomimetics desynchronization algorithm, we first set our goals that will be used as a guidance in designing such an algorithm throughout the dissertation. Our physciomimetics desynchronization algorithm is aimed to be practical, distributed, scalable, minimal, stable, fair without global time. More specifically:

- be practical, the proposed algorithm should be installable and successfully runnable on real hardware.
- be distributed, the proposed algorithm has to work without a central master node. Each node has no global neighbors' information and independently decides its own action based on only local information.
- be scalable, the proposed algorithm should scale well with network size.
- be minimal, the proposed algorithm should incur minimal overhead. Because wireless sensor nodes are resource-limited, the processing, memory, and transmission

overhead should be minimized.

- be stable, in case a network is not over-saturated, the proposed algorithm should be stable under small perturbation. The network system should converge to an equilibrium.
- be fair without global time, the proposed algorithm has to work without global time knowledge. All nodes in a system is not synchronized. Their local clocks can be different in time. In other words, there is no common notion of global time. However, the proposed algorithm should space nodes equivalently in the time domain for single-hop networks and minimizes the deviation of channel utilization per node in multi-hop networks.

1.2 Scope and Assumption

The scope of this dissertation is limited to the following:

- This dissertation considers the wireless sensor network that 1) there is no central master node 2) nodes are not synchronized and lack of global time knowledge 3) nodes are static (*i.e.*, there is no mobile node).
- This dissertation proposes a desynchronization algorithm that is able to work on both single-hop and multi-hop networks.
- The proposed algorithm does not rely on any global information.
- The proposed algorithm is runnable on both TOSSIM simulator (Levis et al. (2003)) and TelosB hardware platform.
- The number of neighboring nodes is limited to under 100 nodes for single-hop networks and under 30 nodes for multi-hop networks.

Additionally, in this dissertation, we assume the following:

- Each node attempts to periodically fire a message with the same time period.
- There is no mobile node in a network.
- There is no global time knowledge. Clocks are not synchronized. Local timestamps of nodes can be the same or different.

1.3 Summary of Contributions

The main contribution of this dissertation is a novel physicomimetics desynchronization algorithm for wireless sensor networks. The proposed algorithm has several desirable properties. First, the algorithm runs distributedly on each sensor node. Central master node and global information is not required. Second, the algorithm works even nodes are not synchronized and do not realize the global time. Third, the algorithm is able to work for both single-hop and multi-hop networks. In addition, the algorithm is lightweight, simple, and practical. The size of a compiled binary is less than 30 kilobytes. The required memory is less than 2 kilobytes. This property is desirable to implement, extend, and apply for resource-limited wireless sensor nodes. Furthermore, the algorithm requires only local 2-hop information and scales well with network size. Finally, the algorithm is stable under small perturbation. We believe that the proposed algorithm can be a primer for several applications such as TDMA protocol, packet collision avoidance, area sensing coverage, cooperative data sampling, and other resource-sharing applications.

1.4 Dissertation Organization

The rest of the dissertation is organized as follows. The next chapter describes desynchronization preliminaries to understand the problem and the traditional framework. This chapter also reviews works in literature and describes the motivation of our algorithm. Chapter 3 presents our desynchronization algorithm and performance evaluation on single-hop networks. In Chapter 4, we analyse the stability of the proposed single-hop algorithm. Then, we extend the proposed algorithm to support multi-hop networks and evaluate the algorithm on various topologies in Chapter 5. The stability analysis of the multi-hop algorithm is presented in Chapter 6. Finally, Chapter 7 concludes the dissertation and discusses the current limitations and directions for further research.

CHAPTER II

PRELIMINARIES, RELATED WORK, AND MOTIVATION

2.1 Desynchronization Preliminaries

Degesys et al. (2007) have introduced the desynchronization primitive and framework for WSNs. The desynchronization framework is depicted as a time circle in Figure 2.1. The perimeter of a time circle represents a configurable time period T of nodes' oscillators. The time position or *phase* of each node represents its turn to perform a task (*e.g.*, accessing a shared resource, sampling data, and firing a message). The system is desynchronized when all nodes are separated in the time circle.

We define terms used in the desynchronization context as follows:

Definition 2.1 (Phase) *A phase ϕ_i of node i is the time position on the circle of a time period T, where $0 \leq \phi_i < T$ and $T \in \mathbb{R}^+$.*

Definition 2.2 (Phase Neighbor) *Node j is a phase neighbor of node i if node i perceives the existence of node j at the phase $\phi_i + \phi_{i,j}$, where $\phi_{i,j}$ is the phase difference between node j and node i,*

$$\phi_{i,j} = \begin{cases} \phi_j - \phi_i & \text{if } \phi_j \geq \phi_i, \\ T - (\phi_i - \phi_j) & \text{if } \phi_j < \phi_i. \end{cases} \tag{2.1}$$

Definition 2.3 (Next Phase Neighbor) *Node j is the next phase neighbor of node i if $\phi_{i,j} = \min_{k \in S}\{\phi_{i,k}\}$, where S is a set of node i's neighbors.*

Definition 2.4 (Previous Phase Neighbor) *Node j is the previous phase neighbor of node i if $\phi_{i,j} = \max_{k \in S}\{\phi_{i,k}\}$, where S is a set of node i's neighbors.*

Definition 2.5 (Desynchrony State) *The system is in the desynchrony state if $\phi_i \neq \phi_j$*

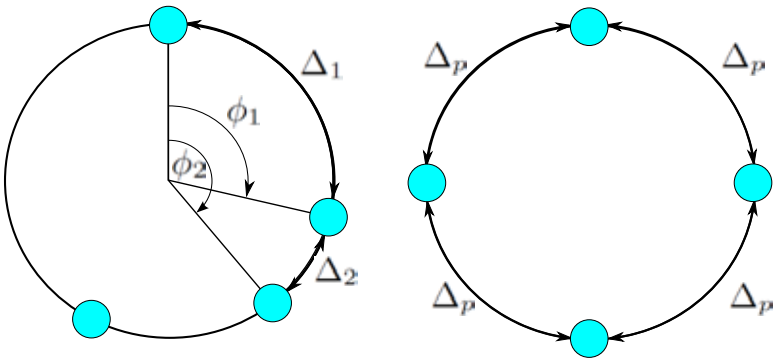

Figure 2.1: Desynchronization framework

for all $i, j \in V$ and $i \neq j$, where V is a set of nodes in a network that cannot share the same phase.

Definition 2.6 (Perfect Desynchrony State) *The system is in the perfect desynchrony state if it is in the desynchrony state and $\phi_{i,j} = T/N$ for all $i \in V$, j is i's previous phase neighbor, and N is the number of nodes in a network that cannot share the same phase.*

We note that two nodes can share the same phase if they are not within the two-hop communication range of each other.

2.2 Related Work

In this section, we review works in literature. We divide related works into two categories. The first category is the works on desynchronization in a temporal domain. The works in this category directly attempt to solve the desynchronization problem in wireless networks. We compare our work directly to these previous works. The second category is the works on robotic circular formation. The works in this category do not explicitly attempt to solve the desynchronization problem in wireless networks. However, their works can be abstracted as desynchronization on a spatial domain. These works are the motivation of our desynchronization algorithm.

2.2.1 Desynchronization on a Temporal Domain in Wireless Networks

To the best of our knowledge, DESYNC (Degesys et al. (2007)) is the first to introduce the desynchronization problem. In DESYNC, a node simply attempts to stay

in the middle between its previous and next phase neighbors. By repeating this simple algorithm, all nodes will eventually be spread out. However, the error from one phase neighbor is also propagated to the other phase neighbors and indefinitely circulated inside the network. Therefore, DESYNC's error is quite high even after convergence. In contrast, our work relies on all received neighbors information that is robust to the error from one phase neighbor. In Degesys and Nagpal (2008), they describe how DESYNC works on multi-hop networks and describe a future extension for DESYNC by exchanging 2-hop neighbors information.

Designed to converge faster than DESYNC, INVERSE-MS (Patel et al. (2007)) is an inverse algorithm of the synchronicity work by Mirollo and Strogatz (1990). At a steady state, INVERSE-MS maintains a dynamic equilibrium (*i.e.*, nodes keep changing time positions while maintaining desynchronization). However, in INVERSE-MS, the time period is distorted whereas our algorithm does not distort the time period.

In EXTENDED-DESYNC (Mühlberger and Kolla (2009)), they propose a desynchronization algorithm that is similar to the extension proposed in Degesys and Nagpal (2008). Each node sends its one-hop neighbors' relative time information to all of its one-hop neighbors. Then, the one-hop neighbors relay such information to two-hop neighbors. Therefore, each node knows 2-hop relative time information. Consequently, each node can presume that there are two-hop neighbors appearing on the time circle. Then, each node uses time information of both one-hop and two-hop neighbors and processes with the same algorithm as in DESYNC. Our multi-hop algorithm is partly based on the same idea.

M-DESYNC (Kang and Wong (2009)) is a localized multi-hop desynchronization algorithm that works on a granularity of time slots. The protocol estimates the required number of time slots with a two-hop maximum degree. This estimation helps M-DESYNC converge very fast. However, M-DESYNC requires that all nodes have a global notion of time in order to share the common perception of time slots. Furthermore, M-DESYNC is claimed to work only on acyclic graph networks. On the contrary, our algorithm does not require a global notion of time and can work on both acyclic and cyclic graph networks.

Motskin et al. (2009) propose a simple, lightweight desynchronization algorithm that is also based on a graph coloring model. Unlike M-DESYNC, the algorithm works

on general graph networks and does not need the global time. To ensure that the selected time slot does not overlap with others', a node needs to listen to the media for a full time period before claiming the slot. The listening mechanism can only avoid collision with one-hop neighbors but cannot avoid collision with two-hops neighbors (*i.e.*, the hidden terminal problem). Furthermore, without a common notion of time, the starting time of each slot is quite random. As a result, several time gaps are too small to be used as time slots. This external fragmentation problem reduces resource utilization of the system. Finally, to converge faster, their algorithm overestimates the number of required time slots. Hence, several big time gaps are also left unused and the resource utilization is undoubtedly low. In our work, nodes gradually adapt their phases to be separated from each other as far as possible. Therefore, the external fragmentation problem is reduced. In addition, our algorithm works well on multi-hop networks; each node can avoid collision with two-hops neighbors.

In DESYNC-ORT (Taechalertpaisarn et al. (2011)), they propose an Orthodontics-inspired desynchronization algorithm. In their work, they use information from all one-hop neighbors and attempt to find nodes that are already in corrected time positions and tie them up together. This method is similar to the Orthodontics method that attempts to tie teeth which are already in corrected positions together. Their result is better than DESYNC in the term of desynchronization error. However, to calculate the correct positions, each node requires to know the total number of nodes in the system in advance. Additionally, the algorithm does not propose to solve the problem in multi-hop networks because nodes in two-hop neighbors can not be tied together with one-hop neighbors. In contrast, our algorithm does not require the total number of nodes in advance. Our algorithm can gradually adapt based on the current number of two-hop neighbors. Additionaly, our algorithm works on multi-hop networks.

Recently, V-DESYNC (Settawatcharawanit et al. (2012)) has been proposed to desynchronize nodes in vehicular ad-hoc networks. Their work has a different objective. They do not focus on fairness (*i.e.*, nodes are not necessary to be equitably separated) because vehicular networks are highly dynamic. In our work, we focus in static wireless sensor networks and attempt to leverage fairness among sensor nodes in resource utilization.

Approach	Properties							
	Period	Time Synced	Equitable Spaced	Multi-hop	Convergence	Error	Scalable	Overhead
DESYNC	Fixed	No	Yes	No	Moderate	High	Poor	Zero
INVERSE-MS	Distorted	No	Yes	No	Fast	Low	Good	Zero
EXTENDED-DESYNC	Fixed	No	Yes	Yes	Moderate	High	Poor	High
M-DESYNC	Fixed	Required	No	Yes	Fast	High	Good	Low
LIGHT-WEIGHT	Fixed	No	No	Yes	Fast	High	Good	Zero
DESYNC-ORT	Fixed	No	Yes	No	Moderate	Low	Good	Zero
V-DESYNC	Fixed	No	No	No	No	High	Good	Zero
Proposed	Fixed	No	Yes	Yes	Moderate	Low	Good	Zero/ Low

Table 2.1: Desynchronization Protocols Comparison

Table 2.1 summarizes the advantages and disadvantages of works in this category. The overhead of the proposed algorithm depends on whether the algorithm works on single-hop or multi-hop mode.

2.2.2 Desynchronization on a Spatial Domain in Robotics

In robotic pattern formation, multiple robots distributedly group and align themselves in geometric patterns such as circle, rectangle, and triangle. Without an explicit argument, robotic pattern formation can be abstracted as desynchronization on a spatial domain. Robots attempt to separate away from each other as far as possible to form such patterns. In other words, robots desynchronize themselves spatially to avoid the collision with each other in the spatial domain.

Several works have done in several pattern formations (Suzuki and Yamashita (1996), Suzuki and Yamashita (1999)). However, the pattern formation that is similar to desynchronization on the temporal domain is the formation on a closed ring. Figure 2.2 illustrates the robotic formation on a closed ring. In Figure 2.2a, initially, robots are randomly placed on any position on the closed ring. The perfect configuration of the formation is illustrated in Figure 2.2b. Robots are equivalently separated away on the

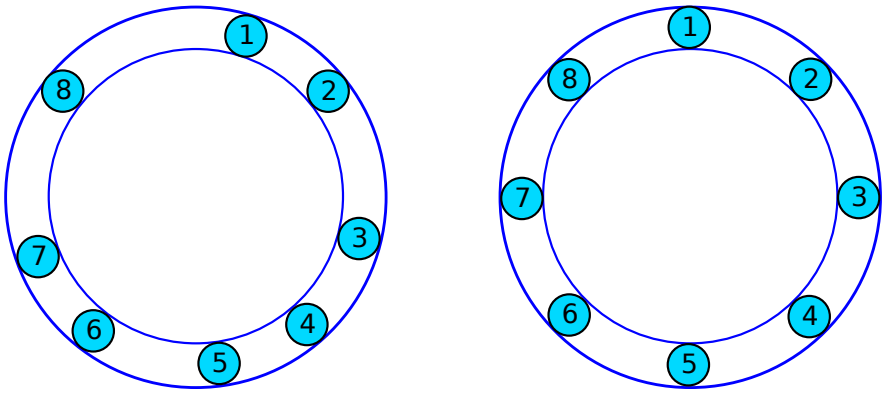

(a) (b)

Figure 2.2: Robotic pattern formation on a closed ring. (a) Robots are randomly placed on a closed ring. (b) In the perfect configuration, robots are equitably separated from each other.

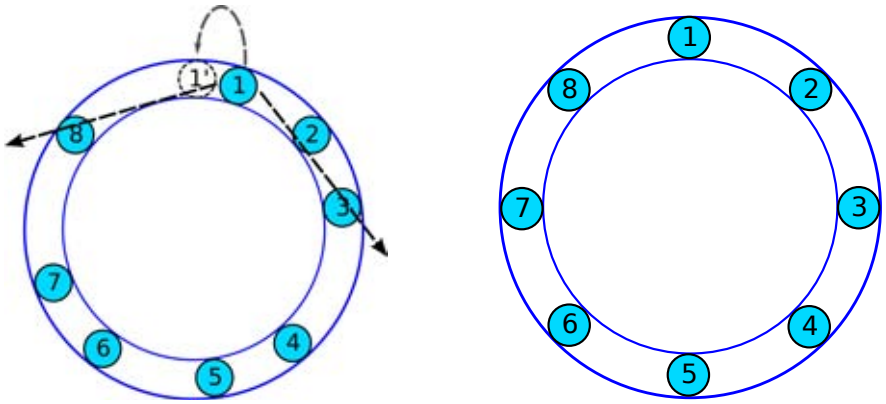

(a) (b)

Figure 2.3: Moving to the midpoint algorithm. (a) Each robot moves to the midpoint between two nearest visible neighbors. (b) The algorithm converges to the perfect configuration.

ring.

Several previous works such as Souissi et al. (2004), Cohen and Peleg (2008), and Flocchini et al. (2008) have proposed algorithms that are similar to each other for robotic formation on a closed ring. These works assume robots have limited visibility range. Each robot attempts to adjust its position to the middle between two nearest robots on its left side and right side (Figure 2.3a). In these works, they prove that this simple algorithm eventually converges to the perfect configuration (Figure 2.3b).

In Boonpinon and Sudsang (2006), heterogeneous robots are distributedly grouped into teams that are equally spread out to cover the monitored area. Each robot has no

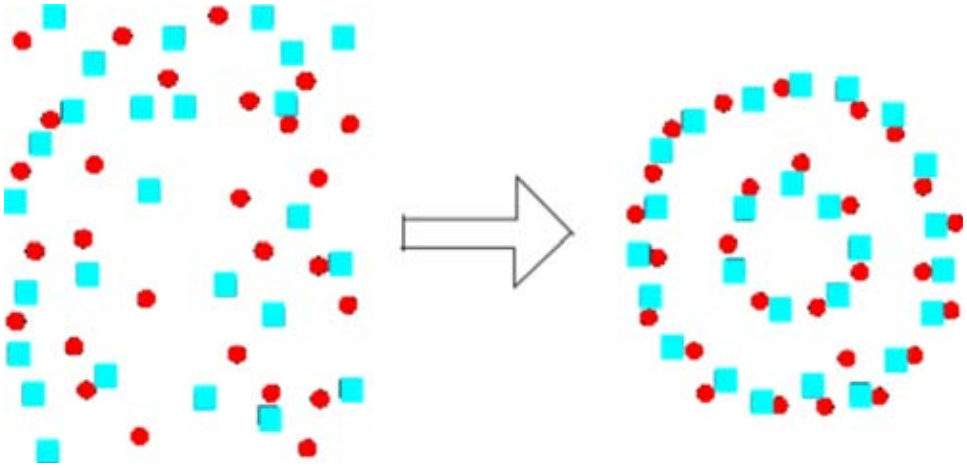

Figure 2.4: Results of Robotic Circular Formation. Robots with two different types form the circle.

global knowledge of others' absolute positions but can detect relative positions of the others with respect to itself as well as the type of the others. To form a circle, an artificial force is used as an abstraction for velocity adaptation of a robot. Robots of different types have attracting forces to each other. Conversely, robots of the same type have repelling forces. As a result, the circle of heterogeneous robots will be formed and robots are nicely spaced on the circle (see Figure 2.4). This work inspires our desynchronization algorithm.

2.2.3 Others

Other works that are related to desynchronization protocols are distributed Time Division Multiple Access (TDMA) protocols. Distributed TDMA protocols are similar to M-DESYNC (Kang and Wong (2009)); their protocols work on a granularity of time slots. As same as M-DESYNC, most of distributed TDMA protocols such as TRAMA (Rajendran et al. (2006)), Parthasarathy Parthasarathy and Gandhi (2005), ED-TDMA (Gong et al. (2010)), and Herman (Herman and Tixeuil (2004)) assume time is already slotted or all nodes are synchronized to achieve the same global clock. In our work, we do not require time synchronization and do not assume already slotted time.

2.3 Motivation

We observe that the desynchronization framework on the temporal domain is similar to the robotic circular formation which can be abstracted as the desynchronization on the spatial domain. In the desynchronization framework on the temporal domain, a node

(like a robot) does not have a global notion of time but each node can measure relative time differences with other nodes. The circle of robots is similar to our circle of the time period. The distribution of robots can be mapped to the distribution of nodes on the time circle. The robotic circular formation of Boonpinon and Sudsang (2006) inspires us to design a novel desynchronization algorithm for wireless sensor networks based on an *artificial force field*. If we abstract the nodes on a time circle as the robots of the same type, the nodes will repel each other and keep time intervals from their neighbors as far as possible. Once all received forces are balanced, nodes are equally spread out on the time circle.

The desynchronization algorithm based on the artificial force field can be classified as a *Physicomimetics* algorithm. A physicomimetics algorithm is an algorithm that imitates principles of physics and can be called *Artificial Physics* or *Virtual Physics* (Spears et al. (2005)). To the best of our knowledge, physicomimetics was introduced in Spears and Gordon (1999) for distributed control of large collections of agents. Then, physicomimetics has been applied mostly in the field of robotics for geometric pattern formation and optimizations such as in Ekanayake and Pathirana (2010), Wang et al. (2010), and Boonpinon and Sudsang (2006). Due to the framework of desynchronization is similar to the framework of robotic geometric pattern formation, we believe that the physicomimetics approach can also solve the desynchronization problem in the temporal domain as well. Therefore, this dissertation presents how physics principles can be imitated to solve the desynchronization problem for wireless sensor networks.

CHAPTER III

PHYSICOMIMETICS DESYNCHRONIZATION ALGORITHM FOR SINGLE-HOP NETWORKS

3.1 Introduction

As we mentioned in the previous chapter, physicomimetics algorithms have been widely used for the robotic pattern formation that can be abstracted as desynchronization in the spatial domain. One of such algorithms is that of Boonpinon and Sudsang (2006). In their work, robots are in an artificial force field. Robots with the same type repel each other to form themselves into a circular shape.

Inspired by their work, in this chapter, we present a novel physicomimetics desynchronization algorithm called *DWARF* (Desynchronization With an ARtificial Force field) for single-hop wireless sensor networks. Each neighboring node has artificial forces to repel other nodes to perform tasks at different time phases. Nodes with closer time phases have stronger forces to repel each other in the time domain. Each node adjusts its time phase proportionally to its received forces. Once the received forces are balanced, nodes are desynchronized

DWARF has the following key contributions:

- DWARF is a distributed desynchronization algorithm using time phases of all neighbors to achieve the desyncrhony state.
- DWARF uses only local information but achieves a global state.
- DWARF does not require time synchronization, does not assume already slotted time, and does not incur any control message overhead.
- DWARF is simple due to low complexity in terms of computation and memory. Therefore, it is suitable for resource-constraint networks, such as wireless sensor networks. Additionally, message complexity is low because the algorithm relies on the timing of the message, not information inside the message.

- We have implemented and evaluated DWARF on TOSSIM, a simulator for wireless sensor networks. Our results indicate that DWARF scales well with network size and outperforms DESYNC significantly by achieving 10 - 63% reduction in desynchronization error.

Therefore, we believe that DWARF can be a primer for various applications and can be extended for multi-hop networks which will be later described in Chapter 5.

In the next section, we present the concept of an artificial force field which is the crucial concept of our desynchronization algorithm.

3.2 Artificial Force Field

An artificial force field is an analogy to the circle of a time period. Nodes are in the same force field if they can communicate with each other.

If node i and node j are on the same force field, they have repelling forces to push one another away. A closer pair of nodes has a higher magnitude of force than a farther pair does. The time interval between two nodes is derived from the phase difference between them. If two nodes have a small phase difference, they have a high magnitude of force and vice versa. In other words, a repelling force is an inverse of a phase difference between two nodes:

$$f_{i,j} = -\frac{1}{\Delta\phi_{i,j}/T}, \Delta\phi_{i,j} \in (-\frac{T}{2}, \frac{T}{2}), \tag{3.1}$$

where $f_{i,j}$ is the repelling force from node j to node i on a time period T and $\Delta\phi_{i,j}$ is the phase difference between node i and j. We note that $\Delta\phi_{i,j}$ is not equal to 0 because if two nodes fire at the same time, their firings collide and two nodes do not record other's firing. Additionally, at $T/2$ or $-T/2$, a node does not repel an opposite node because they are balanced.

A repelling force can be positive (clockwise repelling) or negative (counterclockwise repelling). A positive force is created by a node on the left half of the circle relative to the considered node whereas a negative force is created by a node on the right half. Figure 3.1 represents a field of repelling forces on node 1.

Each node in the force field moves to a new time position or phase proportional to

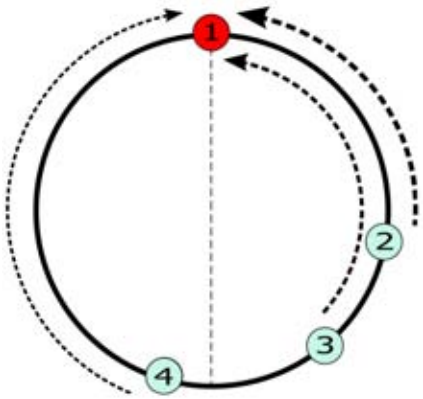

Figure 3.1: Artificial Force Field. Arrow lines represent repelling forces from node 2, 3, and 4 to node 1. A shorter and thicker line is a stronger force. A force from node 4 is a positive force and two forces from node 2 and 3 are negative forces.

the total received force. Given n nodes in a force field, the total force on a node i is the following:

$$\mathcal{F}_i = \sum_{\substack{j=1 \\ j \neq i}}^{n} f_{i,j}. \tag{3.2}$$

Eventually, nodes reach an equilibrium state whereby the total force of the system is close to zero and each pair of phase neighboring nodes has the same time interval. This equilibrium state also indicates the perfect desynchrony state because all nodes are equally spaced on the time circle.

3.3 Algorithm

We assume that, initially, nodes are not desynchronized. Each node sets a timer to fire in T time unit. After setting the timer, each node listens to all neighbors until its timer expires.

When receiving a firing message from its neighbor, the (positive or negative) repelling force from that neighbor is calculated based on the phase difference. When the timer expires, a node broadcasts a firing message to neighbors. Then, the node calculates a new time phase to move on the circle based on the summation of forces from all neighbors and sets a new timer according to the new time phase.

Reasonably, one may wonder how far a node should move or adjust its phase. In

our work, given the total received force $\mathcal{F}_i$, the node i adjusts to a new time phase $\phi_i^{'}$,

$$\phi_i^{'} = (\phi_i + K\mathcal{F}_i) \mod T, \tag{3.3}$$

where ϕ_i is the current phase of the node i.

Undoubtedly, the proper value of the coefficient K leads to the proper new phase. The value of K is similar to a step size which is used in artificial intelligence techniques. Therefore, if the value of K is too small, the system takes much time to converge. On the other hand, if the value of K is too large, the system may overshoot the optimal value and does not converge. We observe that, given the same time period, fewer nodes in the system result in bigger phase difference between two phase neighbors. To be desynchronized, nodes in sparse networks must make a bigger adjustment to their time phases than nodes in dense networks must. Therefore, the same total received force should have a bigger impact on a node in sparse networks than on a node in dense networks. To reflect this observation, the coefficient K is inversely proportional to a power of the number of nodes n,

$$K = c_1 \times n^{-c_2}, \text{ where } c_1, c_2 \geq 0. \tag{3.4}$$

Therefore, we have conducted an experiment to find the proper value of c_1 and c_2.

We set a time period T to 1000 and vary the number of nodes. In the specific number of nodes, we first simulate to see the trend of the value K that leads to small errors. Then, we select a range of good K values. After that, we simulate 100 times to obtain the average desynchronization error for each K value. In each simulation, we randomly set an initial phase of each node between 0 and T (period value). Finally, we select the K value that results in the lowest error. After getting the proper K value for each number of nodes, we plot the relation between K and the number of nodes (Figure 3.2) and use a mathematical tool to calculate the power regression. The obtained relation function between K and n (the trendline in Figure 3.2) consists of c_1 and c_2 values as follows:

$$K = 38.597 \times n^{-1.874}.$$

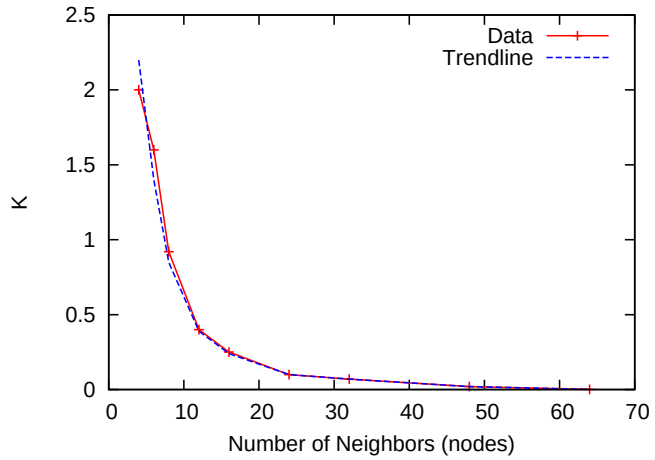

Figure 3.2: Relation of the coefficient K with a number of nodes n

However, this K value is derived by setting T equal to 1000. Therefore, for arbitrary T,

$$K = 38.597 \times n^{-1.874} \times \frac{T}{1000}. \tag{3.5}$$

Proof: From Equation 3.2 and 3.3, the phase of node j is adjusted by $K\mathcal{F}_j = K\sum_{i\neq j}^{n} f_{i,j} = \sum_{i\neq j}^{n} Kf_{i,j}$. Therefore, we can analyze the value of K from only single force $f_{i,j}$.

For a time circle of a period T_p, let θ_p be an angle between two nodes on the circle and Θ_p be an angle between the new adjusted phase and the old phase based on a single force where $\theta_p, \Theta_p \in (0, 2\pi)$. Hence,

$$\frac{\theta_p}{2\pi} = \frac{\Delta\phi_{i,j}}{T_p}, \tag{3.6}$$

and

$$\frac{\Theta_p}{2\pi} = \frac{Kf_{i,j}}{T_p}. \tag{3.7}$$

If θ_1 of T_1 equals to θ_2 of T_2, both of them should be adjusted with the same angle amount $\Theta_1 = \Theta_2$. Thus, from Equation 3.7,

$$\Theta_1 = \Theta_2$$
$$\frac{K_1 f_{i,j(1)}}{T_1} = \frac{K_2 f_{i,j(2)}}{T_2}.$$

From Equation 3.1 and 3.6, $f_{i,j} = \frac{1}{\Delta\phi_{i,j}/T_p} = \frac{2\pi}{\theta_p}$, consequently,

$$\begin{aligned} \frac{K_1 2\pi}{T_1\theta_1} &= \frac{K_2 2\pi}{T_2\theta_2} \\ \frac{K_1}{T_1} &= \frac{K_2}{T_2} \\ K_2 &= K_1\frac{T_2}{T_1}. \end{aligned} \tag{3.8}$$

At $T = 1000$, we get $K = 38.597 \times n^{-1.874}$. Therefore, from Equation 3.8, for arbitrary T,

$$K = 38.597 \times n^{-1.874} \times \frac{T}{1000}.$$

■

All nodes in the artificial force field (in the period circle) iteratively run the same algorithm until the force is balanced (*i.e.*, all nodes are in the desynchrony state). The pseudo-code of this algorithm is shown in Figure 3.3.

3.4 Evaluation

In this section, we evaluate the performance of our proposed algorithm and compare with DESYNC (Degesys et al. (2007)) because DESYNC and our algorithm share the same goal and requirements. Particularly, they do not require time synchronization, do not assume already slotted time, do not need to look into the packet content, and do not incur control packets but still achieve equivalent time spaces. Other protocols (*e.g.*, M-DESYNC (Patel et al. (2007)), Lightweight desynchronization (Motskin et al. (2009))) assume different requirements. Therefore, we only discuss our differences with such protocols in Chapter 2.

The performance metrics in this evaluation are desynchronization error and convergence time. The former indicates how close the current state is to the perfect desynchrony state. The latter indicates how fast the algorithm converges.

1: **Initialization**
2: $T = TimePeriod$ {Configurable Time Period}
3: $n = 1$ {Number of receiving messages including itself}
4: $\mathcal{F} = 0$ {Force Summation}
5: $lastFiringTime = localTime$
6: $currentPhase = localTime$ modulo T
7: Set a firing timer to be T unit time

8: **Upon timer firing**
9: Broadcast a firing message to neighbors
10: $lastFiringTime = localTime$
11: $currentPhase = localTime$ modulo T
12: $K = 38.597 \times n^{-1.874} \times \frac{T}{1000}$
13: $newPhase = currentPhase + (K \times \mathcal{F})$
14: **if** $newPhase < 0$ **then**
15: $\quad newPhase = T + newPhase$
16: **end if**
17: Set a firing timer to be fired at ($newPhase$ modulo T)
18: $\mathcal{F} = 0$
19: $n = 1$

20: **Upon receiving a firing message**
21: $n = n + 1$
22: $phaseDiff = localTime - lastFiringTime$
23: **if** $phaseDiff == 0.5T$ **then**
24: $\quad \mathcal{F} = \mathcal{F} + 0$ {Balanced force}
25: **else if** $phaseDiff < 0.5T$ **then**
26: $\quad \mathcal{F} = \mathcal{F} + |\frac{1}{phaseDiff/T}|$ {Positive force}
27: **else**
28: $\quad \mathcal{F} = \mathcal{F} - |\frac{1}{(T-phaseDiff)/T}|$ {Negative force}
29: **end if**

Figure 3.3: Pseudocode of DWARF algorithm

3.4.1 Evaluation Environment

We implement DWARF on TinyOS 2.1.2 (Levis et al. (2004)), an operating system for wireless sensor networks and evaluate the protocol on TOSSIM (Levis et al. (2003)), a TinyOS simulator. We vary the one-hop network size from 4 to 96 nodes. Each node periodically fires a message that contains only application data with no extra control overhead. This zero overhead is the advantage of both DWARF and DESYNC because, to avoid collision, a node only needs to know the timing of the firing rather than the control information inside a packet. In our simulation, for both DWARF and DESYNC, we use a 2-byte node ID and a 2-byte counter as the data. However, we do use the regular 11-byte CC2420 header for TOSSIM. Therefore, we do not measure the overhead in our evaluation. We set the time period to 1,000 milliseconds and compare our result with

that of DESYNC. Initially, the phase of each node is random in a range of 0 to 1,000.

3.4.2 Varying Step Size in DESYNC

In Degesys et al. (2007), they choose the step size of DESYNC to be 0.95. In this section, we begin by varying the step size of DESYNC to confirm that the step size 0.95 is a proper and fair value for DESYNC to compare with DWARF in our investigated scenario. Figure 3.4, 3.5, and 3.6 show the results of varying step size from 0.10 to 0.95.

The result indicates that too small step size (0.10 to 0.35) leads to slow convergence speed and high error. Increasing step size tends to lead to lower error. Step sizes from 0.65 to 0.95 do not result in much different in term of error but the larger value tends to lead to faster convergence speed. However, increasing step size from 0.80 to 0.95 does not significantly improve the performance. Therefore, we can use 0.95 which is the same value used in Degesys et al. (2007) as the step size for DESYNC to compare with DWARF.

3.4.3 Desynchronization Error

To measure the desynchronization error, we run the simulation for 300 time periods. In each network size, we run the simulation for 30 times. Then, we measure the average root mean square error (RMSE). The error (ERR) is the measured phase difference minus the perfect phase difference:

$$ERR_i = \Delta\phi_{i,j} - T/n,$$

$$RMSE = \sqrt{\frac{\sum_{i=1}^{n} ERR_i^2}{n}},$$

where node j is the next phase neighbor of node i. $\Delta\phi_{i,j}$ is the phase difference between node i and node j on the time period T. Given that n is a total number of nodes, T/n is the perfect phase difference.

However, a smaller absolute error in a dense network is not necessarily better than

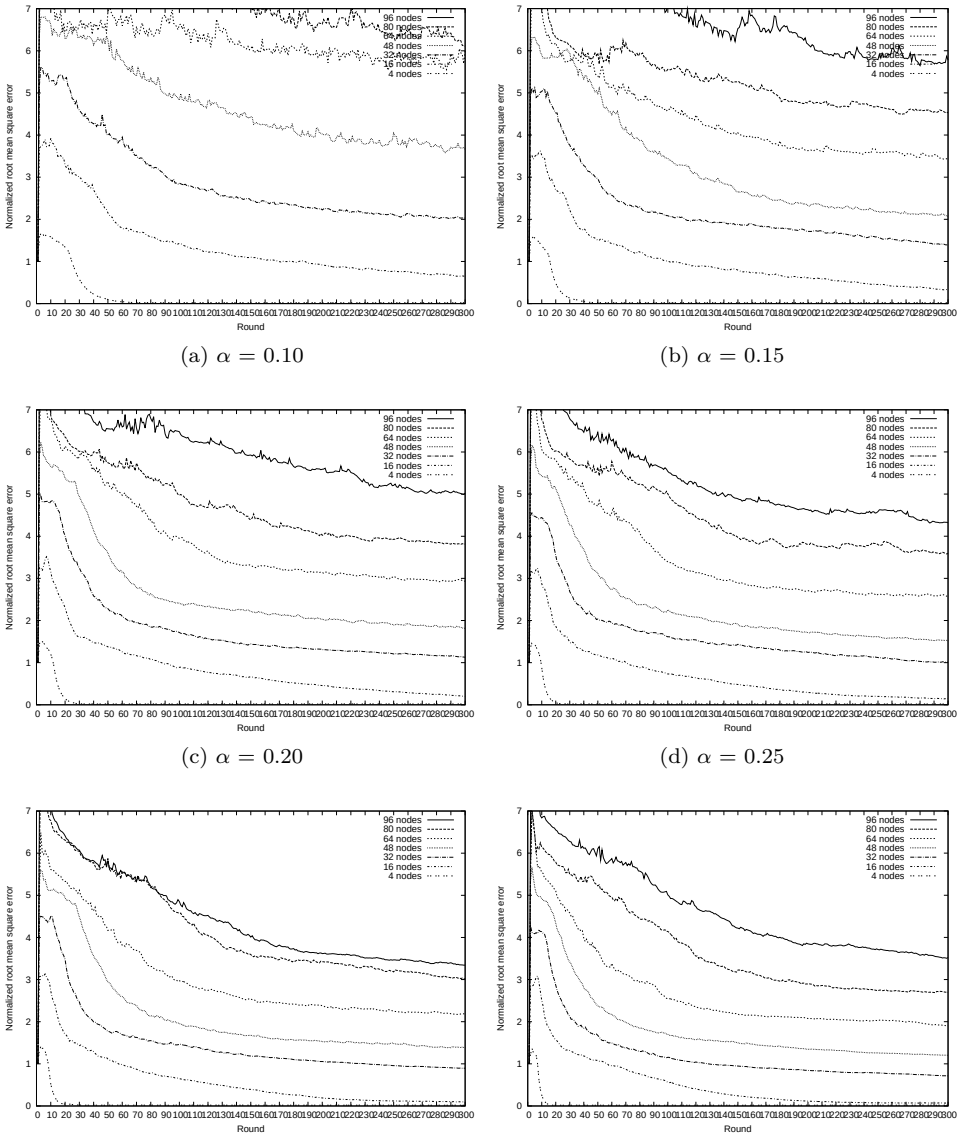

(a) $\alpha = 0.10$

(b) $\alpha = 0.15$

(c) $\alpha = 0.20$

(d) $\alpha = 0.25$

(e) $\alpha = 0.30$

(f) $\alpha = 0.35$

Figure 3.4: DESYNC: Varying step size from 0.10 to 0.35

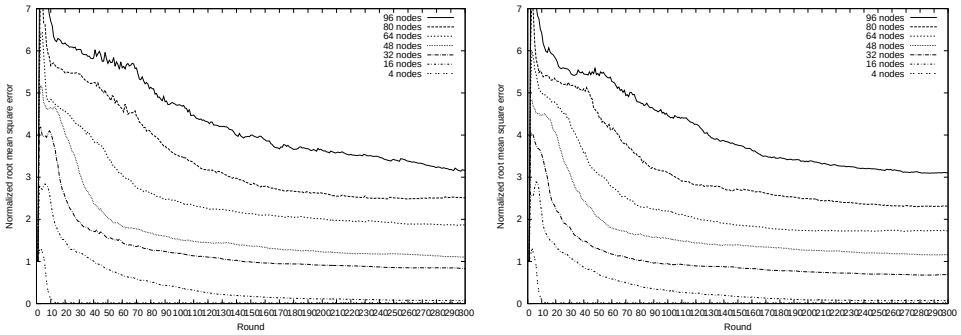

(a) $\alpha = 0.40$

(b) $\alpha = 0.45$

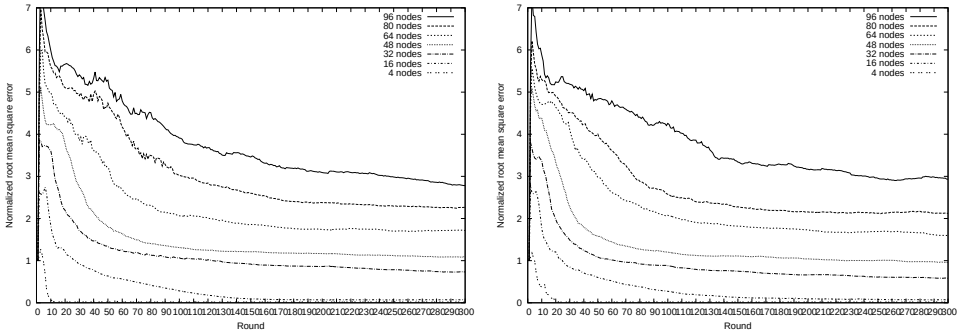

(c) $\alpha = 0.50$

(d) $\alpha = 0.55$

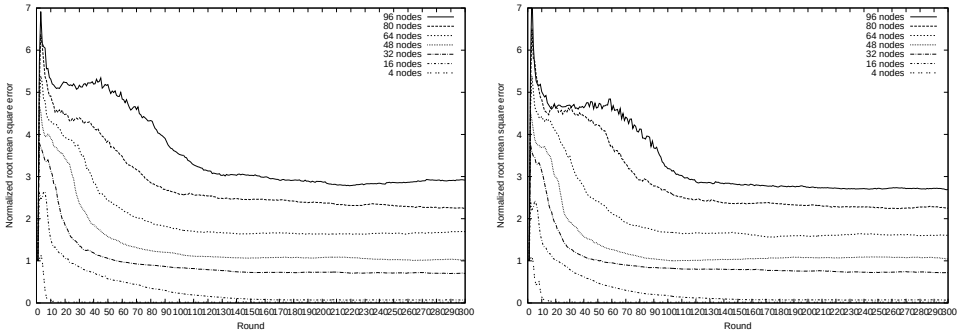

(e) $\alpha = 0.60$

(f) $\alpha = 0.65$

Figure 3.5: DESYNC: Varying step size from 0.40 to 0.65

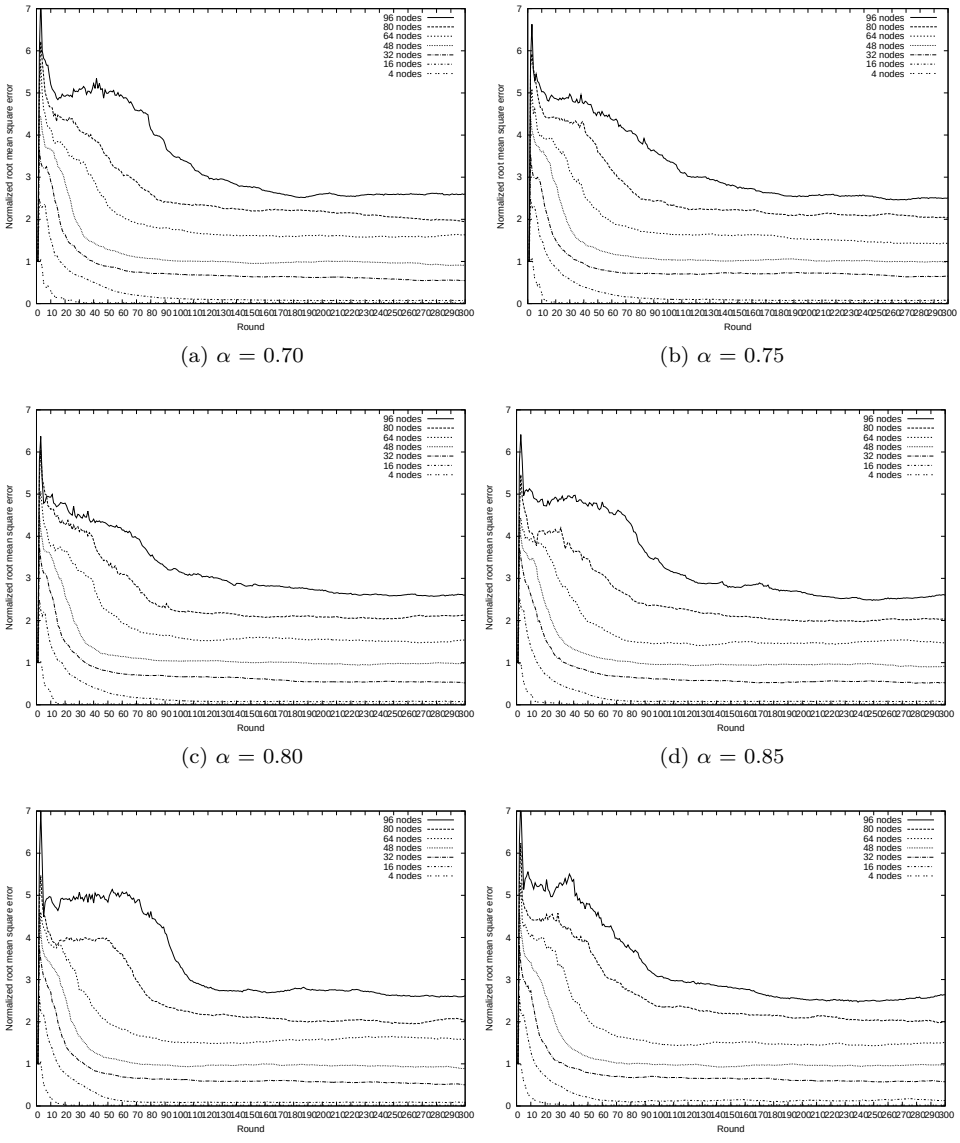

(a) $\alpha = 0.70$ (b) $\alpha = 0.75$

(c) $\alpha = 0.80$ (d) $\alpha = 0.85$

(e) $\alpha = 0.90$ (f) $\alpha = 0.95$

Figure 3.6: DESYNC: Varying step size from 0.70 to 0.95

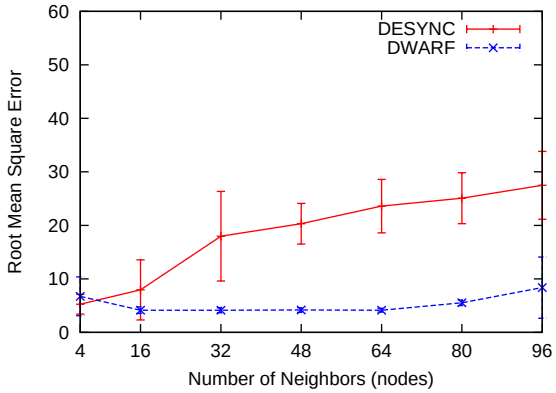

Figure 3.7: Root mean square error after 300 time periods

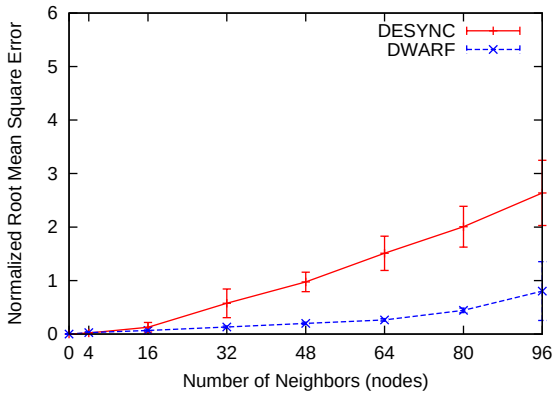

Figure 3.8: Root mean square error normalized by perfect phase difference after 300 time periods

a bigger error in a sparse network because the perfect phase difference in a dense network is also smaller than that in a sparse network. Thus, for a comparable view of each network size, we also measure a normalized root mean square error (NRMSE) that is a ratio of the root mean square error and the perfect phase difference of each network size. Figure 3.7 illustrate the result of absolute desynchronization error and Figure 3.8 illustrates the result of the normalized desynchronization error in each network size after 300 time periods.

The result indicates that, in all network sizes (4 - 96 nodes), DWARF achieves significantly better desynchrony states than DESYNC does. Understandably, using information from all neighbors (as in DWARF) leads to lower errors than using information from only two phase neighbors (as in DESYNC) does. Furthermore, DESYNC's mechanism allows a phase error of a node to propagate to its phase neighbors. A part of this error will propagate back and forth between two phase neighbors as well as circulate

inside the network. As a result, DESYNC's error after convergence is still quite large. In contrast, DWARF is robust to this error propagation. Even though the error propagation may still occur, the impact is not significant. Given that DWARF uses the sum of forces from all neighbors, an error from one neighbor does not overwhelm the system.

We note that we show RMSE and NRMSE after 300 periods because, by that time, the errors of all simulation scenarios seem to be stable. The actual convergence time in most scenarios is much lower than 300 rounds (see the next section).

3.4.4 Convergence Time

In the desynchronization error evaluation, we only measure the performance after 300 time periods. However, the previous result does not indicate whether the protocols have converged or not. Neither does it indicate how fast the protocols have converged. Hence, we also measure the absolute root mean square error and normalized root mean square error for each time period.

In sparse networks (Figure 3.9a and 3.10a), both protocols converge with similar small error but DWARF converges slightly faster. In dense networks (Figure 3.9b and 3.10b) and extremely dense networks (Figure 3.9c and 3.10c), both protocols still converge. Even though DESYNC converges faster in such networks, it converges with a relatively high error compared to that of DWARF. In addition, at the time when DESYNC has converged and DWARF has not converged yet, DWARF's error is already lower than DESYNC's. Furthermore, in dense and extremely dense networks, the normalized root mean square errors of DESYNC after convergence is higher or equal to 1. This means that the error is very large compared to the perfect phase difference. Conversely, the normalized error of DWARF is lower than 1 even in the extremely dense networks. Therefore, DWARF scales well with the network density whereas DESYNC does not.

In a denser network, the errors of DESYNC and DWARF are higher because the probability of message collisions increases (see the next section).

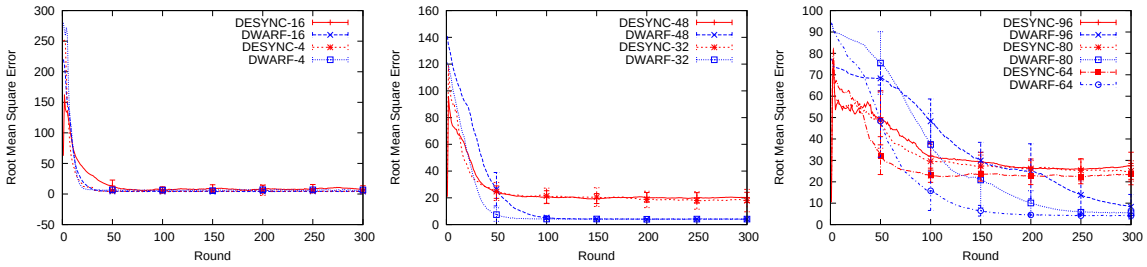

(a) Sparse (b) Dense (c) Extremely Dense

Figure 3.9: Convergence time and absolute root mean square error

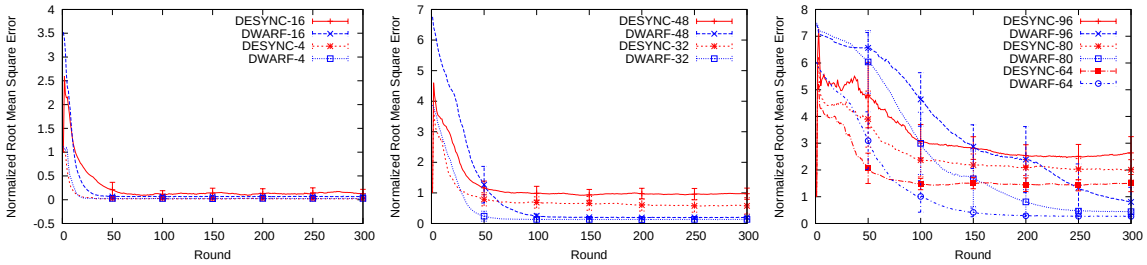

(a) Sparse (b) Dense (c) Extremely Dense

Figure 3.10: Convergence time and root mean square error normalized by expected phase difference

3.4.5 Correlation of Packet Loss and Desynchronization Error

In this section, we investigate the correlation of packet loss and desynchronization error. We only include the results of DWARF in networks of 16, 48, and 80 nodes for 300 time periods (Figure 3.11). However, in networks of 4, 32, 64, and 96 nodes, the results are similar (not shown).

At the beginning, the network is far from the perfect desynchrony state and messages from different nodes are simultaneously fired. This results in lost packets and errors. However, over time, nodes gradually adapt their time phases. Consequently, the number of lost packets and the error also gradually drop.

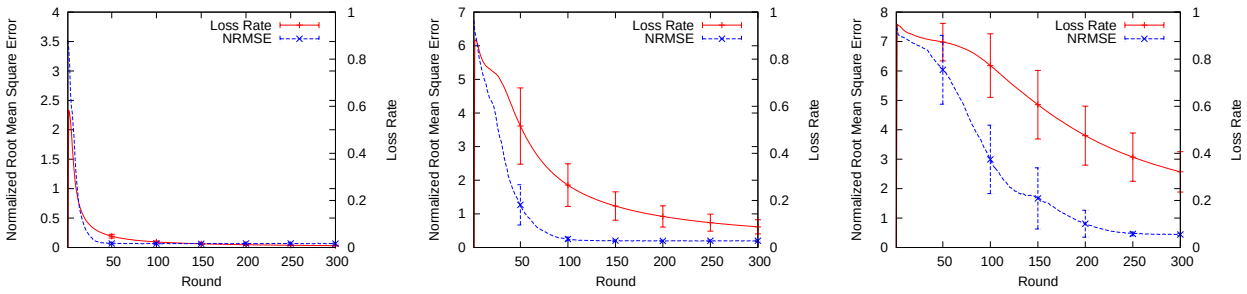

(a) 16 nodes (b) 48 nodes (c) 80 nodes

Figure 3.11: Correlation of packet loss and desynchronization error

3.5 Summary

In this chapter, we present DWARF, a novel desynchronization algorithm that enables nodes in a system to perform tasks at different time. To the best of our knowledge, DWARF is the first desynchronization algorithm that is based on the concept of electromagnetic fields, a foundation of physics. Our algorithm is completely distributed and localized with no reliance on a centralized node or a global notion of time. Due to low complexity in terms of computation, memory, and message overhead, DWARF is suitable for traditional wireless networks as well as resource-constraint wireless sensor networks. Our result indicates that DWARF can significantly outperform DESYNC by reducing 10 - 63% of the desynchronization error. In addition, DWARF scales well with network size given that the normalized error is lower than 1 even in extremely dense networks.

The evaluation result of DWARF is promising. This result indicates that physicomimetics approach is viable for desynchronization. However, the evaluation has been performed on single-hop networks. Typically, wireless sensor networks are multi-hop networks. There are several issues to be concerned in extending DWARF to such networks. We cover such issues and present the multi-hop extension of DWARF in Chapter 5. Additionally, the evaluation does not show the mathematical evidence that the algorithm is stable and does not indicate why the algorithm converges. Therefore, we analyses the stability of the algorithm in the next chapter.

CHAPTER IV

CONVEXITY AND STABILITY ANALYSIS OF THE SINGLE-HOP ALGORITHM

In the previous chapter, we present DWARF, a physicomimetics desynchronization algorithm. From the evaluation results, the algorithm is eventually stable with low desynchronization error. However, it is not obvious that why DWARF is eventually stable with low error. Therefore, in this chapter, we mathematically analyse the stability of the algorithm.

We divide our analysis into two parts. First, we analyse the convexity of the force function. If the force function is convex, the system contains one global minima and no local minima. Therefore, the system could reach the perfect desynchrony state by gradually reducing the overall force of the system. Second, we analyse the stability when the system at the equilibrium. If the system is stable, it can be back to the equilibrium under a small perturbation.

4.1 Convexity Analysis

In this section, our goal is to prove that the force function used in DWARF has one global minima and no local minima. In other words, we will prove that the force function is convex.

Let F_i be the force summation at node i and $\Delta_{i,j} \in (-\frac{T}{2}, \frac{T}{2})$ is an interval between node i and j. If $\Delta_{i,j} > 0$, the node j repels the node i in a positive direction. In contrast, if $\Delta_{i,j} < 0$, the node j repels the node i in a negative direction.

Therefore, for n nodes, F_i can be formulated as the following equation,

$$F_i = \sum_{\substack{j=1 \\ j \neq i}}^{n} \frac{1}{\Delta_{i,j}}. \tag{4.1}$$

The objective function E of the system is the summation of absolute received forces

at all nodes,

$$E = \sum_{i=1}^{n} |F_i| = \sum_{i=1}^{n} \left| \sum_{\substack{j=1 \\ j \neq i}}^{n} \frac{1}{\Delta_{i,j}} \right| \tag{4.2}$$

To prove the function E is a convex function, we must prove that two following conditions are satisfied; 1) the set of all $\Delta_{i,j}$ is a convex set and 2) the Hessian matrix of E is positive semidefinite.

Proposition 4.1 *A set of all possible interval $\Delta_{i,j}$ is a convex set.*

Proof: A set of $(-\frac{T}{2}, \frac{T}{2})$ is a line connecting between $-\frac{T}{2}$ and $\frac{T}{2}$. Therefore, any Δ_{i_1,j_1}, $\Delta_{i_2,j_2} \in (-\frac{T}{2}, \frac{T}{2})$ and $\alpha \in \mathbb{R}$ with $0 \leq \alpha \leq 1$,

$$\alpha\Delta_{i_1,j_1} + (1-\alpha)\Delta_{i_2,j_2} \in (-\frac{T}{2}, \frac{T}{2}).$$

■

Proposition 4.2 *The Hessian of the function E is positive semidefinite.*

Proof: Let H be the Hessian matrix of the objective function E,

$$H = \begin{pmatrix} \frac{\partial^2 E}{\partial \Delta_{1,2}^2} & \frac{\partial^2 E}{\partial \Delta_{1,2} \partial \Delta_{1,3}} & \cdots & \frac{\partial^2 E}{\partial \Delta_{1,2} \partial \Delta_{n,n-1}} \\ \frac{\partial^2 E}{\partial \Delta_{1,3} \partial \Delta_{1,2}} & \frac{\partial^2 E}{\partial \Delta_{1,3}^2} & \cdots & \frac{\partial^2 E}{\partial \Delta_{1,3} \partial \Delta_{n,n-1}} \\ \vdots & \vdots & \ddots & \vdots \\ \frac{\partial^2 E}{\partial \Delta_{n,n-1} \partial \Delta_{1,2}} & \frac{\partial^2 E}{\partial \Delta_{n,n-1} \partial \Delta_{1,3}} & \cdots & \frac{\partial^2 E}{\partial \Delta_{n,n-1}^2} \end{pmatrix}.$$

For any $\Delta_{x,y}$, we derive the first-order derivative as follows,

$$\frac{\partial E}{\partial \Delta_{x,y}} = \frac{\sum_{\substack{j=1 \\ j \neq x}}^{n} \frac{1}{\Delta_{x,j}}}{\left| \sum_{\substack{j=1 \\ j \neq x}}^{n} \frac{1}{\Delta_{x,j}} \right|} \left(-\frac{1}{\Delta_{x,y}^2} \right).$$

For the second-order partial derivatives, if we differentiate with the same $\Delta_{x,y}$,

$$\frac{\partial^2 E}{\partial \Delta_{x,y}^2} = \frac{\sum_{\substack{j=1 \\ j\neq x}}^{n} \frac{1}{\Delta_{x,j}}}{\left|\sum_{\substack{j=1 \\ j\neq x}}^{n} \frac{1}{\Delta_{x,j}}\right|} \left(\frac{2}{\Delta_{x,y}^3}\right).$$

In the other hand, if we differentiate with other $\Delta_{u,v}$, where $u \neq x$ or $v \neq y$, $\frac{\partial^2}{\partial \Delta_{u,v} \partial \Delta_{x,y}} E = 0$.

Therefore, the Hessian matrix of the function E is

$$H = \begin{pmatrix} a_{1,2} & 0 & \cdots & 0 \\ 0 & a_{1,3} & \cdots & 0 \\ \vdots & \vdots & \ddots & \vdots \\ 0 & 0 & \cdots & a_{n,n-1} \end{pmatrix},$$

where $a_{i,j} = \frac{u_i}{|u_i|}\left(\frac{2}{\Delta_{i,j}^3}\right)$ and $u_i = \sum_{\substack{j=1 \\ j\neq i}}^{n} \frac{1}{\Delta_{i,j}}$.

To show that the Hessian matrix of the function E is positive semidefinite, we show that $\vec{\Delta}^T H \vec{\Delta} \geq 0$ for all $\vec{\Delta}$ when $\vec{\Delta} \neq 0$.

$$\begin{aligned} \vec{\Delta}^T H \vec{\Delta} &= \begin{pmatrix} \Delta_{1,2} & \Delta_{1,3} & \cdots & \Delta_{n,n-1} \end{pmatrix} H \begin{pmatrix} \Delta_{1,2} \\ \Delta_{1,3} \\ \vdots \\ \Delta_{n,n-1} \end{pmatrix} \\ &= \sum_{i=1}^{n} \sum_{\substack{j=1 \\ j\neq i}}^{n} \frac{u_i}{|u_i|} \left(\frac{2}{\Delta_{i,j}}\right) \\ &= 2 \sum_{i=1}^{n} \frac{u_i}{|u_i|} \sum_{\substack{j=1 \\ j\neq i}}^{n} \frac{1}{\Delta_{i,j}} \\ &= 2 \sum_{i=1}^{n} \frac{u_i}{|u_i|} u_i = 2 \sum_{i=1}^{n} |u_i| \\ &\geq 0 \end{aligned}$$

Therefore, we conclude that $\vec{\Delta}^T H \vec{\Delta} \geq 0$ and the Hessian matrix of E is positive semidefinite. ■

From Proposition 4.1 and 4.2, we derive the following lemma.

Lemma 4.3 *the function E is a convex function.*

From the above lemma, we finish our proof with the following theorem.

Theorem 4.4 *The system force summation function of DWARF has one global minima and no local minima.*

4.2 Stability Analysis

To prove that the system is stable, we begin by transforming the system into a non-linear dynamic system. The evenness of the number of nodes affects the analysis. Therefore, we divide the non-linear dynamic system into two cases: when n is even and when n is odd where n is the number of nodes.

1) when n is even: Figure 4.1a illustrates the equilibrium of a dynamic system when the number of nodes is even. Noticeably, node 0 and $n/2$ are exactly at the opposite side of each other. At the first snapshot of the system, node 0 adjusts its phase based on the force function of DWARF. After adjustment, we re-label node 1 to 0, node 2 to 1, ..., node $n-1$ to $n-2$, and node 0 to $n-1$ for analysis at the next snapshot (see Figure 4.1b). Therefore, to transform into a difference equation, Δ_1 in the next snapshot is Δ_2 in the previous snapshot, Δ_2 in the next snapshot is Δ_3 in the previous snapshot, and so on. However, Δ_{n-1} and Δ_n in the next snapshot are Δ_n and Δ_1 in the previous snapshot adjusted by the force function, respectively. Therefore, the non-linear dynamic system

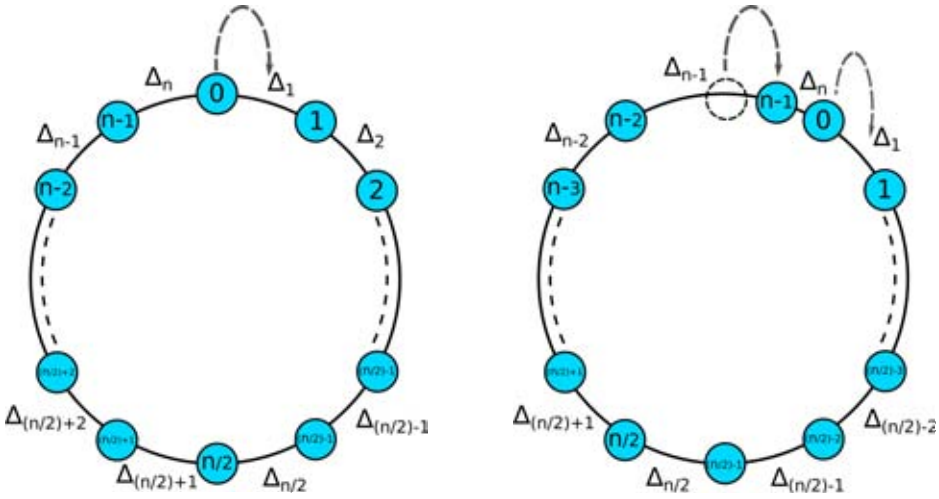

(a) (b)

Figure 4.1: Non-linear dynamic system when n is even. (a) The snapshot of the system at one time step. (b) In next time step after node 0 adjusts its phase, node 1 in previous round is re-labelled to 0, node 2 is re-labelled to 1, and so on.

when n is even can be expressed as the following difference equations:

$$
\begin{aligned}
\Delta_1 =& \Delta_2 \\
\Delta_2 =& \Delta_3 \\
&\vdots \\
\Delta_{n-2} =& \Delta_{n-1} \\
\Delta_{n-1} =& \Delta_n + KT\Bigg(-\frac{1}{\Delta_1} - \frac{1}{\Delta_1+\Delta_2} - \ldots - \frac{1}{\Delta_1+\Delta_2+\ldots+\Delta_{\frac{n}{2}-1}} \\
&+ \frac{1}{\Delta_n} + \frac{1}{\Delta_n+\Delta_{n-1}} + \ldots + \frac{1}{\Delta_n+\Delta_{n-1}+\ldots+\Delta_{\frac{n}{2}+2}} \Bigg) \\
\Delta_n =& \Delta_1 - KT\Bigg(-\frac{1}{\Delta_1} - \frac{1}{\Delta_1+\Delta_2} - \ldots - \frac{1}{\Delta_1+\Delta_2+\ldots+\Delta_{\frac{n}{2}-1}} \\
&+ \frac{1}{\Delta_n} + \frac{1}{\Delta_n+\Delta_{n-1}} + \ldots + \frac{1}{\Delta_n+\Delta_{n-1}+\ldots+\Delta_{\frac{n}{2}+2}} \Bigg)
\end{aligned}
\tag{4.3}
$$

We note that the force from node $n/2$ in the previous snapshot is already balanced when we consider node 0. Therefore, $\Delta_{\frac{n}{2}}$ and $\Delta_{\frac{n}{2}+1}$ do not appear in the force equation

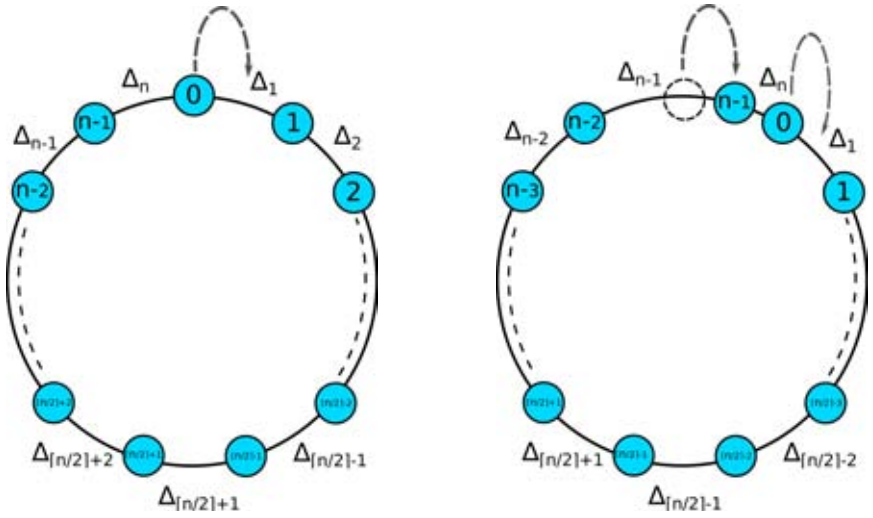

(a) (b)

Figure 4.2: Non-linear dynamic system when n is odd. (a) The snapshot of the system at one time step. (b) In next time step after node 0 adjusts its phase, node 1 in previous round is re-labelled to 0, node 2 is re-labelled to 1, and so on.

for adjusting Δ_{n-1} and Δ_n in the next snapshot.

2) when n is odd: Similarly, Figure 4.2 illustrates the non-linear dynamic system when n is odd. The only difference from when n is even is that there is no node that is opposite to node 0. Therefore, in the difference equations, only $\Delta_{\lceil \frac{n}{2} \rceil}$ from the previous snapshot does not appear in the force equation for adjusting Δ_{n-1} and Δ_n in the next snapshot.

$$
\begin{aligned}
\Delta_1 =& \Delta_2 \\
\Delta_2 =& \Delta_3 \\
&\vdots \\
\Delta_{n-2} =& \Delta_{n-1} \\
\Delta_{n-1} =& \Delta_n + KT\Bigg(-\frac{1}{\Delta_1} - \frac{1}{\Delta_1+\Delta_2} - \ldots - \frac{1}{\Delta_1+\Delta_2+\ldots+\Delta_{\lceil \frac{n}{2} \rceil -1}} \\
&+ \frac{1}{\Delta_n} + \frac{1}{\Delta_n+\Delta_{n-1}} + \ldots + \frac{1}{\Delta_n+\Delta_{n-1}+\ldots+\Delta_{\lceil \frac{n}{2} \rceil +1}} \Bigg) \\
\Delta_n =& \Delta_1 - KT\Bigg(-\frac{1}{\Delta_1} - \frac{1}{\Delta_1+\Delta_2} - \ldots - \frac{1}{\Delta_1+\Delta_2+\ldots+\Delta_{\lceil \frac{n}{2} \rceil -1}}
\end{aligned}
$$

$$+\frac{1}{\Delta_n}+\frac{1}{\Delta_n+\Delta_{n-1}}+\ldots+\frac{1}{\Delta_n+\Delta_{n-1}+\ldots+\Delta_{\lceil\frac{n}{2}\rceil+1}}\Bigg)$$

Due to the non-linear adaptation function, the standard linear dynamic system analysis does not suffice. Therefore, we locally analyse stability of the system around a fixed point which is the equilibrium point. We begin by linear approximation to find the Jacobian at the equilibrium. Then, from the Jacobian, we find the bound of eigenvalues which is the crucial part of stability analysis.

4.2.1 Linear Approximation

The Jacobian (J) of a difference equations system is defined as follows:

$$J=\begin{pmatrix} \frac{\partial\Delta_1}{\partial\Delta_1} & \frac{\partial\Delta_1}{\partial\Delta_2} & \cdots & \frac{\partial\Delta_1}{\partial\Delta_{n-1}} & \frac{\partial\Delta_1}{\partial\Delta_n} \\ \frac{\partial\Delta_2}{\partial\Delta_1} & \frac{\partial\Delta_2}{\partial\Delta_2} & \cdots & \frac{\partial\Delta_2}{\partial\Delta_{n-1}} & \frac{\partial\Delta_2}{\partial\Delta_n} \\ \vdots & \vdots & \ddots & \vdots & \vdots \\ \frac{\partial\Delta_{n-1}}{\partial\Delta_1} & \frac{\partial\Delta_{n-1}}{\partial\Delta_2} & \cdots & \frac{\partial\Delta_{n-1}}{\partial\Delta_{n-1}} & \frac{\partial\Delta_{n-1}}{\partial\Delta_n} \\ \frac{\partial\Delta_n}{\partial\Delta_1} & \frac{\partial\Delta_n}{\partial\Delta_2} & \cdots & \frac{\partial\Delta_n}{\partial\Delta_{n-1}} & \frac{\partial\Delta_n}{\partial\Delta_n} \end{pmatrix} \tag{4.4}$$

We consider the Jacobian when n is even and odd separately. In both cases, after finding the Jacobian, we substitute each Δ_i with T/n which is the phase interval between each node at the equilibrium.

1) n is even:

For $\Delta_i, 1\leq i\leq n-2$, partial derivatives of $\partial\Delta_i/\partial\Delta_j, 1\leq j\leq n$ are the followings:

$$\frac{\partial\Delta_i}{\partial\Delta_j}=\begin{cases} 1 & \text{if } j=i+1 \\ 0 & \text{otherwise} \end{cases}$$

For Δ_{n-1}, we find its partial derivatives as follows:

$$\begin{aligned}
\frac{\partial \Delta_{n-1}}{\partial \Delta_1} =& KT\left(\frac{1}{\Delta_1^2}+\frac{1}{(\Delta_1+\Delta_2)^2}+\cdots+\frac{1}{(\Delta_1+\Delta_2+\cdots+\Delta_{\frac{n}{2}-1})^2}\right)\\
=& KT\left(\frac{n^2}{T^2}\right)\left(\frac{1}{1^2}+\frac{1}{2^2}+\cdots+\frac{1}{(\frac{n}{2}-1)^2}\right)=\frac{Kn^2}{T}\sum_{i=1}^{\frac{n}{2}-1}\frac{1}{i^2}\\
\frac{\partial \Delta_{n-1}}{\partial \Delta_2} =& KT\left(\frac{1}{(\Delta_1+\Delta_2)^2}+\cdots+\frac{1}{(\Delta_1+\Delta_2+\cdots+\Delta_{\frac{n}{2}-1})^2}\right)\\
=& KT\left(\frac{n^2}{T^2}\right)\left(\frac{1}{2^2}+\cdots+\frac{1}{(\frac{n}{2}-1)^2}\right)=\frac{Kn^2}{T}\sum_{i=2}^{\frac{n}{2}-1}\frac{1}{i^2}\\
&\vdots\\
\frac{\partial \Delta_{n-1}}{\partial \Delta_{\frac{n}{2}-1}} =& KT\left(\frac{1}{(\Delta_1+\Delta_2+\cdots+\Delta_{\frac{n}{2}-1})^2}\right)\\
=& KT\left(\frac{n^2}{T^2}\right)\left(\frac{1}{(\frac{n}{2}-1)^2}\right)=\frac{Kn^2}{T}\sum_{i=\frac{n}{2}-1}^{\frac{n}{2}-1}\frac{1}{i^2}\\
\frac{\partial \Delta_{n-1}}{\partial \Delta_{\frac{n}{2}}} =& 0\\
\frac{\partial \Delta_{n-1}}{\partial \Delta_{\frac{n}{2}+1}} =& 0\\
\frac{\partial \Delta_{n-1}}{\partial \Delta_{\frac{n}{2}+2}} =& KT\left(-\frac{1}{(\Delta_n+\Delta_{n-1}+\cdots+\Delta_{\frac{n}{2}+2})^2}\right)\\
=& -KT\left(\frac{n^2}{T^2}\right)\left(\frac{1}{(\frac{n}{2}-1)^2}\right)=-\frac{Kn^2}{T}\sum_{i=\frac{n}{2}-1}^{\frac{n}{2}-1}\frac{1}{i^2}\\
&\vdots\\
\frac{\partial \Delta_{n-1}}{\partial \Delta_{n-1}} =& KT\left(-\frac{1}{(\Delta_n+\Delta_{n-1})^2}-\cdots-\frac{1}{(\Delta_n+\Delta_{n-1}+\cdots+\Delta_{\frac{n}{2}+2})^2}\right)\\
=& -KT\left(\frac{n^2}{T^2}\right)\left(\frac{1}{2^2}+\cdots+\frac{1}{(\frac{n}{2}-1)^2}\right)=-\frac{Kn^2}{T}\sum_{i=2}^{\frac{n}{2}-1}\frac{1}{i^2}\\
\frac{\partial \Delta_{n-1}}{\partial \Delta_n} =& 1+KT\left(-\frac{1}{\Delta_n^2}-\frac{1}{(\Delta_n+\Delta_{n-1})^2}-\cdots-\frac{1}{(\Delta_n+\Delta_{n-1}+\cdots+\Delta_{\frac{n}{2}+2})^2}\right)\\
=& 1-KT\left(\frac{n^2}{T^2}\right)\left(\frac{1}{1^2}+\frac{1}{2^2}+\cdots+\frac{1}{(\frac{n}{2}-1)^2}\right)=1-\frac{Kn^2}{T}\sum_{i=1}^{\frac{n}{2}-1}\frac{1}{i^2}
\end{aligned}$$

For Δ_n, we find its partial derivatives which is similar to Δ_{n-1} as follows.

$$
\begin{aligned}
\frac{\partial \Delta_n}{\partial \Delta_1} =& 1 - \frac{Kn^2}{T} \sum_{i=1}^{\frac{n}{2}-1} \frac{1}{i^2} \\
\frac{\partial \Delta_n}{\partial \Delta_2} =& - \frac{Kn^2}{T} \sum_{i=2}^{\frac{n}{2}-1} \frac{1}{i^2} \\
& \vdots \\
\frac{\partial \Delta_n}{\partial \Delta_{\frac{n}{2}-1}} =& - \frac{Kn^2}{T} \sum_{i=\frac{n}{2}-1}^{\frac{n}{2}-1} \frac{1}{i^2} \\
\frac{\partial \Delta_n}{\partial \Delta_{\frac{n}{2}}} =& 0 \\
\frac{\partial \Delta_n}{\partial \Delta_{\frac{n}{2}+1}} =& 0 \\
\frac{\partial \Delta_n}{\partial \Delta_{\frac{n}{2}+2}} =& \frac{Kn^2}{T} \sum_{i=\frac{n}{2}-1}^{\frac{n}{2}-1} \frac{1}{i^2} \\
& \vdots \\
\frac{\partial \Delta_n}{\partial \Delta_{n-1}} =& \frac{Kn^2}{T} \sum_{i=2}^{\frac{n}{2}-1} \frac{1}{i^2} \\
\frac{\partial \Delta_n}{\partial \Delta_n} =& \frac{Kn^2}{T} \sum_{i=1}^{\frac{n}{2}-1} \frac{1}{i^2}
\end{aligned}
$$

Let $\sum\limits_{s}$ stands for $\sum\limits_{i=s}^{\frac{n}{2}-1} \frac{1}{i^2}$, where $s \in [1, \frac{n}{2} - 1]$ and let $A = Kn^2/T$. The Jacobian matrix of the system, when n is even, is

$$J = \begin{pmatrix} 0 & 1 & \cdots & 0 & 0 & 0 & 0 & \cdots & 0 & 0 \\ 0 & 0 & \ddots & 0 & 0 & 0 & 0 & \cdots & 0 & 0 \\ \vdots & \vdots & \ddots & \ddots & \vdots & \vdots & \vdots & \ddots & \vdots & \vdots \\ 0 & 0 & \cdots & 0 & 1 & 0 & 0 & \cdots & 0 & 0 \\ 0 & 0 & \cdots & 0 & 0 & 1 & 0 & \cdots & 0 & 0 \\ 0 & 0 & \cdots & 0 & 0 & 0 & 1 & \cdots & 0 & 0 \\ \vdots & \vdots & \ddots & \vdots & \vdots & \vdots & \vdots & \ddots & \vdots & \vdots \\ 0 & 0 & \cdots & 0 & 0 & 0 & 0 & \cdots & 1 & 0 \\ A\sum\limits_{1} & A\sum\limits_{2} & \cdots & A\sum\limits_{\frac{n}{2}-1} & 0 & 0 & -A\sum\limits_{\frac{n}{2}-1} & \cdots & -A\sum\limits_{2} & 1-A\sum\limits_{1} \\ 1-A\sum\limits_{1} & -A\sum\limits_{2} & \cdots & -A\sum\limits_{\frac{n}{2}-1} & 0 & 0 & A\sum\limits_{\frac{n}{2}-1} & \cdots & A\sum\limits_{2} & A\sum\limits_{1} \end{pmatrix}. \tag{4.5}$$

2) n is odd:

Similarly, when n is odd, we can find its Jacobian with the same procedure as when n is even. We obtain the similar Jacobian matrix as follows:

$$J = \begin{pmatrix} 0 & 1 & \cdots & 0 & 0 & 0 & \cdots & 0 & 0 \\ 0 & 0 & \ddots & 0 & 0 & 0 & \cdots & 0 & 0 \\ \vdots & \vdots & \ddots & \ddots & \vdots & \vdots & \ddots & \vdots & \vdots \\ 0 & 0 & \cdots & 0 & 1 & 0 & \cdots & 0 & 0 \\ 0 & 0 & \cdots & 0 & 0 & 1 & \cdots & 0 & 0 \\ \vdots & \vdots & \ddots & \vdots & \vdots & \vdots & \ddots & \vdots & \vdots \\ 0 & 0 & \cdots & 0 & 0 & 0 & \cdots & 1 & 0 \\ A\sum\limits_{1} & A\sum\limits_{2} & \cdots & A\sum\limits_{\frac{n}{2}-1} & 0 & -A\sum\limits_{\frac{n}{2}-1} & \cdots & -A\sum\limits_{2} & 1-A\sum\limits_{1} \\ 1-A\sum\limits_{1} & -A\sum\limits_{2} & \cdots & -A\sum\limits_{\frac{n}{2}-1} & 0 & A\sum\limits_{\frac{n}{2}-1} & \cdots & A\sum\limits_{2} & A\sum\limits_{1} \end{pmatrix}. \tag{4.6}$$

4.2.2 Finding Eigenvalues

After finding the Jacobian of the linear approximation at the equilibrium, we find the eigenvalues by solving the equation $|J-\lambda I|=0$. If all eigenvalues lay on a unit circle, the system is stable at the equilibrium. Therefore, we begin by finding the determinant of the matrix $J-\lambda I$. We use row operations to transform the determinant of $|J-\lambda I|$ into the determinant of a triangular matrix. Then, the determinant of the triangular matrix is the multiplication of diagonal entries.

The following procedure is to transform the determinant of $|J-\lambda I|$ into the determinant of triangular matrix when n is even:

$$
|J-\lambda I| = \begin{vmatrix}
-\lambda & 1 & \cdots & 0 & 0 & 0 & 0 & \cdots & 0 & 0 \\
0 & -\lambda & \ddots & 0 & 0 & 0 & 0 & \cdots & 0 & 0 \\
\vdots & \vdots & \ddots & \ddots & \vdots & \vdots & \vdots & \ddots & \vdots & \vdots \\
0 & 0 & \cdots & -\lambda & 1 & 0 & 0 & \cdots & 0 & 0 \\
0 & 0 & \cdots & 0 & -\lambda & 1 & 0 & \cdots & 0 & 0 \\
0 & 0 & \cdots & 0 & 0 & -\lambda & 1 & \cdots & 0 & 0 \\
\vdots & \vdots & \ddots & \vdots & \vdots & \vdots & \ddots & \ddots & \vdots & \vdots \\
0 & 0 & \cdots & 0 & 0 & 0 & 0 & \cdots & 1 & 0 \\
A\sum\limits_{1} & A\sum\limits_{2} & \cdots & A\sum\limits_{\frac{n}{2}-1} & 0 & 0 & -A\sum\limits_{\frac{n}{2}-1} & \cdots & -A\sum\limits_{2}-\lambda & 1-A\sum\limits_{1} \\
1-A\sum\limits_{1} & -A\sum\limits_{2} & \cdots & -A\sum\limits_{\frac{n}{2}-1} & 0 & 0 & A\sum\limits_{\frac{n}{2}-1} & \cdots & A\sum\limits_{2} & A\sum\limits_{1}-\lambda
\end{vmatrix} \tag{4.7}
$$

$$
= \begin{vmatrix}
-\lambda & 1 & \cdots & 0 & 0 & 0 & 0 & \cdots & 0 & 0 \\
0 & -\lambda & \ddots & 0 & 0 & 0 & 0 & \cdots & 0 & 0 \\
\vdots & \vdots & \ddots & \ddots & \vdots & \vdots & \vdots & \ddots & \vdots & \vdots \\
0 & 0 & \cdots & -\lambda & 1 & 0 & 0 & \cdots & 0 & 0 \\
0 & 0 & \cdots & 0 & -\lambda & 1 & 0 & \cdots & 0 & 0 \\
0 & 0 & \cdots & 0 & 0 & -\lambda & 1 & \cdots & 0 & 0 \\
\vdots & \vdots & \ddots & \vdots & \vdots & \vdots & \ddots & \ddots & \vdots & \vdots \\
0 & 0 & \cdots & 0 & 0 & 0 & 0 & \cdots & 1 & 0 \\
1 & 0 & \cdots & 0 & 0 & 0 & 0 & \cdots & -\lambda & 1-\lambda \\
1-A\sum\limits_{1} & -A\sum\limits_{2} & \cdots & -A\sum\limits_{\frac{n}{2}-1} & 0 & 0 & A\sum\limits_{\frac{n}{2}-1} & \cdots & A\sum\limits_{2} & A\sum\limits_{1}-\lambda
\end{vmatrix} \tag{4.8}
$$

$$
= \begin{vmatrix}
-\lambda+\frac{1}{\lambda^{n-2}} & 0 & \cdots & 0 & 0 & 0 & 0 & \cdots & 0 & \frac{1-\lambda}{\lambda^{n-2}} \\
\frac{1}{\lambda^{n-3}} & -\lambda & \cdots & 0 & 0 & 0 & 0 & \cdots & 0 & \frac{1-\lambda}{\lambda^{n-3}} \\
\frac{1}{\lambda^{n-4}} & 0 & \ddots & 0 & 0 & 0 & 0 & \cdots & 0 & \frac{1-\lambda}{\lambda^{n-4}} \\
\vdots & \vdots & \ddots & \ddots & \vdots & \vdots & \vdots & \ddots & \vdots & \vdots \\
\frac{1}{\lambda^{\frac{n}{2}-2}} & 0 & \cdots & 0 & -\lambda & 0 & 0 & \cdots & 0 & \frac{1-\lambda}{\lambda^{\frac{n}{2}-2}} \\
\frac{1}{\lambda^{\frac{n}{2}-3}} & 0 & \cdots & 0 & 0 & -\lambda & 0 & \cdots & 0 & \frac{1-\lambda}{\lambda^{\frac{n}{2}-3}} \\
\vdots & \vdots & \ddots & \vdots & \vdots & \vdots & \ddots & \ddots & \vdots & \vdots \\
\frac{1}{\lambda} & 0 & \cdots & 0 & 0 & 0 & 0 & \ddots & 0 & \frac{1-\lambda}{\lambda} \\
1 & 0 & \cdots & 0 & 0 & 0 & 0 & \cdots & -\lambda & 1-\lambda \\
1-A\sum\limits_{1} & -A\sum\limits_{2} & \cdots & -A\sum\limits_{\frac{n}{2}-1} & 0 & 0 & A\sum\limits_{\frac{n}{2}-1} & \cdots & A\sum\limits_{2} & A\sum\limits_{1}-\lambda
\end{vmatrix} \tag{4.9}
$$

$$
= \begin{vmatrix}
-\lambda+\frac{1}{\lambda^{n-2}} & 0 & \cdots & 0 & 0 & 0 & 0 & \cdots & 0 & \frac{1-\lambda}{\lambda^{n-2}} \\
\lambda^2 & -\lambda & \cdots & 0 & 0 & 0 & 0 & \cdots & 0 & 0 \\
\lambda^3 & 0 & \ddots & 0 & 0 & 0 & 0 & \cdots & 0 & 0 \\
\vdots & \vdots & \ddots & \ddots & \vdots & \vdots & \vdots & \ddots & \vdots & \vdots \\
\lambda^{\frac{n}{2}} & 0 & \cdots & 0 & -\lambda & 0 & 0 & \cdots & 0 & 0 \\
\lambda^{\frac{n}{2}+1} & 0 & \cdots & 0 & 0 & -\lambda & 0 & \cdots & 0 & 0 \\
\vdots & \vdots & \ddots & \vdots & \vdots & \vdots & \ddots & \ddots & \vdots & \vdots \\
\lambda^{n-2} & 0 & \cdots & 0 & 0 & 0 & 0 & \ddots & 0 & 0 \\
\lambda^{n-1} & 0 & \cdots & 0 & 0 & 0 & 0 & \cdots & -\lambda & 0 \\
1-A\sum\limits_{1} & -A\sum\limits_{2} & \cdots & -A\sum\limits_{\frac{n}{2}-1} & 0 & 0 & A\sum\limits_{\frac{n}{2}-1} & \cdots & A\sum\limits_{2} & A\sum\limits_{1}-\lambda
\end{vmatrix} \tag{4.10}
$$

$$
= \begin{vmatrix}
-\lambda+\frac{1}{\lambda^{n-2}} & 0 & \cdots & 0 & 0 & 0 & 0 & \cdots & 0 & \frac{1-\lambda}{\lambda^{n-2}} \\
\lambda^2 & -\lambda & \cdots & 0 & 0 & 0 & 0 & \cdots & 0 & 0 \\
\lambda^3 & 0 & \ddots & 0 & 0 & 0 & 0 & \cdots & 0 & 0 \\
\vdots & \vdots & \ddots & \ddots & \vdots & \vdots & \vdots & \ddots & \vdots & \vdots \\
\lambda^{\frac{n}{2}} & 0 & \cdots & 0 & -\lambda & 0 & 0 & \cdots & 0 & 0 \\
\lambda^{\frac{n}{2}+1} & 0 & \cdots & 0 & 0 & -\lambda & 0 & \cdots & 0 & 0 \\
\vdots & \vdots & \ddots & \vdots & \vdots & \vdots & \ddots & \ddots & \vdots & \vdots \\
\lambda^{n-2} & 0 & \cdots & 0 & 0 & 0 & 0 & \ddots & 0 & 0 \\
\lambda^{n-1} & 0 & \cdots & 0 & 0 & 0 & 0 & \cdots & -\lambda & 0 \\
B & 0 & \cdots & 0 & 0 & 0 & 0 & \cdots & 0 & A\sum\limits_{1}-\lambda
\end{vmatrix} \tag{4.11}
$$

$$= \begin{vmatrix} -\lambda + \frac{1}{\lambda^{n-2}} + \frac{B}{A\sum\limits_{1} -\lambda}\left(\frac{\lambda-1}{\lambda^{n-2}}\right) & 0 & \cdots & 0 & 0 & 0 & 0 & \cdots & 0 & 0 \\ \lambda^2 & -\lambda & \cdots & 0 & 0 & 0 & 0 & \cdots & 0 & 0 \\ \lambda^3 & 0 & \ddots & 0 & 0 & 0 & 0 & \cdots & 0 & 0 \\ \vdots & \vdots & \ddots & \ddots & \vdots & \vdots & \vdots & \ddots & \vdots & \vdots \\ \lambda^{\frac{n}{2}} & 0 & \cdots & 0 & -\lambda & 0 & 0 & \cdots & 0 & 0 \\ \lambda^{\frac{n}{2}+1} & 0 & \cdots & 0 & 0 & -\lambda & 0 & \cdots & 0 & 0 \\ \vdots & \vdots & \ddots & \vdots & \vdots & \vdots & \ddots & \ddots & \vdots & \vdots \\ \lambda^{n-2} & 0 & \cdots & 0 & 0 & 0 & 0 & \ddots & 0 & 0 \\ \lambda^{n-1} & 0 & \cdots & 0 & 0 & 0 & 0 & \cdots & -\lambda & 0 \\ B & 0 & \cdots & 0 & 0 & 0 & 0 & \cdots & 0 & A\sum\limits_{1} -\lambda \end{vmatrix} \tag{4.12}$$

where

$$B = 1 - A\sum_{1} - \lambda A\sum_{2} - \lambda^2 A\sum_{3} - \cdots - \lambda^{\frac{n}{2}-2} A\sum_{\frac{n}{2}-1} + \lambda^{\frac{n}{2}+1} A\sum_{\frac{n}{2}-1} + \cdots + \lambda^{n-2} A\sum_{2}. \tag{4.13}$$

Similarly, we use the same procedure to find the determinant of $|J - \lambda I|$ when n is odd. The result matrix is the same as above except that

$$B = 1 - A\sum_{1} - \lambda A\sum_{2} - \lambda^2 A\sum_{3} - \cdots - \lambda^{\lceil \frac{n}{2} \rceil - 1} A\sum_{\frac{n}{2}-1} + \lambda^{\lceil \frac{n}{2} \rceil + 1} A\sum_{\frac{n}{2}-1} + \cdots + \lambda^{n-2} A\sum_{2}. \tag{4.14}$$

We note that the difference between Equation 4.13 and 4.14 is the exponents of λ at two middle terms.

The determinant of a triangular matrix is the product of diagonal terms. That is

$$|J-\lambda I| = \left(-\lambda + \frac{1}{\lambda^{n-2}} + \frac{B}{A\sum\limits_{1} -\lambda}\left(\frac{\lambda-1}{\lambda^{n-2}}\right)\right)(-\lambda)(-\lambda)\cdots(-\lambda)(-\lambda)\left(A\sum_{1} -\lambda\right) = 0.$$

For terms $-\lambda$, it is obvious that we have repeated eigenvalues λ that are equal to 0 and lay on a unit circle.

For the last term $A\sum_{1} -\lambda$, the value of λ depends on n as follows:

$$\begin{aligned} A\sum_{1} -\lambda &= 0 \\ \lambda &= A\sum_{1} \\ \lambda &= 0.038597n^{0.126}\sum_{i=1}^{\frac{n}{2}-1}\frac{1}{i^2} \geq 0. \end{aligned}$$

In this case, $\lambda \geq 0$, however, we have to find the least upper limit of n that leads to $\lambda \leq 1$. From the Reimann zeta function $\zeta(2) = \sum_{i=1}^{\infty}\frac{1}{i^2} = \pi^2/6 \approx 1.645$, so that $\sum_{i=1}^{\frac{n}{2}-1}\frac{1}{i^2} \leqslant 1.645$. We substitute $\sum_{i=1}^{\frac{n}{2}-1}\frac{1}{i^2}$ with 1.645 to find the least upper limit of n:

$$\begin{aligned} \lambda = 0.038597n^{0.126}\sum_{i=1}^{\frac{n}{2}-1}\frac{1}{i^2} &\leq 1 \\ 0.038597n^{0.126}(1.645) &\leq 1 \\ n &\leq 3.178 \times 10^9. \end{aligned} \tag{4.15}$$

Therefore, if the number of nodes n is less than 3.178×10^9 nodes, the eigenvalue λ lies between 0 and 1 in this case.

For the first term, $-\lambda + \frac{1}{\lambda^{n-2}} + \frac{B}{A\sum_{1} -\lambda}\left(\frac{\lambda-1}{\lambda^{n-2}}\right)$, the λ must not be 0. If n is even, we derive the polynomial of λ as follows:

$$\begin{aligned} 0 =& -\lambda + \frac{1}{\lambda^{n-2}} + \frac{B}{A\sum_{1} -\lambda}\left(\frac{\lambda-1}{\lambda^{n-2}}\right) \\ 0 =& -\lambda^{n-1} + 1 + \frac{B}{A\sum_{1} -\lambda}(\lambda-1) \\ 0 =& \lambda^n - \lambda^{n-1}A\sum_{1} -\lambda + A\sum_{1} + B(\lambda-1) \\ 0 =& \lambda^n - \lambda^{n-1}A\sum_{1} -\lambda + A\sum_{1} \\ &+ \lambda - \lambda A\sum_{1} -\lambda^2 A\sum_{2} -\lambda^3 A\sum_{3} - \cdots - \lambda^{\frac{n}{2}-1}A\sum_{\frac{n}{2}-1} \\ &+ \lambda^{\frac{n}{2}+2}A\sum_{\frac{n}{2}-1} + \cdots + \lambda^{n-2}A\sum_{3} + \lambda^{n-1}A\sum_{2} \end{aligned}$$

$$
\begin{aligned}
&-1+A\sum_{1}+\lambda A\sum_{2}+\lambda^2 A\sum_{3}+\cdots+\lambda^{\frac{n}{2}-2}A\sum_{\frac{n}{2}-1}\\
&-\lambda^{\frac{n}{2}+1}A\sum_{\frac{n}{2}-1}-\cdots-\lambda^{n-2}A\sum_{2}\\
0=&\lambda^n-A\lambda^{n-1}\left(\sum_{1}-\sum_{2}\right)-A\lambda^{n-2}\left(\sum_{2}-\sum_{3}\right)-\cdots-A\lambda^{\frac{n}{2}+2}\left(\sum_{\frac{n}{2}-2}-\sum_{\frac{n}{2}-1}\right)\\
&-A\lambda^{\frac{n}{2}+1}\sum_{\frac{n}{2}-1}-A\lambda^{\frac{n}{2}-1}\sum_{\frac{n}{2}-1}-A\lambda^{\frac{n}{2}-2}\left(\sum_{\frac{n}{2}-2}-\sum_{\frac{n}{2}-1}\right)-\cdots-A\lambda^2\left(\sum_{2}-\sum_{3}\right)\\
&-A\lambda\left(\sum_{1}-\sum_{2}\right)+2A\sum_{1}-1\\
0=&\lambda^n-\frac{A\lambda^{n-1}}{1^2}-\frac{A\lambda^{n-2}}{2^2}-\cdots-\frac{A\lambda^{\frac{n}{2}+2}}{(\frac{n}{2}-2)^2}-\frac{A\lambda^{\frac{n}{2}+1}}{(\frac{n}{2}-1)^2}\\
&-\frac{A\lambda^{\frac{n}{2}-1}}{(\frac{n}{2}-1)^2}-\frac{A\lambda^{\frac{n}{2}-2}}{(\frac{n}{2}-2)^2}-\cdots-\frac{A\lambda^2}{2^2}-\frac{A\lambda}{1^2}+2A\sum_{1}-1
\end{aligned}
$$

To get the eigenvalues, we have to solve the polynomial

$$f_{even}(\lambda)=\lambda^n-\frac{A\lambda^{n-1}}{1^2}-\frac{A\lambda^{n-2}}{2^2}-\cdots-\frac{A\lambda^{\frac{n}{2}+1}}{(\frac{n}{2}-1)^2}-\frac{A\lambda^{\frac{n}{2}-1}}{(\frac{n}{2}-1)^2}-\cdots-\frac{A\lambda^2}{2^2}-\frac{A\lambda}{1^2}+2A\sum_{1}-1=0. \tag{4.16}$$

Similarly, if n is odd, we have to solve the polynomial

$$f_{odd}(\lambda)=\lambda^n-\frac{A\lambda^{n-1}}{1^2}-\frac{A\lambda^{n-2}}{2^2}-\cdots-\frac{A\lambda^{\lceil\frac{n}{2}\rceil}}{(\frac{n}{2}-1)^2}-\frac{A\lambda^{\lceil\frac{n}{2}\rceil-1}}{(\frac{n}{2}-1)^2}-\cdots-\frac{A\lambda^2}{2^2}-\frac{A\lambda}{1^2}+2A\sum_{1}-1=0. \tag{4.17}$$

However, according to the Abel's Impossibility theorem (or Abel-Ruffini theorem), we cannot find a general algebraic solution to polynomial equations of degree five or higher (Faucette (1996)). Therefore, instead of finding the exact values, we find the upper and lower bound of the eigenvalues to ensure that they lay on a unit circle.

4.2.3 The Bound of Eigenvalues

To find the bound of polynomial roots (*i.e.* our eigenvalues), we follow the following theorem of Hirst and Macey (Hirst and Macey (1997)).

Theorem 4.5 (Hirst and Macey Bound) *Given $f : \mathbb{C} \to \mathbb{C}$ defined by $f(z) = z^n + a_{n-1}z^{n-1} + \ldots + a_1 z + a_0$, where $a_0, a_1, \ldots, a_n \in \mathcal{C}$, and n a positive integer. If z is a zero of f, then*

$$|z| \leq \max\left\{1, \sum_{i=0}^{n-1} |a_i|\right\}.$$

Therefore, to bound all eigenvalues within a unit circle, $\sum_{i=0}^{n-1} |a_i|$ must be less than or equal 1. From both Equation 4.16 and 4.17,

$$\begin{aligned}
\sum_{i=0}^{n-1} |a_i| = \left|2A\sum_{i=1}^{\frac{n}{2}-1}\frac{1}{i^2} - 1\right| + 2\left(\frac{A}{1^2} + \frac{A}{2^2} + \cdots + \frac{A}{(\frac{n}{2}-1)^2}\right) &\leq 1 \\
\left|2A\sum_{i=1}^{\frac{n}{2}-1}\frac{1}{i^2} - 1\right| + 2A\sum_{i=1}^{\frac{n}{2}-1}\frac{1}{i^2} &\leq 1 \\
\left|2A\sum_{i=1}^{\frac{n}{2}-1}\frac{1}{i^2} - 1\right| &\leq 1 - 2A\sum_{i=1}^{\frac{n}{2}-1}\frac{1}{i^2} \\
-1 + 2A\sum_{i=1}^{\frac{n}{2}-1}\frac{1}{i^2} \leq 2A\sum_{i=1}^{\frac{n}{2}-1}\frac{1}{i^2} - 1 &\leq 1 - 2A\sum_{i=1}^{\frac{n}{2}-1}\frac{1}{i^2}, \qquad (4.18)
\end{aligned}$$

where $A = Kn^2/T = 38.597n^{-1.874}(T/1000)(n^2/T) = 0.038597n^{0.126}$.

For the first case, $-1 + 2A\sum_{i=1}^{\frac{n}{2}-1}\frac{1}{i^2} \leq 2A\sum_{i=1}^{\frac{n}{2}-1}\frac{1}{i^2} - 1$ is always true regardless of the number of nodes n. Therefore, we consider the second case:

$$\begin{aligned}
2A\sum_{i=1}^{\frac{n}{2}-1}\frac{1}{i^2} - 1 &\leq 1 - 2A\sum_{i=1}^{\frac{n}{2}-1}\frac{1}{i^2} \\
4A\sum_{i=1}^{\frac{n}{2}-1}\frac{1}{i^2} &\leq 2 \\
0.038597n^{0.126}\sum_{i=1}^{\frac{n}{2}-1}\frac{1}{i^2} &\leq \frac{1}{2}. \qquad (4.19)
\end{aligned}$$

When n is large, $\sum_{i=1}^{\frac{n}{2}-1} \frac{1}{i^2}$ is approximately equal to the Reimann zeta function $\zeta(2) = \sum_{i=1}^{\infty} \frac{1}{i^2} = \pi^2/6 \approx 1.645$. Therefore, we get the following:

$$\begin{aligned} 0.038597n^{0.126}(1.645) &\leq \frac{1}{2} \\ n^{0.126} &\leq 7.87499981 \\ n &\leq 1.29 \times 10^7. \end{aligned} \tag{4.20}$$

Thus, if the number of nodes n is less than 1.29×10^7 nodes, every eigenvalue lies in a unit circle. Therefore, the non-linear dynamic system of the proposed desynchronization algorithm is locally stable at the equilibrium. In other words, if there is a small perturbation around the equilibrium, the system is able to converge back to the equilibrium.

4.3 Summary

In this chapter, we prove that the force function used in DWARF for phase adjustment is convex. Due to convexity, there is only global minima and no local minima. Therefore, one of the reasons that the system converges (nodes are nicely spread) is that DWARF attempts to reduce the value of the objective function (*i.e.*, the overall force in the system) overtime and eventually reach a value near the global minima.

However, in practice, the system does not always converge. To converge, the system must meet two criteria. First, the value of the step size K must be proper (see Section 3.3). Second, the number of nodes within a time period must not be too high. Otherwise, the system may be over-saturated.

Then, we analyse the stability by transforming the system into a dynamic system. However, the stability analysis of standard dynamic systems does not suffice because the force function is non-linear and the transformation matrix to find the eigenvalues cannot be formed. Therefore, we locally approximate the system at the equilibrium and analyze the stability. The result is that the system is locally stable at the equilibrium under small perturbation.

CHAPTER V

MULTI-HOP PHYSICOMIMETICS DESYNCHRONIZATION ALGORITHM

5.1 Introduction

In Chapter 3, we present DWARF, a physicomimetics desynchronization algorithm based on the artificial force field concept for wireless sensor networks. We have evaluated and compared DWARF with other algorithms in a single-hop topology. The results are promising.

In this chapter, we extend the artificial force field concept to multi-hop networks. We begin by applying DWARF directly to a simple multi-hop topology and indicate how the algorithm fails on such a topology in Section 5.2. Then, we propose two simple but elegant resolutions to extend DWARF for multi-hop networks in Section 5.3. Section 5.4 explains the algorithm that applies such resolutions. Then, in Section 5.5, we evaluate and compare our algorithm to other algorithms. We also propose the optimization to reduce communication overhead and present the robustness to message loss of the algorithm in this section. Finally, Section 5.6 summarizes the chapter.

5.2 First Multi-hop Experiment and Hidden Terminal Problem

To see how DWARF works on a multi-hop network, we set a simple 3-node chain topology as illustrated in Figure 5.1. In this topology, node 1 can receive firing messages from node 2 but cannot receive from node 3, node 2 can receive firing messages from both node 1 and 3, and node 3 can receive firing messages from node 2 but cannot receive from node 1.

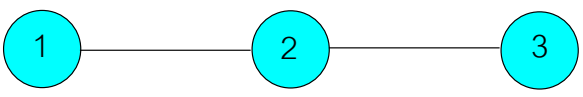

Figure 5.1: A simple multi-hop network.

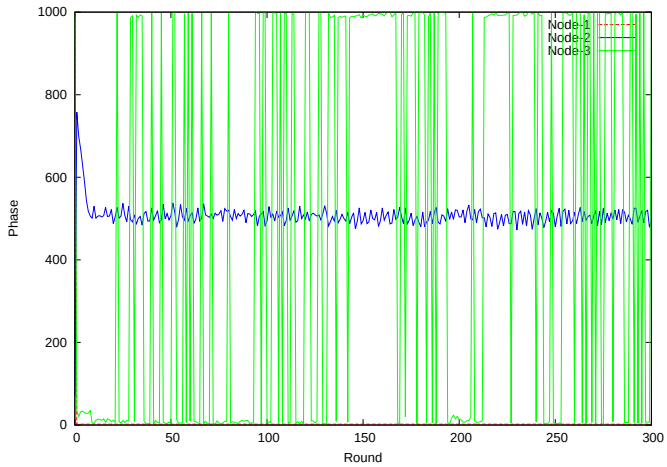

Figure 5.2: Message collision on a 3-node multi-hop chain network. The period T is 1000 milliseconds. Node 1 is at phase 0 whereas node 3 is approximately at the same phase as node 1.

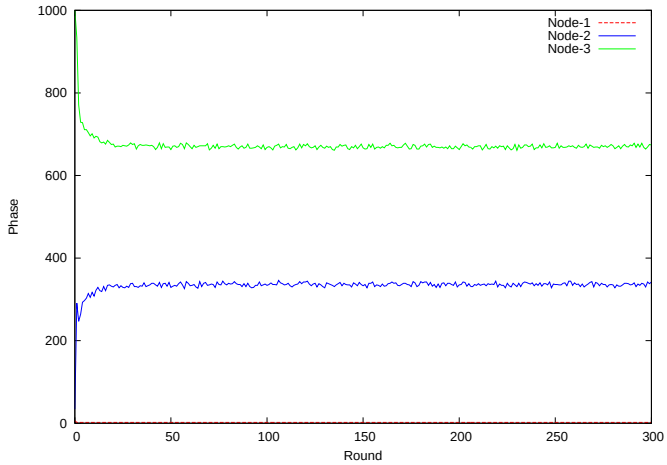

Figure 5.3: The perfect desynchrony state of a 3-node multi-hop chain network, The period T is 1000 milliseconds. Node 1 is at phase 0 whereas others are separated by T/3 milliseconds.

We have simulated DWARF by setting the period to 1000 milliseconds. Nodes wake up randomly. The simulation result is shown in Figure 5.2. Node 2's and node 3's phases are plotted relatively to the node 1's phase (*i.e.*, the node 1's phase is relatively plotted to itself at 0). The noisy vertical line is the wrapping-around phase of node 3. The result shows that node 1 and node 3 fire messages approximately at the same phase. This causes the message collision at node 2. However, the expected result (*i.e.* perfect desynchrony state) should be that three nodes are separated equivalently because all nodes will interfere each other if they fire messages at the same phase. The expected result is shown in Figure 5.3 where each node is equivalently separated from each other

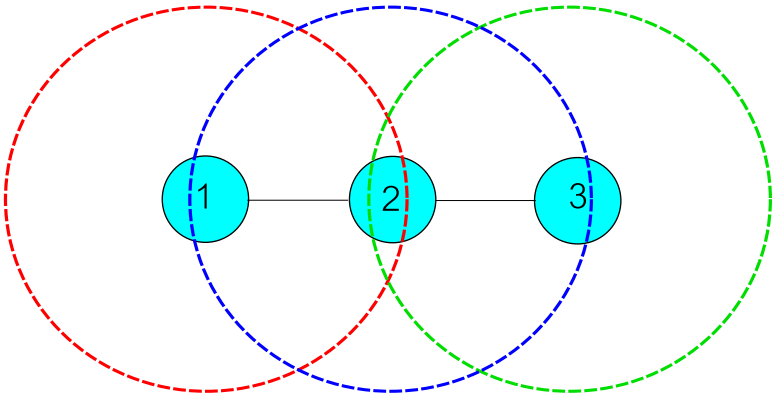

Figure 5.4: The hidden terminal problem.

approximately by 1000/3 milliseconds.

The problematic result is caused by the hidden terminal problem as demonstrated in Figure 5.4; node 1 and node 3 are hidden to each other in this multi-hop topology. While node 3 is firing a message, node 1 senses a wireless channel and does not detect any signal from node 3 because the signal from node 3 is not strong enough within the signal sensing range of node 1 and vice versa. Therefore, in DWARF, node 1 and node 3 notice only that there are two nodes, which are itself and node 2, in their perceived networks. Therefore, node 1 and node 3 simultaneously attempt to adjust their phases to the opposite side of node 2 in their time circles which are the same phase. As a result, their firing messages collide at node 2.

The hidden terminal problem does not only affect the performance of DWARF but also affect that of DESYNC. This is due to the fact that, in DESYNC, a node adjusts its phase based on firing messages from its perceived phase neighbors. In Degesys and Nagpal (2008) and Mühlberger and Kolla (2009), EXTENDED-DESYNC, which is the extension of DESYNC, is proposed to solve the hidden terminal problem based on a relative time relaying mechanism. Based on the similar idea, we extend DWARF to support multi-hop topologies. However, only relative time relaying mechanism does not lead DWARF to an optimal solution in some cases. Therefore, this dissertation also proposes a *force absorption* mechanism for extending DWARF to support multi-hop networks.

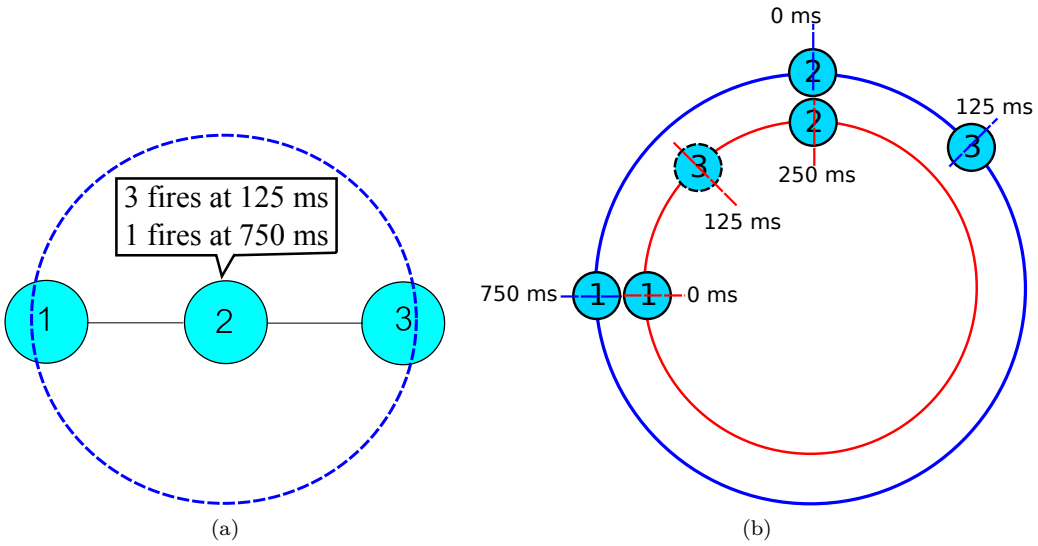

Figure 5.5: A node includes its one-hop neighbors' firing times into a firing message. (a) Node 2 fires a message containing node 1's and node 2's firing timestamps that it perceives. (b) Node 1 misunderstands the time phase of node 3 because local time of node 1 and local time of node 2 are different.

5.3 DWARF with Multi-hop Extension (M-DWARF)

5.3.1 Relative Time Relaying

The first idea to solve the hidden terminal problem is straightforward. If a node does not know the firing times of its second-hop neighbors, its one-hop neighbors relay such information. Therefore, instead of firing only to notify its firing time, each node includes their one-hop neighbors' firing times into a firing message.

However, due to our assumption that nodes' clocks are not synchronized, relying on second-hop neighbors' firing timestamps from its one-hop neighbors could lead to wrong phase adjustment. This problematic scenario is demonstrated in Figure 5.5. Figure 5.5a illustrates the firing message of node 2 that contains timestamps of its one-hop neighbors. Figure 5.5b shows the problem. The inner circle represents the local time of node 1 and the outer circle represents the local time of node 2. The figure indicates that the local reference times (at 0 millisecond) of node 1 and node 2 are different. Therefore, if node 1 uses the node 3's firing time relayed by node 2, which is 125 milliseconds, node 1 will misunderstand the exact time phase of node 3. The misunderstood phase of node 3 is depicted as a dash circle.

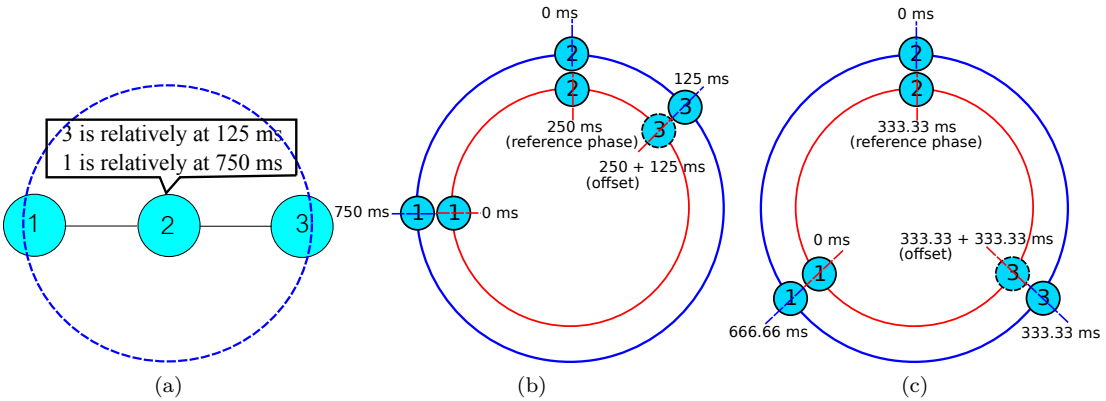

Figure 5.6: EXT-DWARF: A node includes its one-hop neighbors' relative phases into a firing message. (a) Node 2 fires a message containing node 1's and node 2's relative phases. (b) Node 1 marks the node 2's phase as a reference phase and uses it as an offset for calculating the node 3's phase. (c) Eventually, nodes are in the perfect desynchrony state.

This problem can be simply solved by using relative phases instead of actual local times. Each node fires a message that includes relative phases of its one-hop neighbors. A receiving node marks the firing phase of the firing node as a reference phase. Then, the receiving node perceives its second-hop neighbors' phases as relative phases offset by the reference phase. Figure 5.6 shows how extended DWARF desynchronizes a 3-node multi-hop chain network.

5.3.2 Force Absorption

As we mentioned earlier, DWARF with the relative time relaying mechanism does not solve some cases. These cases are when there are at least two second-hop neighbors that can share the same phase without interference. For example, in a 4-node chain network illustrated in Figure 5.7a, node 2 and node 3 are physically far beyond two hops. Therefore, they can fire messages at the same time phase as shown in Figure 5.7b. However, in extended DWARF, node 0 perceives that node 2 and node 3 are at the same phase. Therefore, there are two forces from node 2 and node 3 to repel node 0 forward but there is only force from node 1 to repel node 0 backward. Consequently, node 0 cannot stay at the middle between node 1 and the group of node 2 and 3 (see Figure 5.7c).

Therefore, we propose a novel force absorption mechanism for multi-hop desynchronization based on the artificial force field. The objective of this mechanism is to absorb the overwhelming force from at least two nodes that can fire at the same phase without

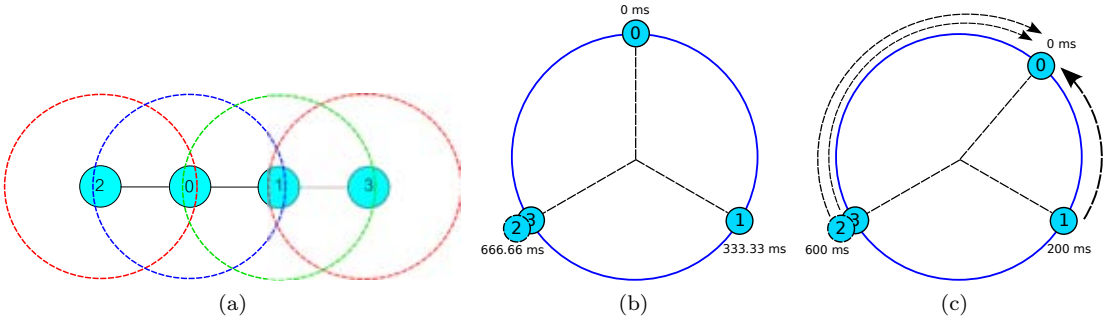

Figure 5.7: The problem of the single-hop DWARF algorithm. (a) A 4-node chain topology. The transmission signal of node 2 does not interfere any receiver of node 3 and vice versa. (b) In the node 0's local view, the expected result is that node 2 and node 3 can share the same phase without interference. (c) In extended DWARF, node 0 is not in the expected phase because there are two forward repelling forces from node 2 and node 3 while there is one backward repelling force from node 1.

interference.

The mechanism is as follows. A node receives a full repelling force from the next/previous phase neighbor as in DWARF. However, a force from the second-next/second-previous phase neighbor is partially absorbed by the next/previous phase neighbor. The magnitude of the absorbed force depends on the phase interval between the next/previous and the second-next/second-previous phase neighbors. The closer that the second-next/second-previous phase neighbor moves to the next/previous phase neighbor results in the lower magnitude of the absorbed force. Eventually, when the second-next/second-previous phase neighbor moves to the same phase as the next/previous phase neighbor, the additional force from the second-next/second-previous phase neighbor is fully absorbed. Consequently, the magnitude of two forces repelling the considered node is approximately equal to only magnitude of one force. This principle is applied recursively; the force from the third-next/third-previous phase neighbor is absorbed by the second-next/second-previous phase neighbor, the force from the fourth-next/fourth-previous phase neighbor is absorbed by the third-next/third-previous phase neighbor, and so forth. Figure 5.8 illustrates this mechanism. In Figure 5.8a, the force from node 2 to node 0 is absorbed by node 3 (the absorbed force is displayed in a blur line). Thus, from node 2, there is only small magnitude of force left to node 0. Eventually, in Figure 5.8b, node 2 moves to the same phase as node 3 because they do not interfere each other and the force from node 2 is fully absorbed. Consequently, the network can be in the perfect desynchrony state.

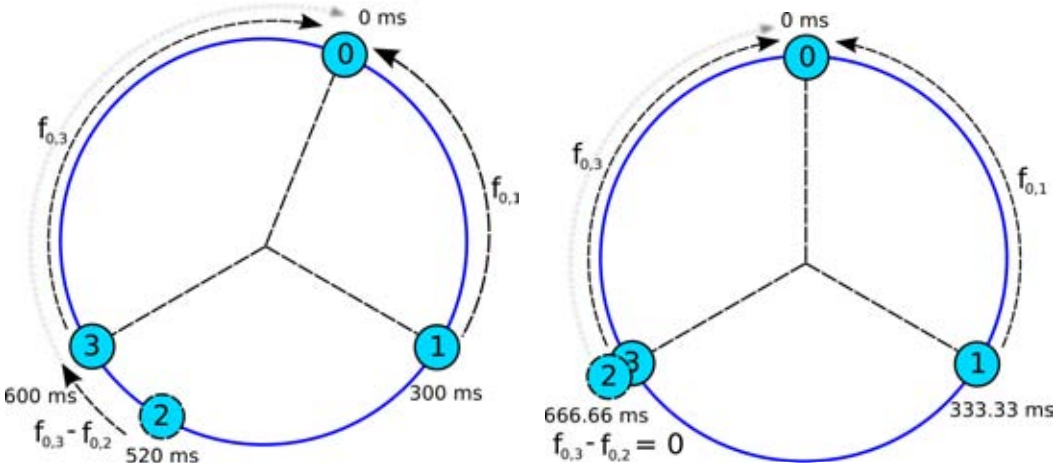

Figure 5.8: EXT-DWARF with force absorption. The blur line represented an absorbed force. (a) When node 2 and 3 are apart, the force from node 2 affects node 0 but the force is partly absorbed. (b) When node 2 and 3 are at the same phase, the force from node 2 is fully absorbed.

Let $f_{i,j}$ be a full repelling force from node j to node i, $f'_{i,j}$ be an absorbed force from node j to node i, T is the time period, and $\Delta\phi_{i,j}$ is the phase difference between node i and j. The force function for multi-hop networks is the following:

$$
\begin{aligned}
f_{i,j} &= \frac{1}{\Delta\phi_{i,j}/T}, \text{where } \Delta\phi_{i,j} \in (-\frac{T}{2}, \frac{T}{2}) \\
f'_{i,i+1} &= f_{i,i+1} \\
f'_{i,i-1} &= f_{i,i-1} \\
f'_{i,j} &= f_{i,x} - f_{i,j}, \text{where } j \notin \{i-1, i+1\} \text{ and } x = (j - \frac{\Delta\phi_{i,j}}{|\Delta\phi_{i,j}|}) \mod n. \qquad (5.1)
\end{aligned}
$$

For $f_{i,x}$, if node j repels node i forward, x is $j+1$. In contrast, if node j repels node i backward, x is $j-1$. At $T/2$ or $-T/2$, a node does not repel an opposite node because they are balanced.

For example, in Figure 5.8, node 0 calculates the force from node 2 as the following:

$$
\begin{aligned}
f'_{0,2} &= f_{0,3} - f_{0,2} \\
&= \frac{1}{\Delta\phi_{0,3}/T} - \frac{1}{\Delta\phi_{0,2}/T}.
\end{aligned}
$$

Noticeably, if node 2 moves close to node 3, the value of $\Delta\phi_{0,2}$ is close to the value

of $\Delta\phi_{0,3}$. Then, the magnitude of force $f_{0,2}$ is reduced. Finally, when $\Delta\phi_{0,2}$ is equal to $\Delta\phi_{0,3}$ as in Figure 5.8b, the magnitude of force $f_{0,2}$ becomes 0. In other words, the force is fully absorbed.

5.4 M-DWARF Algorithm

The M-DWARF algorithm is similar to DWARF (see Chapter 3). However, M-DWARF has two proposed mechanisms to support multi-hop topologies: relative time relaying and force absorption. Initially, nodes are not desynchronized. Each node sets a timer to fire in T time unit and listens to all one-hop neighbors.

When receiving a firing message from its one-hop neighbor, the receiving node marks the current time to be the relative phase reference. Then, the node reads relative phases of its two-hop neighbors which are included within the firing message. After that, the node calculates their two-hop neighbors' phases by using the relative phase reference as the offset.

When the timer expires, the node broadcasts a firing message containing relative phases of its one-hop neighbors. Then, the node calculates a new time phase to move on the phase circle. The calculation is based on the summation of artificial forces from all phase neighbors within two-hops where some forces are absorbed. Then, the node sets a new timer according to the new calculated phase.

As same as DWARF, a node adjusts its phase as follows. Given the total received absorbed force $\mathcal{F}_i$, the node i adjusts to a new time phase $\phi_i^{'}$,

$$\phi_i^{'} = (\phi_i + K\mathcal{F}_i) \mod T, \tag{5.2}$$

where ϕ_i is the current phase of the node i.

We choose the coefficient K as same as in DWARF:

$$K = 38.597 \times n^{-1.874} \times \frac{T}{1000}, \tag{5.3}$$

where n is the number of phase neighbors within two hops and T is the time period. We refer to Section 3.3 that proves and describes in details how we get the value of the

coefficient K. In short, the value of the coefficient K is inverse proportional to the number of nodes n and proportional to the time period T.

All nodes in the artificial force field (in the period circle) iteratively run the same algorithm until the force is balanced. The pseudo-code of this algorithm is shown in Figure 5.9.

5.5 Evaluation

In this section, we evaluate the performance of M-DWARF, EXTENDED-DESYNC (Mühlberger and Kolla (2009)), and LIGHTWEIGHT (Motskin et al. (2009)). All of these algorithms do not require time synchronization. We begin by measuring the desynchronization error and convergence time on single-hop networks because the extension for multi-hop networks should work on single-hop networks as well. Then, we evaluate on several multi-hop topologies which are used in the previous work (Degesys and Nagpal (2008)).

5.5.1 Evaluation Environment

We implement M-DWARF, EXTENDED-DESYNC, and LIGHTWEIGHT on TinyOS 2.1.2 and evaluate them on the TOSSIM simulator. In our simulation, for all algorithms, we use 2-byte sender node ID, and 2-byte neighbor ID. For M-DWARF and EXTENDED-DESYNC, we use 2-byte relative phase for each one-hop neighbor. The regular 11-byte CC2420 header is also used. The time period is set to 1000, 2000, and 3000 milliseconds. The step size (α) of EXTENDED-DESYNC is set to 0.95 as same as in Chapter 3. The phase of each node is initially random in a range of 0 to the period length

5.5.2 Single-hop Networks (Fully-connected Topology) Evaluation

We begin by evaluating M-DWARF on single-hop networks. In M-DWARF and EXTENDED-DESYNC, each firing message contains relative phases of one-hop neighbors. Therefore, to limit the size of a message, we vary the one-hop network size from 4 to 32 nodes.

1: **Initialization**
2: $T = TimePeriod$ {Configurable Time Period}
3: $n = 1$ {Number of neighbors within two hops including itself}
4: $\mathcal{F} = 0$ {Force Summation}
5: $phasesBuffer = Array$ {Buffer for phases of neighbors within two hops}
6: $lastFiringTime = localTime$
7: $currentPhase = localTime$ modulo T
8: Set a firing timer to be T unit time

9: **Upon timer firing**
10: Broadcast a firing message containing relative phases of one-hop neighbors
11: $lastFiringTime = localTime$
12: $currentPhase = localTime$ modulo T
13: $K = 38.597 \times n^{-1.874} \times \frac{T}{1000}$
14: $\mathcal{F}$ = call Calculate total force
15: $newPhase = currentPhase + (K \times \mathcal{F})$
16: **if** $newPhase < 0$ **then**
17: $newPhase = T + newPhase$
18: **end if**
19: Set a firing timer to be fired at ($newPhase$ modulo T)
20: $\mathcal{F} = 0$
21: $n = 1$

22: **Calculate total force**
23: $sortedBuffer$ = Sort $phasesBuffer$
24: $forwardForce = \frac{1}{(T - sortedBuffer[length-1])/T}$
25: $backwardForce = \frac{1}{sortedBuffer[0]/T}$
26: **for** i in range of 1 to length of sorted $phasesBuffer$ - 2 **do**
27: **if** $phasesBuffer[i] > 0.5T$ **then**
28: $forwardForce = forwardForce + (\frac{1}{(T - phasesBuffer[i+1])/T} - \frac{1}{(T - phasesBuffer[i])/T})$
29: **else**
30: $backwardForce = backwardForce + (\frac{1}{phaseBuffer[i-1]/T} - \frac{1}{phaseBuffer[i]/T})$
31: **end if**
32: **end for**
33: return $forwardForce - backwardForce$

34: **Upon receiving a firing message from** $nodeId$
35: $phaseDiff = localTime - lastFiringTime$
36: $phasesBuffer[nodeId] = phaseDiff$
37: $reference = phaseDiff$
38: **for** each $twoHopNodeId$ of two-hop neighbors in $message$ **do**
39: **if** $twoHopNodeId$ is not in $phasesBuffer$ **then**
40: $phasesBuffer[twoHopNodeId] = message[twoHopNodeId][relativePhase] + reference$
41: $n = n + 1$
42: **end if**
43: **end for**

Figure 5.9: Pseudocode of M-DWARF algorithm

5.5.2.1 Desynchronization Error

We run the simulation for 300 time periods to measure the desynchronization error. In each network size, we run the simulation for 30 times. Then, we measure the average

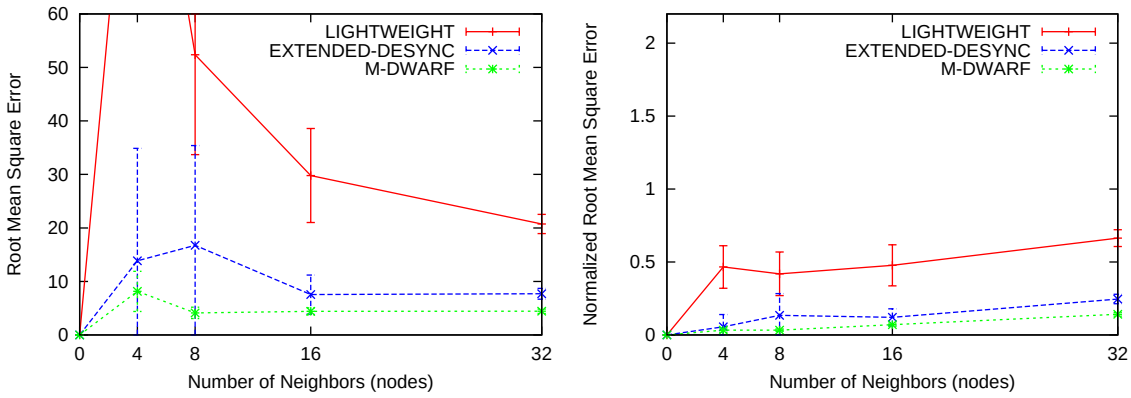

(a) (b)

Figure 5.10: (a) Root mean square error after 300 time periods. (b) Root mean square error normalized by perfect phase difference after 300 time periods.

root mean square error (RMSE) and normalized root mean square error (see details in Section 3.4.3). Figure 5.10a illustrates the result of absolute desynchronization error and Figure 5.10b illustrates the result of the normalized desynchronization error in each network size after 300 time periods.

The result indicates that, in all network sizes (4 - 32 nodes), M-DWARF achieves significantly better desynchrony states than EXTENDED-DESYNC and LIGHTWEIGHT do. The EXTENDED-DESYNC's mechanism has the same pitfall as that of DESYNC because they are based on the same mechanism. The pitfall is that the phase error of a node propagates to its phase neighbors and this error will propagate back and forth between two phase neighbors. This results in a large error after convergence. In contrast, M-DWARF is robust to this error propagation as same as DWARF because both M-DWARF and DWARF use the total received forces from all neighbors. An error from one neighbor does not overwhelm the system. For LIGHTWEIGHT, the desynchronization errors of small networks are extremely large because the algorithm randomly chooses the free time slot without considering the equitably separation. However, when the network size becomes larger, the error becomes lower because the perfect phase interval length is reduced.

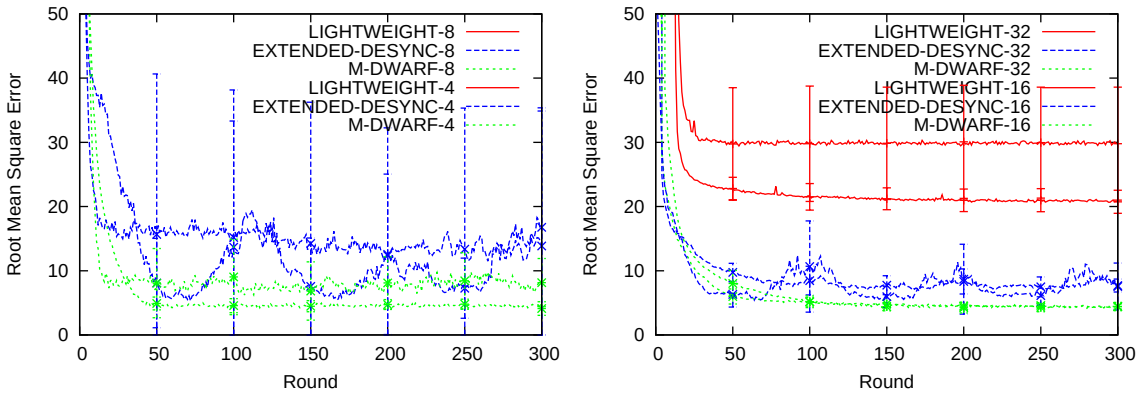

(a) Sparse (b) Dense

Figure 5.11: Convergence time and absolute root mean square error

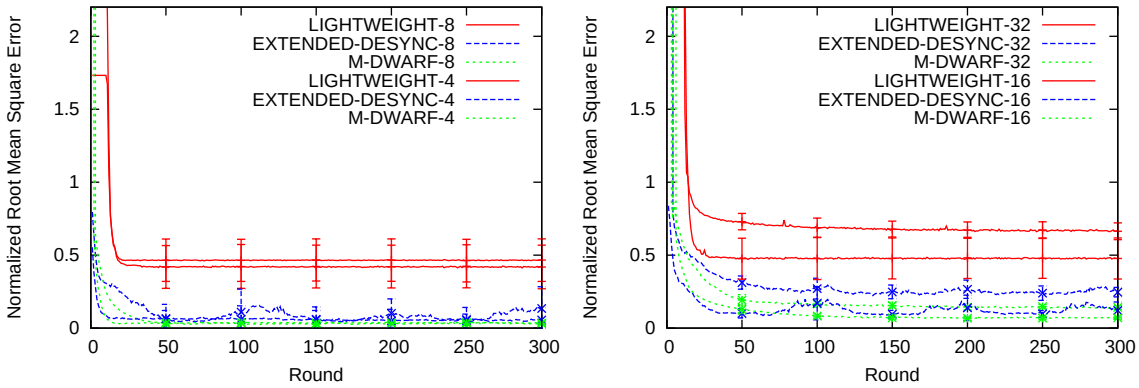

(a) Sparse (b) Dense

Figure 5.12: Convergence time and root mean square error normalized by expected phase difference

5.5.2.2 Convergence Time

In this section, we measure the absolute root mean square error and normalized root mean square error for each time period to investigate the convergence time. Figure 5.11a and 5.12a show the results of sparse networks whereas Figure 5.11b and 5.12b show the results of dense networks.

In all network sizes, the convergence speed of M-DWARF is comparable to that of EXTENDED-DESYNC. However, M-DWARF converges with the lowest desynchronization error. For LIGHTWEIGHT, the algorithm converges fast and stable. However, due to the random slot selection process, the desynchronization errors in all network sizes are

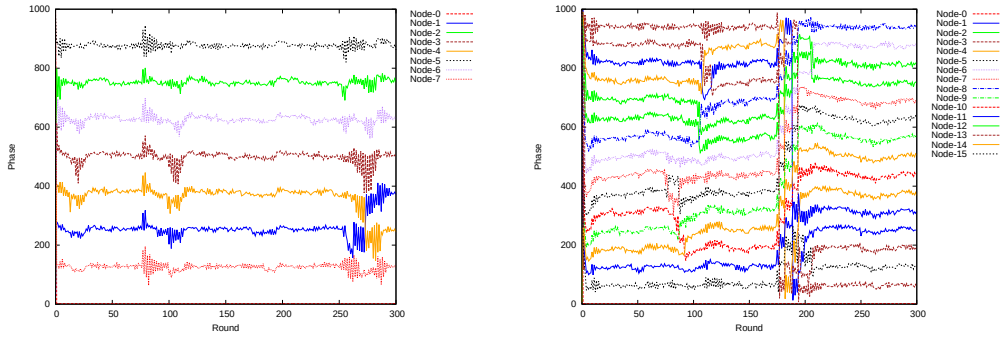

(a) 8 nodes (b) 16 nodes

Figure 5.13: Fluctuation in some cases of EXTENDED-DESYNC.

large.

We note that the errors of EXTENDED-DESYNC for 8-node and 16-node networks are fluctuate. This is due to the fact that, in our 30 EXTENDED-DESYNC simulations, there are some cases in 8-node and 16-node networks that the phases of some nodes are highly fluctuate as depicted in Figure 5.13. These cases affect the average value. This behaviour is caused by the mechanism of EXTENDED-DESYNC (and DESYNC) that relies on only two phase neighbors information as described earlier in Chapter 3.

The result of single-hop networks indicates that M-DWARF that augments DWARF with two mechanisms still performs very well on single-hop networks without loss of generality.

5.5.3 Impact of Topologies

For multi-hop networks, we evaluate M-DWARF on several topologies including star, chain, cycle, butterfly, and mesh topologies. In each topology, we simulate for 30 times and show the relative phase graph results. We show the phase graphs that represent the average case and the problematic case of each algorithm. We note that, in all topologies, LIGHTWEIGHT achieves the similar results. For LIGHTWEIGHT, each node randomly chooses the beginning of a time slot by avoiding the collision with one-hop neighbors. Therefore, on average, LIGHTWEIGHT causes several inequivalent interval gaps between two consecutive phase neighbor nodes. Moreover, there are several problematic cases that at least two nodes within two-hop communication choose the same

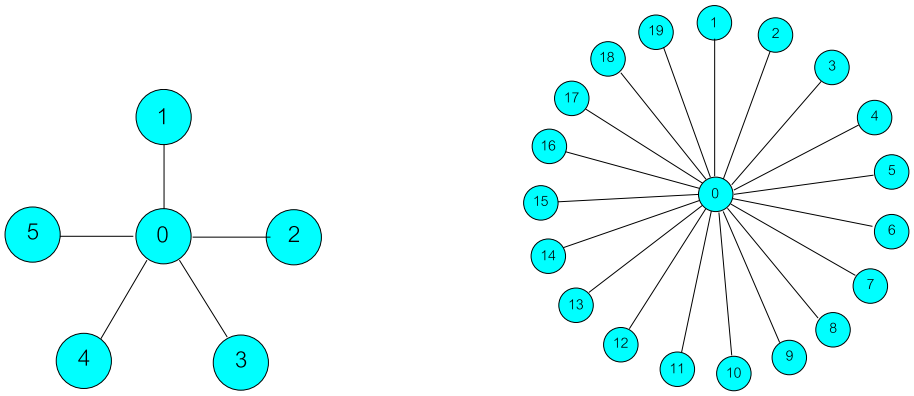

(a) 6 nodes (b) 20 nodes

Figure 5.14: Star topology

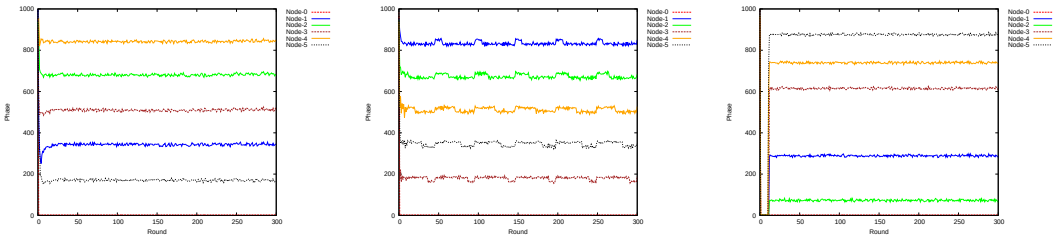

(a) M-DWARF (b) EXTENDED-DESYNC (c) LIGHTWEIGHT

Figure 5.15: 6-node star topology evaluation (average case).

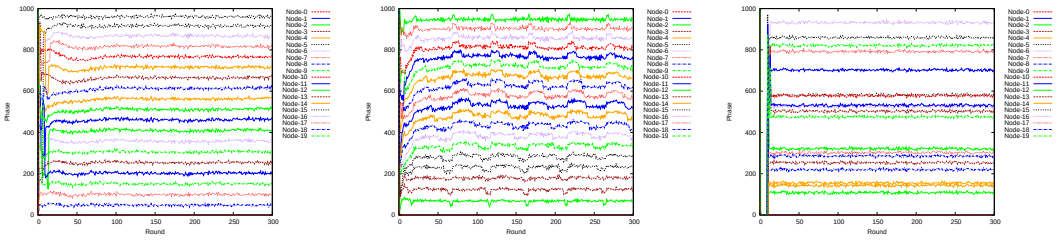

(a) M-DWARF (b) EXTENDED-DESYNC (c) LIGHTWEIGHT

Figure 5.16: 20-node star topology evaluation (average case).

beginning of a time slot because they cannot receive firing messages from each other. Thus, in all topologies, we only describe the behaviour of M-DWARF and EXTENDED-DESYNC.

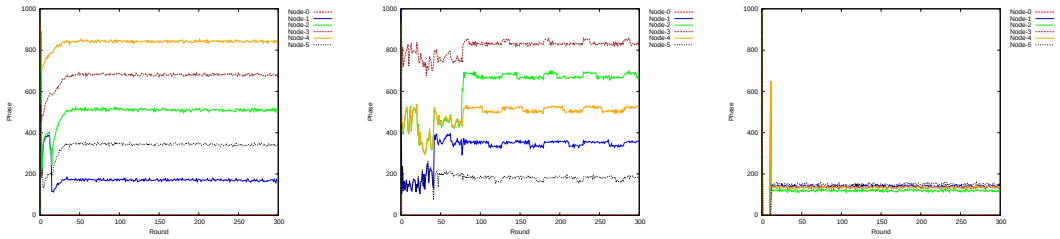

(a) M-DWARF (b) EXTENDED-DESYNC (c) LIGHTWEIGHT

Figure 5.17: 6-node star topology evaluation (problematic case).

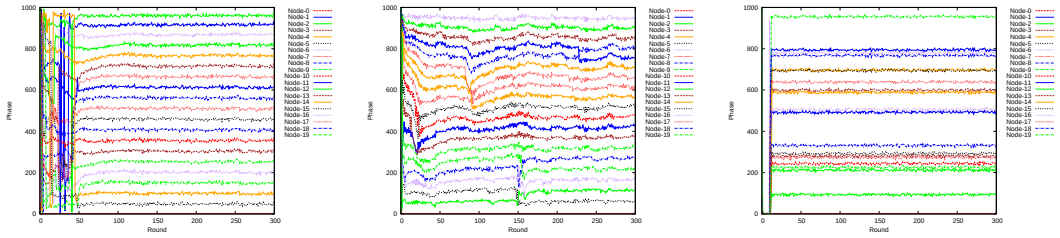

(a) M-DWARF (b) EXTENDED-DESYNC (c) LIGHTWEIGHT

Figure 5.18: 20-node star topology evaluation (problematic case).

5.5.3.1 Star Topology

The star topology is the simplest case for multi-hop desynchronization. There is one center node that can transmit and receive messages with all other nodes in the network. In contrast, other nodes can transmit and receive only with the center node. Figure 5.14 illustrates 6-node and 20-node star topologies that we use for algorithms evaluation. In the star topology, every node is connected to each other within two-hop communication. As a result, all nodes must use different time slots.

Figure 5.15 and 5.16 shows the simulation results of three algorithms on 6-node and 20-node star topologies respectively. Due to the relative phase relaying mechanism, both M-DWARF and EXTENDED-DESYNC perceive relative phases of neighbors within two hops, which are all nodes in the system. Consequently, both algorithms can separate 6 nodes into almost equivalent 6 time slots. However, M-DWARF achieves almost perfect desynchony whereas EXTENDED-DESYNC slightly fluctuates in the sparse 6-node network and highly fluctuates in the dense 20-node network. Figure 5.17 and 5.18 shows the problematic cases. For M-DWARF, there is no problem in the sparse networks, but, in the dense networks, nodes take more time to become stable. The reason is that, when

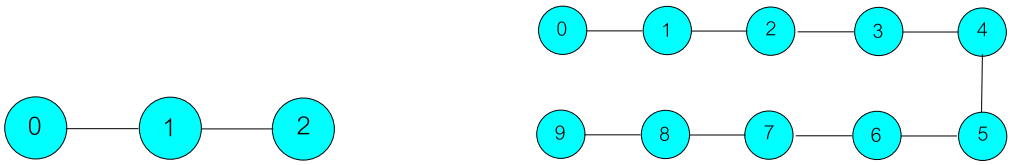

(a) 3 nodes (b) 10 nodes

Figure 5.19: Chain topology

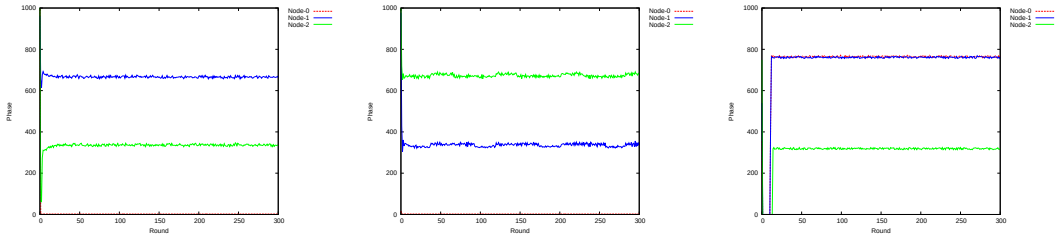

(a) M-DWARF (b) EXTENDED-DESYNC (c) LIGHTWEIGHT

Figure 5.20: 3-node chain topology evaluation (average case).

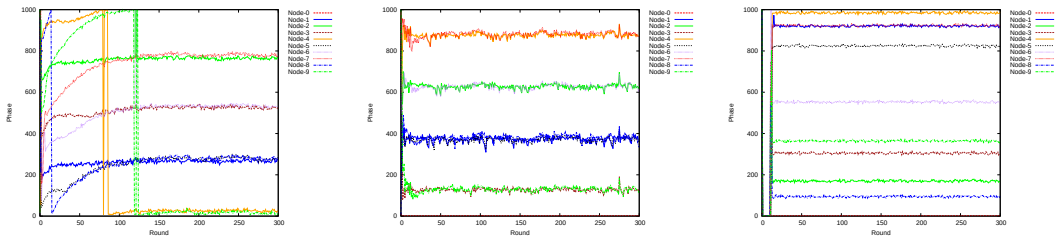

(a) M-DWARF (b) EXTENDED-DESYNC (c) LIGHTWEIGHT

Figure 5.21: 10-node chain topology evaluation (average case).

the network is dense, the usable time interval gap for each node is shortened. Therefore, if several nodes start closely to each other at the initial configuration, forces are highly absorbed. As a result, they takes more time to separate away from each other. In the case of EXTENDED-DESYNC, the fluctuated error from one node can propagate throughout the networks because each node relies on only information of two phase neighbors.

5.5.3.2 Chain Topology

The chain topology is one of the simplest topologies. Every node is lined up without a loop. The 3-node and 10-node chain topologies are depicted in Figure 5.19. For 3 nodes, this case is simple because all three nodes cannot share the same phase. In most cases as shown in Figure 5.20, both M-DWARF and EXTENDED-DESYNC perform very

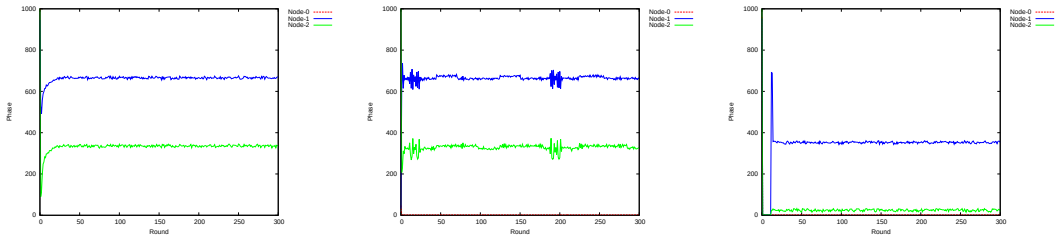

(a) M-DWARF (b) EXTENDED-DESYNC (c) LIGHTWEIGHT

Figure 5.22: 3-node chain topology evaluation (problematic case).

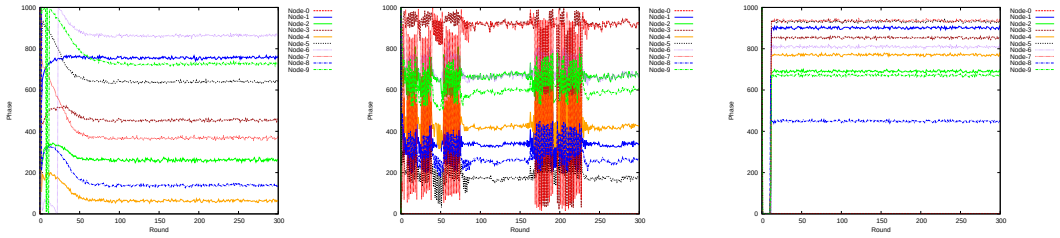

(a) M-DWARF (b) EXTENDED-DESYNC (c) LIGHTWEIGHT

Figure 5.23: 10-node chain topology evaluation (problematic case).

well. All nodes are equivalently separated. However, M-DWARF is slightly smoother than EXTENDED-DESYNC.

For 10 nodes, some nodes that are farther than two hops are able to use the same phase. There are several optimal solutions. For exmaple, the first optimal solution is that there are four groups of nodes that use different phases. Each node within the same group can use the same phase. These four groups are $\{0, 3, 6, 9\}, \{1, 4, 7\}, \{2, 5, 8\}$, and $\{6\}$. Another optimal solution is $\{0, 4, 9\}, \{1, 5, 8\}, \{3, 6\}$, and $\{2, 7\}$. We note that, in our 30 simulations, M-DWARF could achieve the perfect desynchrony state with 4 slots as in Figure 5.21a, but EXTENDED-DEESYNC never achieve the perfect desynchrony state (there are 5 slots in Figure 5.21b because node 0 is at phase 0).

In some problematic cases, the phases of EXTENDED-DESYNC are slightly fluctuate in the sparse networks (Figure 5.22b) and highly fluctuate in the dense networks (Figure 5.23b). Additionally, for both EXTENDED-DESYNC and M-DWARF, each node attempts to gradually adjust its phase in the range between previous and next phase neighbors. Therefore, if the initial configuration is not proper, nodes may be not able to adjust their phases over the range of such neighbors and the networks cannot get

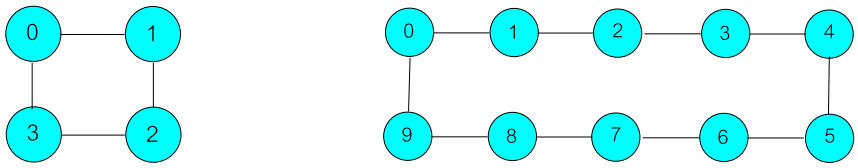

(a) 4 nodes (b) 10 nodes

Figure 5.24: Cycle topology

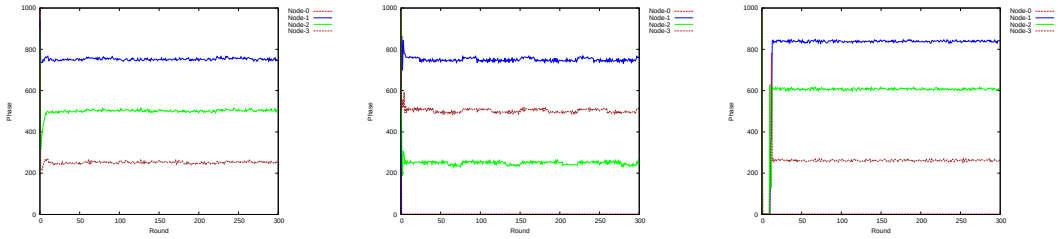

(a) M-DWARF (b) EXTENDED-DESYNC (c) LIGHTWEIGHT

Figure 5.25: 4-node cycle topology evaluation (average case).

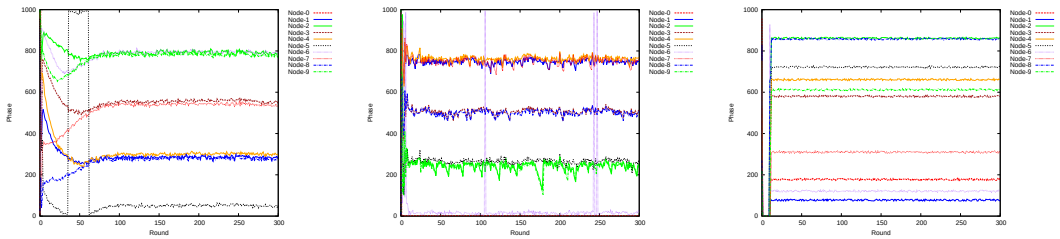

(a) M-DWARF (b) EXTENDED-DESYNC (c) LIGHTWEIGHT

Figure 5.26: 10-node cycle topology evaluation (average case).

into the perfect desynchrony state. Figure 5.23a and 5.23b illustrate this problem.

5.5.3.3 Cycle Topology

The cycle topology is simlar to the chain topology. All nodes are lined up but the first and last nodes are connected together to form a closed loop. Figure 5.24 depicts 4-node and 10-node cycle topologies.

For 4-node cycle networks, all nodes are within two hops from each other. Therefore, every node knows phases of other nodes and no node shares the same phase. On average, both M-DWARF and EXTENDED-DESYNC achieve the perfect desynchrony state as shown in Figure 5.25a and 5.25b. For 10-node networks, some optimal solutions

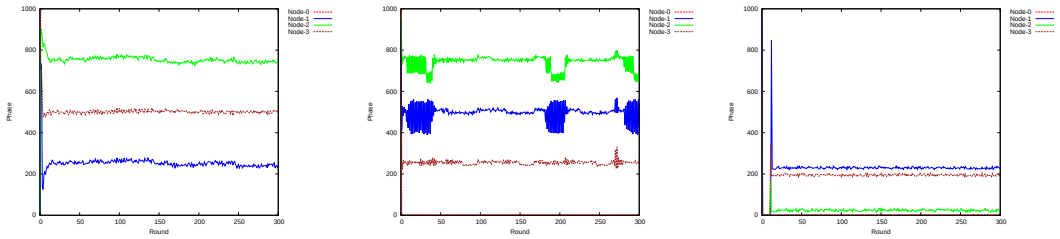

(a) M-DWARF (b) EXTENDED-DESYNC (c) LIGHTWEIGHT

Figure 5.27: 4-node cycle topology evaluation (problematic case).

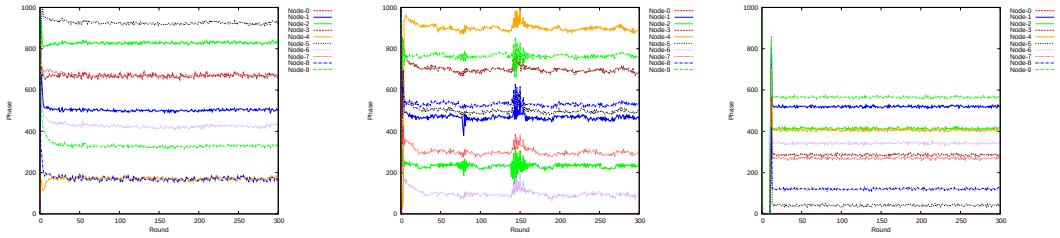

(a) M-DWARF (b) EXTENDED-DESYNC (c) LIGHTWEIGHT

Figure 5.28: 10-node cycle topology evaluation (problematic case).

are different from the optimal solutions in the case of the 10-node chain topology because node 0 and 9 cannot share the same phase in the cycle topology. Both M-DWARF and EXTENDED-DESYNCE can achieve the perfect desynchrony state in this case (see Figure 5.26a and 5.26b). However, again, the phases of EXTENDED-DESYNC are fluctuate.

In some problematic cases, the result is similar to the problematic result of the chain topology with the same reason that the initial configuration affects how nodes adjust theirs phases to the proper phases. Figure 5.27a, 5.27b, 5.28a, and 5.28b illustrate the problem.

5.5.3.4 Dumbbell Topology

The dumbbell topology is commonly used in practice. It is one form of the transit-stub networks. In a dumbbell network, there are a number of nodes connected to a single relay node. The relay node is connected to another relay node at another side. Another number of nodes are connected to that final relay node to create a dumbbell topology. Figure 5.29 depicts 6-node and 20-node dumbbell networks.

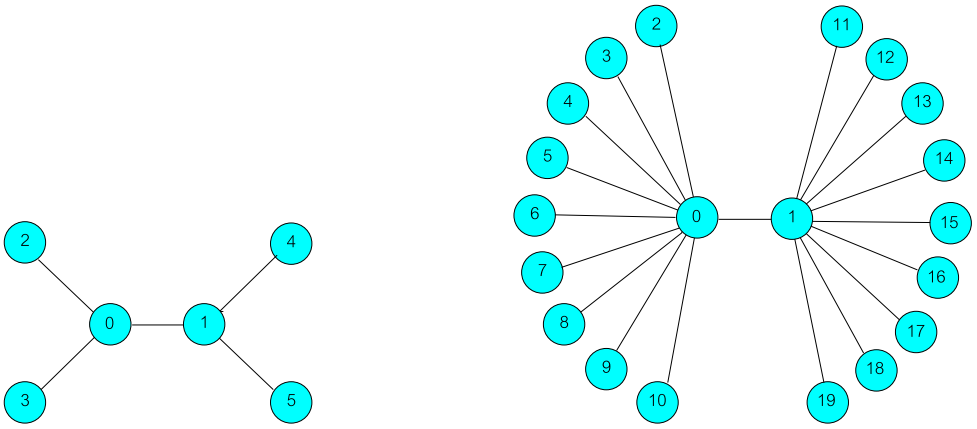

(a) 6 nodes (b) 20 nodes

Figure 5.29: Dumbbell topology

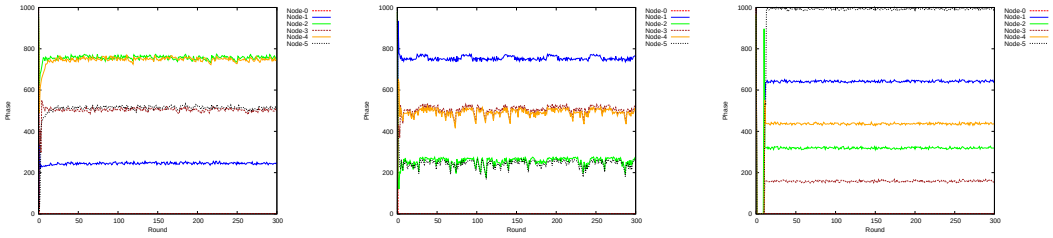

(a) M-DWARF (b) EXTENDED-DESYNC (c) LIGHTWEIGHT

Figure 5.30: 6-node dumbbell topology evaluation (average case).

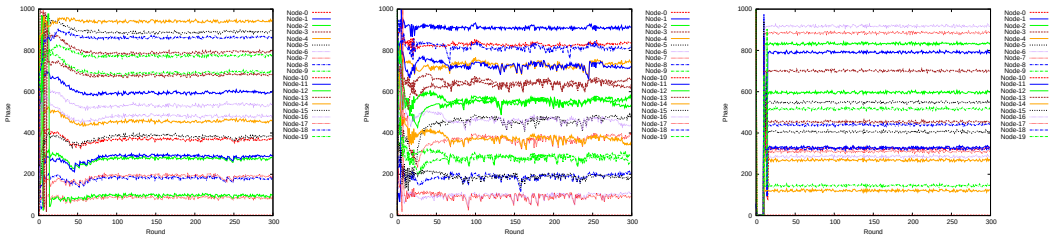

(a) M-DWARF (b) EXTENDED-DESYNC (c) LIGHTWEIGHT

Figure 5.31: 20-node dumbbell topology evaluation (average case).

Obviously, a node at one end can share the same phase with another node at the other end because they are far from each other beyond two hops. Therefore, for 6-node networks, the optimal solution requires 4 slots. Each slot interval is $T/4$. For 20-node networks, the optimal solution requires 11 slots. Each slot interval is $T/11$. In Figure 5.30a and 5.30b, both M-DWARF and EXTENDED-DESYNC achieve the optimal solution for 6-node networks. However, again, M-DWARF is more stable than

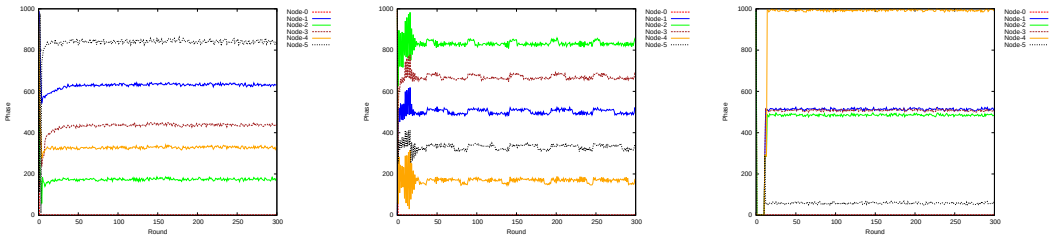

(a) M-DWARF (b) EXTENDED-DESYNC (c) LIGHTWEIGHT

Figure 5.32: 6-node dumbbell topology evaluation (problematic case).

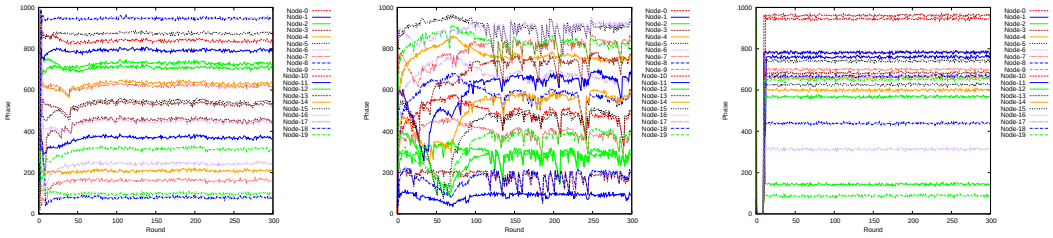

(a) M-DWARF (b) EXTENDED-DESYNC (c) LIGHTWEIGHT

Figure 5.33: 20-node dumbbell topology evaluation (problematic case).

EXTENDED-DESYNC.

When the network is dense, EXTENDED-DESYNC is highly fluctuate. If one node adapts their phase too fast, several nodes are affected because there are many two-hop neighbors in the dumbbell networks as illustrated in Figure 5.33b. In contrast, in M-DWARF, the fast adaptation of one node does not has high impact to other nodes because nodes do not rely on only their two phase neighbors but use all information from neighbors within two hops as the force function.

5.5.3.5 Mesh Topology

We use the 10-node mesh topology described in Degesys and Nagpal (2008) as depicted in Figure 5.34. A solid line represents one-hop connectivity whereas a dash line represents two-hop connectivity. In Degesys and Nagpal (2008), they state the best case of this topology is that eight slots are required. However, in our simulation, we discover the better solution that requires only six slots as illustrated in Figure 5.35a for M-DWARF and Figure 5.35b for EXTENDED-DESYNC. The problematic case for bot M-DWARF and EXTENDED-DESYNC is that the initial configuration is not proper. However, as

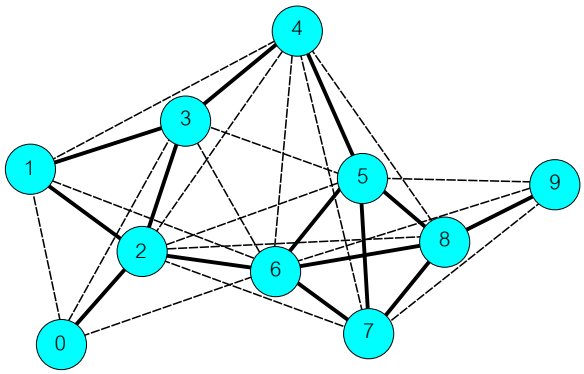

Figure 5.34: 10-node multi-hop network. A solid line represents 1-hop connectivity. A dash line represents 2-hop connectivity. Any two nodes that are connected within 2-hop connectivity can interfere each other transmission.

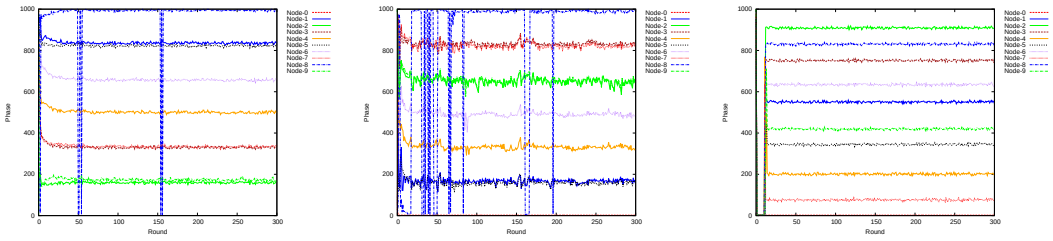

(a) M-DWARF (b) EXTENDED-DESYNC (c) LIGHTWEIGHT

Figure 5.35: 10-node mesh topology evaluation (average case).

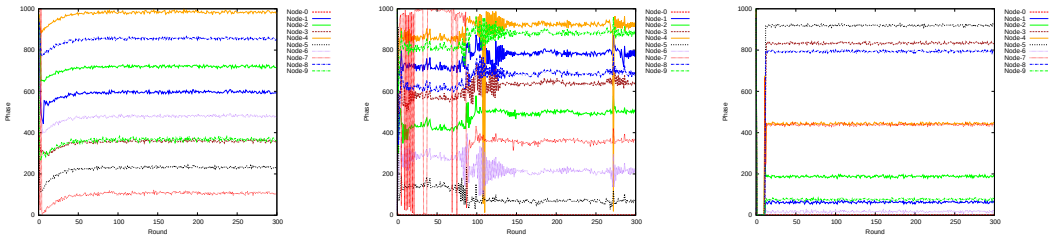

(a) M-DWARF (b) EXTENDED-DESYNC (c) LIGHTWEIGHT

Figure 5.36: 10-node mesh topology evaluation (problematic case).

expected, EXTENDED-DESYNCE is affected from highly fluctuation.

5.5.4 Impact of Period Length

In previous experiments, we set the time period to 1,000 milliseconds. In this experiment, we vary the period from 1,000 to 3,000 milliseconds. To obviously see the impact of period length, we use the star topology which is the multi-hop topology that all nodes perceive all 2-hop neighbors and set the number of nodes to 30 nodes. With this

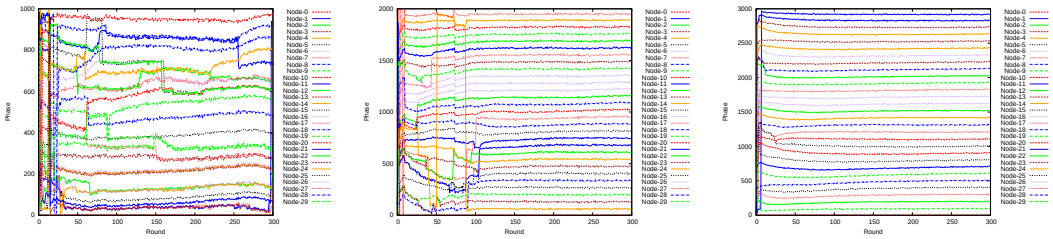

(a) $T = 1000$ ms (b) $T = 2000$ ms (c) $T = 3000$ ms

Figure 5.37: Impact of period length (T) in M-DWARF

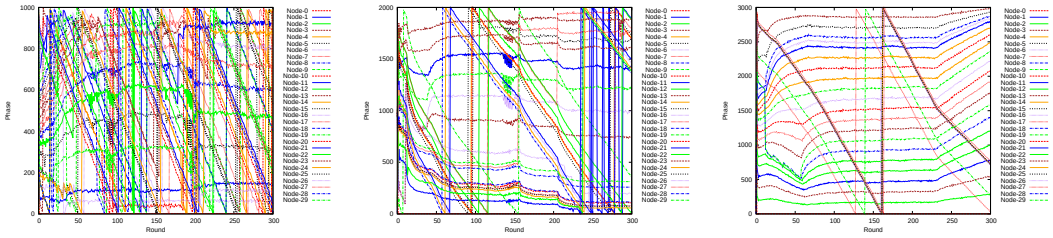

(a) $T = 1000$ ms (b) $T = 2000$ ms (c) $T = 3000$ ms

Figure 5.38: Impact of period length (T) in EXTENDED-DESYNC

topology and the number of nodes, the network is saturated within the 1,000-millisecond period.

Figure 5.37 and 5.38 show the phase graphs when varying period length of M-DWARF and EXTENDED-DESYNC respectively. At the 1,000-millisecond period, the network is saturated for 30 nodes. First, we notice that this result is different from 30 nodes in the single-hop networks that we evaluate in Chapter 3 which nodes are well-spread in a time period. In the single-hop DWARF algorithm, a firing message does not contain any overhead, whereas, in the multi-hop M-DWARF algorithm, a firing message contains one-hop neighbors relative phases. Therefore, the firing message of multi-hop M-DWARF takes longer firing time than that of single-hop DWARF. Consequently, the time gap between two firing messages is reduced in M-DWARF.

With the same period length, there are more nodes in EXTENDED-DESYNC than in M-DWARF that stay at the same phase and their firing messages collide. When the period length is increased to 2,000 and 3,000 milliseconds, the free time gap is also increased. Therefore, the number of collisions is reduced and nodes are better spread in both algorithms.

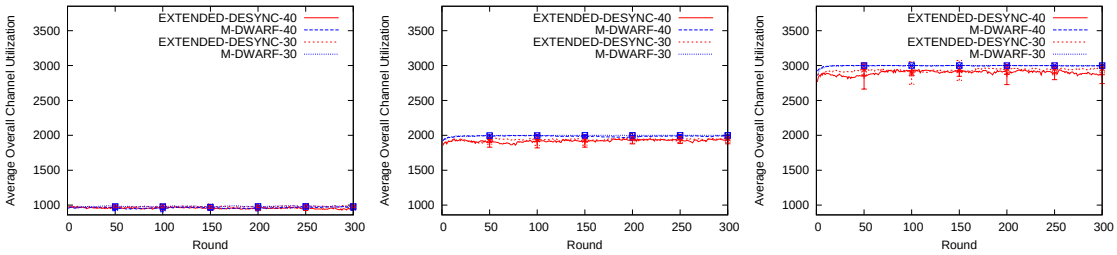

(a) $T = 1000$ ms (b) $T = 2000$ ms (c) $T = 3000$ ms

Figure 5.39: Average channel utilization of 30 and 40 node networks

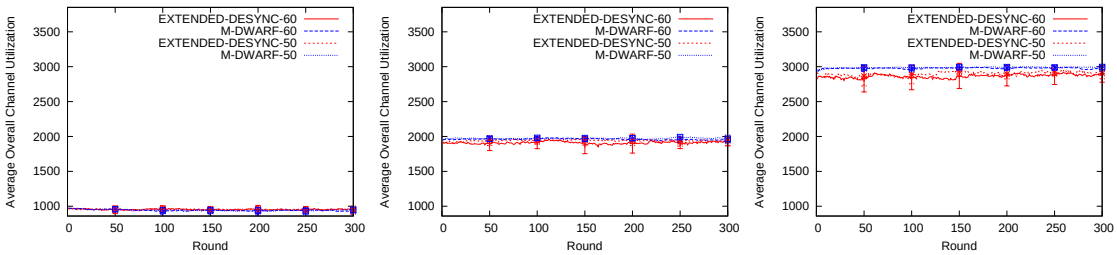

(a) $T = 1000$ ms (b) $T = 2000$ ms (c) $T = 3000$ ms

Figure 5.40: Average channel utilization of 50 and 60 node networks

5.5.5 Channel Utilization and Fairness

In this section, we measure the average channel utilization of M-DWARF and EXTENDED-DESYNC. The channel can be utilized by one node if there is no collision during an amount of time between a node's firing to another node's firing. Figure 5.39 shows the results of networks with 30 and 40 nodes and Figure 5.40 shows the results of networks with 50 and 60 nodes. At the 1000-millisecond period, the average channel utilizations of 30 to 60 nodes networks are almost the same because the network are already saturated and there are several collisions. The number of colliding nodes are also approximately the same for both algorithms. When the period length is increased, M-DWARF performs better than EXTENDED-DESYNC because there are less collisions in M-DWARF. However, we note that this benefit is not significant (only around 50 milliseconds improvement).

Then, we measure the fairness of nodes utilizing the channel. If we average the channel utilization per node, the result is approximately the same for M-DWARF and EXTENDED-DESYNC but M-DWARF is insignificantly slightly better (which is the rea-

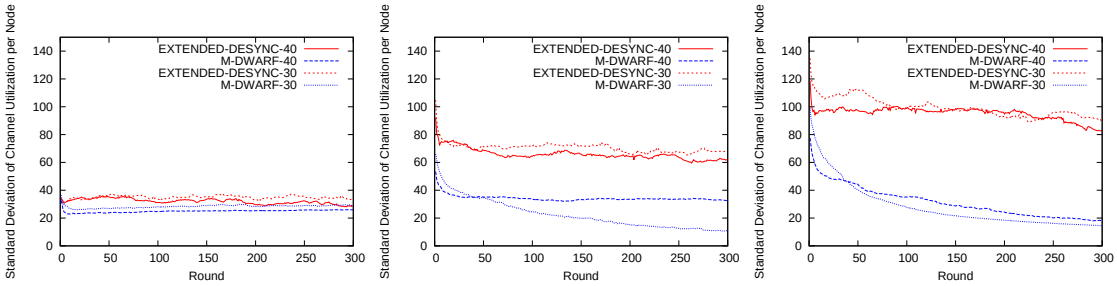

(a) $T = 1000$ ms (b) $T = 2000$ ms (c) $T = 3000$ ms

Figure 5.41: Average standard deviation of channel utilization per node of 30 and 40 node networks

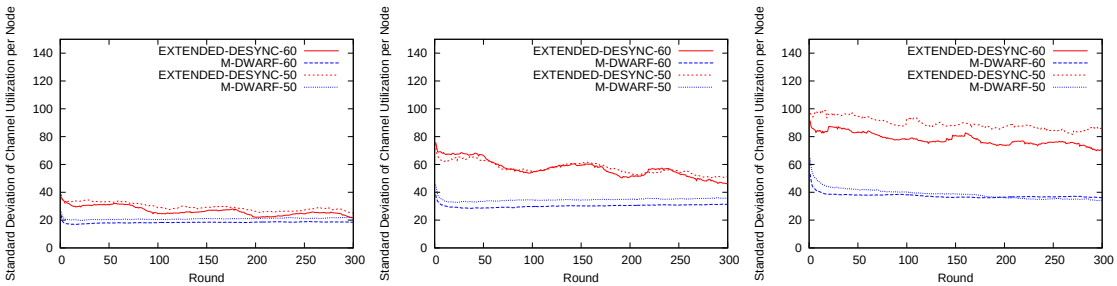

(a) $T = 1000$ ms (b) $T = 2000$ ms (c) $T = 3000$ ms

Figure 5.42: Average standard deviation of channel utilization per node of 50 and 60 node networks

son why the average channel utilization of M-DWARF is only slightly better). However, to measure the fairness, we are interested in the value of the average standard deviation of the channel utilization per node. If nodes fairly utilize the network, this value is low. The results of 30 and 40 nodes networks are shown in Figure 5.41 and the results of 50 and 60 nodes networks are shown in Figure 5.42. In saturated networks (*i.e.* 1000-millisecond period), the fairness of both M-DWARF and EXTENDED-DESYNC is approximately the same when the time passes. However, the difference of fairness becomes significantly large when the period length is increased. The average standard deviation of the channel utilization per node of EXTENDED-DESYNC is 30 - 400% higher than that of M-DWARF. Therefore, M-DWARF achieves better fairness. One of the main reasons that nodes in M-DWARF fairly utilize a network is that the stability of M-DWARF is better than that of EXTENDED-DESYNC which still has error-fluctuation (see Chapter 3).

5.5.6 Overhead Optimization and Robustness to Loss

Due to the fact that the firing message contains relative phases of one-hop neighbors. If there are too many neighbors, the algorithm incurs large overhead. Therefore, in this evaluation, we attempt to reduce such overhead. We straightforwardly reduce the number of relative phases broadcastings. We only periodically attach neighbors' relative phases in a firing message. Therefore, in most firing messages, relative phases are not included. Each node keeps track of phase neighbors within two hops even it does not receive a new firing message. We set a time-to-live for each record to 3 periods. If a node does not receive the phase information from arbitrary node within 3 periods, it removes that node from its records. To investigate how much we can reduce the overhead, we vary a saving gain parameter β which is the frequency to exclude relative phases from a firing message; for example, $\beta = 0$ means including relative phases in every firing message, $\beta = 1$ means including relative phases in every two firing messages, $\beta = 2$ means including relative phases in every three firing messages, and so on.

We evaluate this optimization scheme on the 10-node star topology. We vary the saving gain β from 0 to 20. The result is shown in Figure 5.43. From the figure, we find that, even we reduce the number of relative phases broadcastings, the system still converges to the perfect desynchrony state in most cases. However, if the saving gain is greater than 16, the system converges slowly or may not converge because the information that a node keeps is removed. This result indicates two important insights. First, by trading off with convergence speed, we can drastically reduce the overhead by a factor of 16 in our investigated scenario. Second, even each node does not receive relative phases for many consecutive times. The algorithm still works. Therefore, the proposed algorithm tolerates to packet loss.

5.6 Summary

This chapter presents M-DWARF, the multi-hop extension of DWARF which is presented in Chapter 3. In multi-hop networks, the hidden terminal problem directly affects the performance of desynchronization algorithms. M-DWARF solves such a problem with two mechanisms: relative phase relaying and force absorption. The relative phase relaying mechanism help nodes notice the presence of two-hop neighbors. The force absorption mechanism help reduce the force from two-hop neighbors that can stay at the

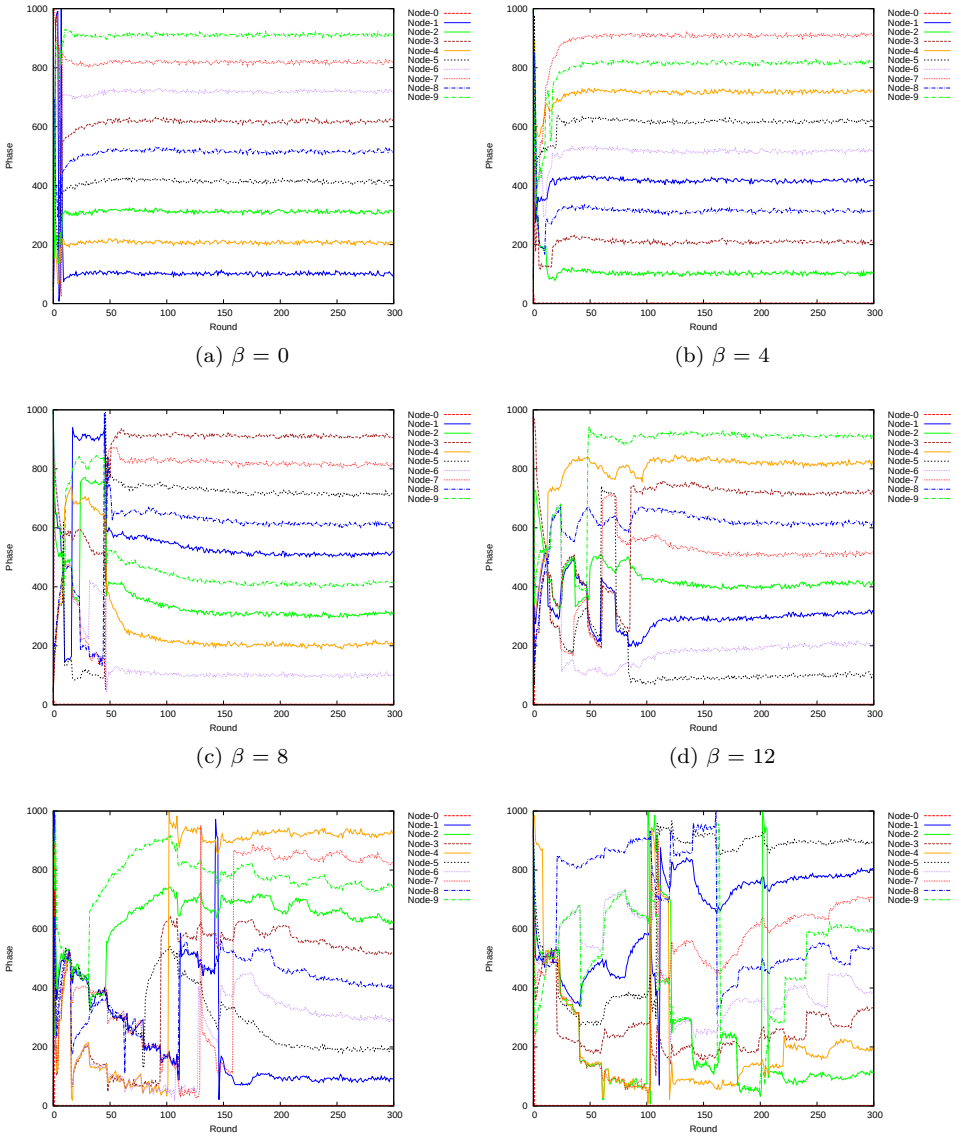

(a) $\beta = 0$ (b) $\beta = 4$

(c) $\beta = 8$ (d) $\beta = 12$

(e) $\beta = 16$ (f) $\beta = 20$

Figure 5.43: Optimized M-DWARF: Varying saving gain from 0 to 20.

same phase.

M-DWARF has several benefits. First, the algorithm runs distributedly on each sensor node. No central master node is required. Second, the algorithm works even nodes are not synchronized and do not realize global time. Third, the algorithm is able to work for both single-hop and multi-hop networks. In addition, the algorithm is lightweight, simple, and practical. The code size of the core algorithm is less than 500 lines of code. The size of a compiled binary is less than 30 kilobytes. The required memory is less than 2 kilobytes. This property is desirable to implement, extend, and apply for resource-limited wireless sensor nodes. Furthermore, the algorithm requires only local 2-hop information and scales well with network size.

In the next chapter, we analyse the stability under small perturbation of M-DWARF.

CHAPTER VI

STABILITY ANALYSIS OF THE MULTI-HOP ALGORITHM

The multi-hop stability analysis in this chapter is more complicated than the analysis of single-hop networks (Chapter 4) due to the connectivity and topology affect the analysis. We begin by formalizing components of forces to a general form. Then, we transform the system into a dynamic system equations and locally analyse at the equilibrium.

6.1 Definition

We first define several variables and notations to be used throughout the analysis in this chapter.

We define n to be the number of nodes in the system and T be the time period. We assume n is even. However, in the case of odd n, the system can be analysed with the same procedure.

We define $c_{i,j}$ to be a connectivity status in two-hop communication from node j to node i. If node i perceives the presence of node j (as a one-hop neighbor or by relaying relative phase), $c_{i,j}$ is 1. Otherwise, $c_{i,j}$ is 0. For example, in a simple 3-node chain network with node labelled 0, 1, and 2 respectively, if communication links are symmetry, the values of $c_{0,1}, c_{1,0}, c_{1,2}$, and $c_{2,1}$ are 1 whereas the values of $c_{0,2}$ and $c_{2,0}$ are 0. We assume that nodes are labelled sequentially in increasing order from 0 to $n-1$ according the the increasing phase in the global period ring.

We define the modulo notation $[x]_n$ to stand for $x \mod n$ for brevity.

We define Δ_i to be a phase interval between node i and node $[i+1]_n$, where $\Delta_i \in (0, T]$.

6.2 Force Component

To construct a dynamic system, we first analyse how force with the absorption mechanism affects the system equations. As described in Chapter 5, a force can be absorbed if it is not originated from the closest phase neighbor. Therefore, respect to the node i's point of view, some forces have no effect to node i whereas some forces do. We classify forces that affect node i into three components: closest component, resistance component, and absorption component. The final form of forces that affect node i will be in the following form:

$$\begin{aligned} F_i =&(\text{closest component} + \text{resistance component} - \text{absorption component})_{positive} \\ &- (\text{closest component} + \text{resistance component} - \text{absorption component})_{negative}. \end{aligned} \tag{6.1}$$

Closest component: Respect to the node i's point of view, the closest component is the force from the closest phase neighbor of node i and node i perceives its presence. This force is not absorbed by any node. This force component from node j to node i will appear in the equation if, between node j and node i, node i does not perceive the presence of any node. In other words, node j is the closest perceived phase neighbor of node i. We firstly define the closest component for node i by using the combination of logic and algebraic expression as follows (we use it only for clarification purpose and we will change it to pure algebraic expression later),

$$\begin{aligned} &\Bigg((c_{i,[i+(n-1)]_n}) f^+_{i,[i+(n-1)]_n} + (\neg c_{i,[i+(n-1)]_n} \wedge c_{i,[i+(n-2)]_n}) f^+_{i,[i+(n-2)]_n} \\ &+ (\neg c_{i,[i+(n-1)]_n} \wedge \neg c_{i,[i+(n-2)]_n} \wedge c_{i,[i+(n-3)]_n}) f^+_{i,[i+(n-3)]_n} + \cdots \\ &+ (\neg c_{i,[i+(n-1)]_n} \wedge \neg c_{i,[i+(n-2)]_n} \wedge \cdots \wedge \neg c_{i,[i+(\frac{n}{2}+2)]_n} \wedge c_{i,[i+(\frac{n}{2}+1)]_n}) f^+_{i,[i+(\frac{n}{2}+1)]_n} \Bigg) \\ &- \Bigg((c_{i,[i+1]_n}) f^-_{i,[i+1]_n} + (\neg c_{i,[i+1]_n} \wedge c_{i,[i+2]_n}) f^-_{i,[i+2]_n} \\ &+ (\neg c_{i,[i+1]_n} \wedge \neg c_{i,[i+2]_n} \wedge c_{i,[i+3]_n}) f^-_{i,[i+3]_n} + \cdots \\ &+ (\neg c_{i,[i+1]_n} \wedge \neg c_{i,[i+2]_n} \wedge \cdots \wedge \neg c_{i,[i+(\frac{n}{2}-2)]_n} \wedge c_{i,[i+(\frac{n}{2}-1)]_n}) f^-_{i,[i+(\frac{n}{2}-1)]_n} \Bigg), \end{aligned} \tag{6.2}$$

where $f^{+}_{i,[j]_n}$ is a positive (clockwise) force and $f^{-}_{i,[j]_n}$ is a negative (counter-clockwise) force. We note that $f^{+}_{i,[j]_n}$ appears only when $c_{i,[j]_n} = 1$ and all $c_{i,[k]_n} = 0$, where $j < k < i + n$. Similary, $f^{-}_{i,[j]_n}$ appears only when $c_{i,[j]_n} = 1$ and all $c_{i,[k]_n} = 0$, where $i < k < j$.

Then, we convert the logic expression into the algebraic expression. For *logical negation*, $\neg c_{i,[j]_n}$ can be algebraically expressed as $(1 - c_{i,[j]_n})$. For *logical and* ($\wedge$), we can express algebraically by using multiplication instead. For example, $c_{i,[j]_n} \wedge c_{i,[k]_n}$ can be expressed as $c_{i,[j]_n} c_{i,[k]_n}$. Therefore, Equation 6.2 can be expressed algebraically as the following,

$$
\begin{aligned}
&\Bigg((c_{i,[i+(n-1)]_n}) f^{+}_{i,[i+(n-1)]_n} + ((1 - c_{i,[i+(n-1)]_n}) c_{i,[i+(n-2)]_n}) f^{+}_{i,[i+(n-2)]_n} \\
&+ ((1 - c_{i,[i+(n-1)]_n})(1 - c_{i,[i+(n-2)]_n}) c_{i,[i+(n-3)]_n}) f^{+}_{i,[i+(n-3)]_n} + \cdots \\
&+ ((1 - c_{i,[i+(n-1)]_n})((1 - c_{i,[i+(n-2)]_n}) \cdots (1 - c_{i,[i+(\frac{n}{2}+2)]_n}) c_{i,[i+(\frac{n}{2}+1)]_n}) f^{+}_{i,[i+(\frac{n}{2}+1)]_n} \Bigg) \\
&- \Bigg((c_{i,[i+1]_n}) f^{-}_{i,[i+1]_n} + ((1 - c_{i,[i+1]_n}) c_{i,[i+2]_n}) f^{-}_{i,[i+2]_n} \\
&+ ((1 - c_{i,[i+1]_n})(1 - c_{i,[i+2]_n}) c_{i,[i+3]_n}) f^{-}_{i,[i+3]_n} + \cdots \\
&+ ((1 - c_{i,[i+1]_n})((1 - c_{i,[i+2]_n}) \cdots (1 - c_{i,[i+(\frac{n}{2}-2)]_n}) c_{i,[i+(\frac{n}{2}-1)]_n}) f^{-}_{i,[i+(\frac{n}{2}-1)]_n} \Bigg) \\
&= \sum_{j=i+(\frac{n}{2}+1)}^{i+(n-1)} f^{+}_{i,[j]_n} c_{i,[j]_n} \prod_{k=1}^{i+n-(j+1)} (1 - c_{i,[i+(n-k)]_n}) - \sum_{j=i+1}^{i+(\frac{n}{2}-1)} f^{-}_{i,[j]_n} c_{i,[j]_n} \prod_{k=1}^{j-1} (1 - c_{i,[i+k]_n}).
\end{aligned}
\tag{6.3}
$$

Let $R^{+}_{i,j}$ be $\prod_{k=1}^{i+n-(j+1)}(1 - c_{i,[i+(n-k)]_n}) \in 0, 1$ and $R^{-}_{i,j}$ be $\prod_{k=1}^{j-1}(1 - c_{i,[i+k]_n}) \in 0, 1$. We derive the following form of the closet component to be used in our analysis,

$$
\sum_{j=i+(\frac{n}{2}+1)}^{i+(n-1)} f^{+}_{i,[j]_n} c_{i,[j]_n} R^{+}_{i,j} - \sum_{j=i+1}^{i+(\frac{n}{2}-1)} f^{-}_{i,[j]_n} c_{i,[j]_n} R^{-}_{i,j}. \tag{6.4}
$$

Resistance component: Respect to the node i's point of view, there is a resistance component originated from node j if the following criteria are satisfied:

- Node i perceives the presence of node j.

- There is at least one node k following node j in the time period ring (in each force direction).
- Node i perceives the presence of node k.

For example, respect to the node 0's point of view, if node 1 is the closest phase neighbor of node 0 and there is node 2 following node 1 in clockwise direction, and node 0 perceives the presence of both node 1 and node 2, then, there is a force difference between node 1 and node 2 in the form of $f_{0,1} - f_{0,2}$ (see Chapter 5). The part $f_{0,1}$ is called *resistance* component and the part $f_{0,2}$ is called *absorption* component which we will describe later. We note that, if there is no node following the closest phase neighbor in each direction, there is no resistance and absorption components.

Therefore, we define the resistance component for node i by using the combination of logic and algebraic expression as follows,

$$
\begin{aligned}
&\Bigg(((c_{i,[i+(n-2)]_n} \vee c_{i,[i+(n-3)]_n} \vee \cdots \vee c_{i,[i+(\frac{n}{2}+1)]_n}) \wedge c_{i,[i+(n-1)]_n}) f^{+}_{i,[i+(n-1)]_n} \\
&+ ((c_{i,[i+(n-3)]_n} \vee c_{i,[i+(n-4)]_n} \vee \cdots \vee c_{i,[i+(\frac{n}{2}+1)]_n}) \wedge c_{i,[i+(n-2)]_n}) f^{+}_{i,[i+(n-2)]_n} \\
&+ \cdots + ((c_{i,[i+(\frac{n}{2}+1)]_n}) \wedge c_{i,[i+(\frac{n}{2}+2)]_n}) f^{+}_{i,[i+(\frac{n}{2}+2)]_n} \Bigg) \\
&- \Bigg(((c_{i,[i+2]_n} \vee c_{i,[i+3]_n} \vee \cdots \vee c_{i,[i+(\frac{n}{2}-1)]_n}) \wedge c_{i,[i+1]_n}) f^{-}_{i,[i+1]_n} \\
&+ ((c_{i,[i+3]_n} \vee c_{i,[i+4]_n} \vee \cdots \vee c_{i,[i+(\frac{n}{2}-1)]_n}) \wedge c_{i,[i+2]_n}) f^{-}_{i,[i+2]_n} \\
&+ \cdots + ((c_{i,[i+(\frac{n}{2}-1)]_n}) \wedge c_{i,[i+(\frac{n}{2}-2)]_n}) f^{-}_{i,[i+(\frac{n}{2}-2)]_n} \Bigg). \qquad (6.5)
\end{aligned}
$$

Then, we convert the logical expression into the algebraic expression.

Let $s^{+}(v^{+}_{i,k})$ be an *algebraic or* function to represent a *logical or* expression of $(c_{i,[i+(n-k)]_n} \vee c_{i,[i+(n-k-1)]_n} \vee \cdots \vee c_{i,[i+(\frac{n}{2}+1)]_n})$, where $v^{+}_{i,k} = c_{i,[i+(\frac{n}{2}+1)]_n} 2^{\frac{n}{2}-1-k} + \cdots + c_{i,[i+(n-k-1)]_n} 2^{1} + c_{i,[i+(n-k)]_n} 2^{0}$.

Similarly, let $s^{-}(v^{-}_{i,k})$ be an algebraic function to represent a *logical or* expression

of $(c_{i,[i+k]_n} \vee c_{i,[i+(k+1)]_n} \vee \cdots \vee c_{i,[i+(\frac{n}{2}-1)]_n})$, where $v^-_{i,k} = c_{i,[i+(\frac{n}{2}-1)]_n} 2^{\frac{n}{2}-1-k} + \cdots + c_{i,[i+(k+1)]_n} 2^1 + c_{i,[i+k]_n} 2^0$.

We note that, if we write a binary string $c_{i,[i+(\frac{n}{2}+1)]_n} \cdots c_{i,[i+(n-k-1)]_n} c_{i,[i+(n-k)]_n}$, v^+_k is an integer value in base 10 of this binary string where $v^+_{i,k} \in \{0, 1, \cdots, 2^{\frac{n}{2}-k} - 1\}$. If all $c_{i,[j]_n} = 0$, then $v^+_{i,k} = 0$. The result is similar for $v^-_{i,k}$.

Let $I_A(x)$ be an indicator function as follows,

$$I_A(x) = \begin{cases} 1 & \text{if } x \in A \\ 0 & \text{if } x \notin A. \end{cases} \tag{6.6}$$

Therefore, $s^+(v^+_{i,k}) = I_{\mathbb{N}-\{0\}}(v^+_{i,k})$ and $s^-(v^-_{i,k}) = I_{\mathbb{N}-\{0\}}(v^-_{i,k})$.

From Equation 6.5, we derive the equivalent algebraic expression as follows,

$$\begin{aligned} &\Big(((s^+(v^+_{i,2}))c_{i,[i+(n-1)]_n}) f^+_{i,[i+(n-1)]_n} + ((s^+(v^+_{i,3}))c_{i,[i+(n-2)]_n}) f^+_{i,[i+(n-2)]_n} \\ &+ \cdots + ((s^+(v^+_{i,\frac{n}{2}-1}))c_{i,[i+(\frac{n}{2}+2)]_n}) f^+_{i,[i+(\frac{n}{2}+2)]_n} \Big) \\ &- \Big(((s^-(v^-_{i,2}))c_{i,[i+1]_n}) f^-_{i,[i+1]_n} + ((s^-(v^-_{i,3}))c_{i,[i+2]_n}) f^-_{i,[i+2]_n} \\ &+ \cdots + ((s^-(v^-_{i,\frac{n}{2}-1}))c_{i,[i+(\frac{n}{2}-2)]_n}) f^-_{i,[i+(\frac{n}{2}-2)]_n} \Big). \end{aligned} \tag{6.7}$$

Let $S^+_{i,j} = s^+(v^+_{i,i+n-j+1}) \in \{0, 1\}$ and $S^-_{i,j} = s^-(v^-_{i,j-i+1}) \in \{0, 1\}$. We derive the following form for the resistance component to be used in our analysis,

$$\sum_{j=i+(\frac{n}{2}+2)}^{i+(n-1)} f^+_{i,[j]_n} c_{i,[j]_n} S^+_{i,j} - \sum_{j=i+1}^{i+(\frac{n}{2}-2)} f^-_{i,[j]_n} c_{i,[j]_n} S^-_{i,j}. \tag{6.8}$$

Absorption component: Respect to the node i's point of view, there is an absorption component originated from node j if the following criteria are satisfied:

- Node i perceives the presence of node j.

- There is at least one node k stays between node i and node j in the time period ring (in each force direction).
- Node i perceives the presence of node k.

Therefore, we define the absorption component for node i by using the combination of logic and algebraic expression as follows,

$$\begin{aligned}
&\Bigg(((c_{i,[i+(n-1)]_n}) \wedge c_{i,[i+(n-2)]_n}) f^{+}_{i,[i+(n-2)]_n} \\
&+ ((c_{i,[i+(n-1)]_n} \vee c_{i,[i+(n-2)]_n}) \wedge c_{i,[i+(n-3)]_n}) f^{+}_{i,[i+(n-3)]_n} \\
&+ \cdots + ((c_{i,[i+(n-1)]_n} \vee c_{i,[i+(n-2)]_n} \vee \cdots \vee c_{i,[i+(\frac{n}{2}+2)]_n}) \wedge c_{i,[i+(\frac{n}{2}+1)]_n}) f^{+}_{i,[i+(\frac{n}{2}+1)]_n} \Bigg) \\
&- \Bigg(((c_{i,[i+1]_n}) \wedge c_{i,[i+2]_n}) f^{-}_{i,[i+2]_n} \\
&+ ((c_{i,[i+1]_n} \vee c_{i,[i+2]_n}) \wedge c_{i,[i+3]_n}) f^{-}_{i,[i+3]_n} \\
&+ \cdots + ((c_{i,[i+1]_n} \vee c_{i,[i+2]_n} \vee \cdots \vee c_{i,[i+(\frac{n}{2}-2)]_n}) \wedge c_{i,[i+(\frac{n}{2}-1)]_n}) f^{-}_{i,[i+(\frac{n}{2}-1)]_n} \Bigg).
\end{aligned} \tag{6.9}$$

Based on the same procedure deriving the resistance component, we derive the following form for the absorption component to be used in our analysis,

$$\sum_{j=i+(\frac{n}{2}+1)}^{i+(n-2)} f^{+}_{i,[j]_n} c_{i,[j]_n} T^{+}_{i,j} - \sum_{j=i+2}^{i+(\frac{n}{2}-1)} f^{-}_{i,[j]_n} c_{i,[j]_n} T^{-}_{i,j}, \tag{6.10}$$

where $T^{+}_{i,j}$ and $T^{-}_{i,j}$ are the algebraic expressions of the *logical or* terms in Equation 6.9.

Therefore, respect to the node i's point of view, the total force at node i is as follows,

$$F_i = \left(\sum_{j=i+(\frac{n}{2}+1)}^{i+(n-1)} f^{+}_{i,[j]_n} c_{i,[j]_n} R^{+}_{i,j} + \sum_{j=i+(\frac{n}{2}+2)}^{i+(n-1)} f^{+}_{i,[j]_n} c_{i,[j]_n} S^{+}_{i,j} - \sum_{j=i+(\frac{n}{2}+1)}^{i+(n-2)} f^{+}_{i,[j]_n} c_{i,[j]_n} T^{+}_{i,j} \right)$$

$$- \left(\sum_{j=i+1}^{i+(\frac{n}{2}-1)} f^-_{i,[j]_n} c_{i,[j]_n} R^-_{i,j} + \sum_{j=i+1}^{i+(\frac{n}{2}-2)} f^-_{i,[j]_n} c_{i,[j]_n} S^-_{i,j} - \sum_{j=i+2}^{i+(\frac{n}{2}-1)} f^-_{i,[j]_n} c_{i,[j]_n} T^-_{i,j} \right). \quad (6.11)$$

In the next section, we analyse the stability of the M-DWARF algorithm based on the derived total force.

6.3 Stability Analysis

As same as the analysis of single-hop networks, to prove that the system is stable, we begin by transforming the system into a non-linear dynamic system.

Let $f^+_{i,j}$ and $f^-_{i,j}$ be the positive and negative forces from node j to node i respectively,

$$f^+_{i,j} = \frac{T}{\sum_{k=j}^{i-1} \Delta_{[k]_n}} \text{ and } f^-_{i,j} = \frac{T}{\sum_{k=i}^{j-1} \Delta_{[k]_n}}, \quad (6.12)$$

where $\Delta_k \in (0, T]$ is the phase difference between node $[k+1]_n$ and node k.

From Equation 6.11, the total force at node i is

$$F_i = \left(\sum_{j=i+(\frac{n}{2}+1)}^{i+(n-1)} f^+_{i,[j]_n} c_{i,[j]_n} R^+_{i,j} + \sum_{j=i+(\frac{n}{2}+2)}^{i+(n-1)} f^+_{i,[j]_n} c_{i,[j]_n} S^+_{i,j} - \sum_{j=i+(\frac{n}{2}+1)}^{i+(n-2)} f^+_{i,[j]_n} c_{i,[j]_n} T^+_{i,j} \right)$$
$$- \left(\sum_{j=i+1}^{i+(\frac{n}{2}-1)} f^-_{i,[j]_n} c_{i,[j]_n} R^-_{i,j} + \sum_{j=i+1}^{i+(\frac{n}{2}-2)} f^-_{i,[j]_n} c_{i,[j]_n} S^-_{i,j} - \sum_{j=i+2}^{i+(\frac{n}{2}-1)} f^-_{i,[j]_n} c_{i,[j]_n} T^-_{i,j} \right). \quad (6.13)$$

Let Δ_i be the current phase difference between node $[i+1]_n$ and node i and Δ'_i be the phase difference between node $[i+1]_n$ and node i in the next time period. The dynamic system of a multi-hop network running the M-DWARF algorithm is as follows:

$$\Delta'_0 = \Delta_0 + KF_1 - KF_0$$
$$\Delta'_1 = \Delta_1 + KF_2 - KF_1$$
$$\vdots$$

$$\Delta'_{n-1} = \Delta_{n-1} + KF_0 - KF_{n-1} \tag{6.14}$$

We write the transition of Δ_i in a general form as the following,

$$\Delta'_i = \Delta_i + KF_{[i+1]_n} - KF_i. \tag{6.15}$$

Then, we linearly approximate the dynamic system at the equilibrium.

6.3.1 Linear Approximation

The Jacobian (J) of a difference equations system is defined as follows:

$$J = \begin{pmatrix} \frac{\partial \Delta'_0}{\partial \Delta_0} & \frac{\partial \Delta'_0}{\partial \Delta_1} & \cdots & \frac{\partial \Delta_{0'}}{\partial \Delta_{n-1}} \\ \frac{\partial \Delta'_1}{\partial \Delta_0} & \frac{\partial \Delta'_1}{\partial \Delta_1} & \cdots & \frac{\partial \Delta'_1}{\partial \Delta_{n-1}} \\ \vdots & \vdots & \ddots & \vdots \\ \frac{\partial \Delta'_{n-1}}{\partial \Delta_0} & \frac{\partial \Delta'_{n-1}}{\partial \Delta_1} & \cdots & \frac{\partial \Delta'_{n-1}}{\partial \Delta_{n-1}} \end{pmatrix} \tag{6.16}$$

Therefore, from Equation 6.15, each element in a row of Jacobian is

$$\frac{\partial \Delta'_i}{\partial \Delta_p} = \frac{\partial \Delta_i}{\partial \Delta_p} + K\frac{\partial F_{[i+1]_n}}{\partial \Delta_p} - K\frac{\partial F_i}{\partial \Delta_p}, p \in \{0, 1, \cdots, n-1\}. \tag{6.17}$$

For the first term, $\frac{\partial \Delta_i}{\partial \Delta_p}$ is 1 if $p = i$. . If $p \neq i$, this term is zero. Formally,

$$\frac{\partial \Delta_i}{\partial \Delta_p} = \begin{cases} 1 & \text{if } p = i \\ 0 & \text{otherwise.} \end{cases} \tag{6.18}$$

Then, we find $\frac{\partial F_i}{\partial \Delta_p}$ as follows:

$$\frac{\partial F_i}{\partial \Delta_i} = T\left(\sum_{j=i+2}^{i+(\frac{n}{2}-2)} \frac{c_{i,[j]_n}(R_{i,j} + S_{i,j} - T_{i,j})}{(\sum_{k=i}^{j-1} \Delta_{[k]_n})^2} \right.$$

$$
\begin{aligned}
&+\frac{c_{i,[i+(\frac{n}{2}-1)]_n}(R_{i,i+(\frac{n}{2}-1)}-T_{i,i+(\frac{n}{2}-1)})}{(\sum_{k=i}^{i+(\frac{n}{2}-2)}\Delta_{[k]_n})^2}\\
&+\frac{c_{i,[i+1]_n}(R_{i,i+1}+S_{i,i+1})}{(\Delta_i)^2}\Bigg)\\
\frac{\partial F_i}{\partial \Delta_{[m]_n}} &= T\Bigg(\sum_{j=m+1}^{i+(\frac{n}{2}-2)}\frac{c_{i,[j]_n}(R_{i,j}+S_{i,j}-T_{i,j})}{(\sum_{k=i}^{j-1}\Delta_{[k]_n})^2}\\
&+\frac{c_{i,[i+(\frac{n}{2}-1)]_n}(R_{i,i+(\frac{n}{2}-1)}-T_{i,i+(\frac{n}{2}-1)})}{(\sum_{k=i}^{i+(\frac{n}{2}-2)}\Delta_{[k]_n})^2}\Bigg),\\
&\text{for } m=i+1,i+2,\cdots,i+(\frac{n}{2}-3)\\
\frac{\partial F_i}{\partial \Delta_{[i+(\frac{n}{2}-2)]_n}} &= T\Bigg(\frac{c_{i,[i+(\frac{n}{2}-1)]_n}(R_{i,i+(\frac{n}{2}-1)}-T_{i,i+(\frac{n}{2}-1)})}{(\sum_{k=i}^{i+(\frac{n}{2}-2)}\Delta_{[k]_n})^2}\Bigg)\\
\frac{\partial F_i}{\partial \Delta_{[m]_n}} &= 0,\ \text{for } m=i+(\frac{n}{2}-1),i+\frac{n}{2}\\
\frac{\partial F_i}{\partial \Delta_{[i+(\frac{n}{2}+1)]_n}} &= T\Bigg(-\frac{c_{i,[i+(\frac{n}{2}+1)]_n}(R_{i,i+(\frac{n}{2}+1)}-T_{i,i+(\frac{n}{2}+1)})}{(\sum_{k=i+(\frac{n}{2}+1)}^{i+(n-1)}\Delta_{[k]_n})^2}\Bigg)\\
\frac{\partial F_i}{\partial \Delta_{[m]_n}} &= T\Bigg(-\sum_{j=i+(\frac{n}{2}+2)}^{m}\frac{c_{i,[j]_n}(R_{i,j}+S_{i,j}-T_{i,j})}{(\sum_{k=j}^{i-1}\Delta_{[k]_n})^2}\\
&-\frac{c_{i,[i+(\frac{n}{2}+1)]_n}(R_{i,i+(\frac{n}{2}+1)}-T_{i,i+(\frac{n}{2}+1)})}{(\sum_{k=i+(\frac{n}{2}+1)}^{i+(n-1)}\Delta_{[k]_n})^2}\Bigg),\\
&\text{for } m=i+(\frac{n}{2}+2),i+(\frac{n}{2}+3),\cdots,i+(n-2)\\
\frac{\partial F_i}{\partial \Delta_{[i+(n-1)]_n}} &= T\Bigg(-\sum_{j=i+(\frac{n}{2}+2)}^{i+(n-2)}\frac{c_{i,[j]_n}(R_{i,j}+S_{i,j}-T_{i,j})}{(\sum_{k=j}^{i-1}\Delta_{[k]_n})^2}\\
&-\frac{c_{i,[i+(\frac{n}{2}+1)]_n}(R_{i,i+(\frac{n}{2}+1)}-T_{i,i+(\frac{n}{2}+1)})}{(\sum_{k=i+(\frac{n}{2}+1)}^{i+(n-1)}\Delta_{[k]_n})^2}\\
&+\frac{c_{i,[i+(n-1)]_n}(R_{i,i+(n-1)}+S_{i,i+(n-1)})}{(\Delta_{[i+(n-1)]_n})^2}\Bigg). \qquad (6.19)
\end{aligned}
$$

For $\frac{\partial F_{[i+1]_n}}{\partial \Delta_p}$, we can find by replacing i with $i+1$ in Equation 6.19. The result is as follows:

$$
\frac{\partial F_{[i+1]_n}}{\partial \Delta_{[i+1]_n}} = T\Bigg(\sum_{j=i+3}^{i+(\frac{n}{2}-1)}\frac{c_{[i+1]_n,[j]_n}(R_{i+1,j}+S_{i+1,j}-T_{i+1,j})}{(\sum_{k=i+1}^{j-1}\Delta_{[k]_n})^2}
$$

$$+\frac{c_{[i+1]_n,[i+\frac{n}{2}]_n}(R_{i+1,i+\frac{n}{2}}-T_{i+1,i+\frac{n}{2}})}{(\sum_{k=i+1}^{i+(\frac{n}{2}-1)}\Delta_{[k]_n})^2}$$
$$+\frac{c_{[i+1]_n,[i+2]_n}(R_{i+1,i+2}+S_{i+1,i+2})}{(\Delta_{[i+1]_n})^2}\Bigg)$$

$$\frac{\partial F_{[i+1]_n}}{\partial \Delta_{[m]_n}}=T\Bigg(\sum_{j=m+1}^{i+(\frac{n}{2}-1)}\frac{c_{[i+1]_n,[j]_n}(R_{i+1,j}+S_{i+1,j}-T_{i+1,j})}{(\sum_{k=i+1}^{j-1}\Delta_{[k]_n})^2}$$
$$+\frac{c_{[i+1]_n,[i+\frac{n}{2}]_n}(R_{i+1,i+\frac{n}{2}}-T_{i+1,i+\frac{n}{2}})}{(\sum_{k=i+1}^{i+(\frac{n}{2}-1)}\Delta_{[k]_n})^2}\Bigg),$$
$$\text{for } m=i+2,i+3,\cdots,i+(\frac{n}{2}-2)$$

$$\frac{\partial F_{[i+1]_n}}{\partial \Delta_{i+(\frac{n}{2}-1)}}=T\Bigg(\frac{c_{[i+1]_n,[i+\frac{n}{2}]_n}(R_{i+1,i+\frac{n}{2}}-T_{i+1,i+\frac{n}{2}})}{(\sum_{k=i+1}^{i+(\frac{n}{2}-1)}\Delta_{[k]_n})^2}\Bigg)$$

$$\frac{\partial F_{[i+1]_n}}{\partial \Delta_{[}m]_n}=0,\ \text{for } m=i+\frac{n}{2},i+(\frac{n}{2}+1)$$

$$\frac{\partial F_{[i+1]_n}}{\partial \Delta_{[i+(\frac{n}{2}+2)]_n}}=T\Bigg(-\frac{c_{[i+1]_n,[i+(\frac{n}{2}+2)]_n}(R_{i+1,i+(\frac{n}{2}+2)}-T_{i+1,i+(\frac{n}{2}+2)})}{(\sum_{k=i+(\frac{n}{2}+2)}^{i+n}\Delta_{[k]_n})^2}\Bigg)$$

$$\frac{\partial F_{[i+1]_n}}{\partial \Delta_{[m]_n}}=T\Bigg(-\sum_{j=i+(\frac{n}{2}+3)}^{m}\frac{c_{[i+1]_n,[j]_n}(R_{i+1,j}+S_{i+1,j}-T_{i+1,j})}{(\sum_{k=j}^{i}\Delta_{[k]_n})^2}$$
$$-\frac{c_{[i+1]_n,[i+(\frac{n}{2}+2)]_n}(R_{i+1,i+(\frac{n}{2}+2)}-T_{i+1,i+(\frac{n}{2}+2)})}{(\sum_{k=i+(\frac{n}{2}+2)}^{i+n}\Delta_{[k]_n})^2}\Bigg),$$
$$\text{for } m=i+(\frac{n}{2}+3),i+(\frac{n}{2}+4),\cdots,i+(n-1)$$

$$\frac{\partial F_{[i+1]_n}}{\partial \Delta_i}=T\Bigg(-\sum_{j=i+(\frac{n}{2}+3)}^{i+(n-1)}\frac{c_{[i+1]_n,[j]_n}(R_{i+1,j}+S_{i+1,j}-T_{i+1,j})}{(\sum_{k=j}^{i}\Delta_{[k]_n})^2}$$
$$-\frac{c_{[i+1]_n,[i+(\frac{n}{2}+2)]_n}(R_{i+1,i+(\frac{n}{2}+2)}-T_{i+1,i+(\frac{n}{2}+2)})}{(\sum_{k=i+(\frac{n}{2}+2)}^{i+n}\Delta_{[k]_n})^2}$$
$$-\frac{c_{[i+1]_n,i}(R_{i+1,i}+S_{i+1,i})}{(\Delta_i)^2}\Bigg). \tag{6.20}$$

Consequently, from Equation 6.17, 6.18, 6.19, and 6.20, we find $\frac{\partial \Delta_i'}{\partial \Delta_p}$ as the following:

$$\frac{\partial \Delta_i'}{\partial \Delta_i}=1+KT\Bigg(-\sum_{j=i+(\frac{n}{2}+3)}^{i+(n-1)}\frac{c_{[i+1]_n,[j]_n}(R_{i+1,j}+S_{i+1,j}-T_{i+1,j})}{(\sum_{k=j}^{i}\Delta_{[k]_n})^2}$$
$$-\frac{c_{[i+1]_n,[i+(\frac{n}{2}+2)]_n}(R_{i+1,i+(\frac{n}{2}+2)}-T_{i+1,i+(\frac{n}{2}+2)})}{(\sum_{k=i+(\frac{n}{2}+2)}^{i+n}\Delta_{[k]_n})^2}$$

$$
\begin{aligned}
&- \frac{c_{[i+1]_n,i}(R_{i+1,i}+S_{i+1,i})}{(\Delta_i)^2} \\
&- \sum_{j=i+2}^{i+(\frac{n}{2}-2)} \frac{c_{i,[j]_n}(R_{i,j}+S_{i,j}-T_{i,j})}{(\sum_{k=i}^{j-1}\Delta_{[k]_n})^2} \\
&- \frac{c_{i,[i+(\frac{n}{2}-1)]_n}(R_{i,i+(\frac{n}{2}-1)}-T_{i,i+(\frac{n}{2}-1)})}{(\sum_{k=i}^{i+(\frac{n}{2}-2)}\Delta_{[k]_n})^2} \\
&- \frac{c_{i,[i+1]_n}(R_{i,i+1}+S_{i,i+1})}{(\Delta_i)^2}\Bigg)
\end{aligned}
$$

$$
\begin{aligned}
\frac{\partial\Delta_i'}{\partial\Delta_{[i+1]_n}} = KT\Bigg(&\sum_{j=i+3}^{i+(\frac{n}{2}-1)} \frac{c_{[i+1]_n,[j]_n}(R_{i+1,j}+S_{i+1,j}-T_{i+1,j})}{(\sum_{k=i+1}^{j-1}\Delta_{[k]_n})^2} \\
&+ \frac{c_{[i+1]_n,[i+\frac{n}{2}]_n}(R_{i+1,i+\frac{n}{2}}-T_{i+1,i+\frac{n}{2}})}{(\sum_{k=i+1}^{i+(\frac{n}{2}-1)}\Delta_{[k]_n})^2} \\
&+ \frac{c_{[i+1]_n,[i+2]_n}(R_{i+1,i+2}+S_{i+1,i+2})}{(\Delta_{[i+1]_n})^2} \\
&- \sum_{j=i+2}^{i+(\frac{n}{2}-2)} \frac{c_{i,[j]_n}(R_{i,j}+S_{i,j}-T_{i,j})}{(\sum_{k=i}^{j-1}\Delta_{[k]_n})^2} \\
&- \frac{c_{i,[i+(\frac{n}{2}-1)]_n}(R_{i,[i+(\frac{n}{2}-1)]_n}-T_{i,i+(\frac{n}{2}-1)})}{(\sum_{k=i}^{i+(\frac{n}{2}-2)}\Delta_{[k]_n})^2}\Bigg)
\end{aligned}
$$

$$
\begin{aligned}
\frac{\partial\Delta_i'}{\partial\Delta_{[m]_n}} = KT\Bigg(&\sum_{j=m+1}^{i+(\frac{n}{2}-1)} \frac{c_{[i+1]_n,[j]_n}(R_{i+1,j}+S_{i+1,j}-T_{i+1,j})}{(\sum_{k=i+1}^{j-1}\Delta_{[k]_n})^2} \\
&+ \frac{c_{[i+1]_n,[i+\frac{n}{2}]_n}(R_{i+1,i+\frac{n}{2}}-T_{i+1,i+\frac{n}{2}})}{(\sum_{k=i+1}^{i+(\frac{n}{2}-1)}\Delta_{[k]_n})^2} \\
&- \sum_{j=m+1}^{i+(\frac{n}{2}-2)} \frac{c_{i,[j]_n}(R_{i,j}+S_{i,j}-T_{i,j})}{(\sum_{k=i}^{j-1}\Delta_{[k]_n})^2} \\
&- \frac{c_{i,[i+(\frac{n}{2}-1)]_n}(R_{i,i+(\frac{n}{2}-1)}-T_{i,i+(\frac{n}{2}-1)})}{(\sum_{k=i}^{i+(\frac{n}{2}-2)}\Delta_{[k]_n})^2},\Bigg),
\end{aligned}
$$

$$
\text{for } m = i+2, i+3, \cdots, i+(\frac{n}{2}-3)
$$

$$
\begin{aligned}
\frac{\partial\Delta_i'}{\partial\Delta_{[i+(\frac{n}{2}-2)]_n}} = KT\Bigg(&\frac{c_{[i+1]_n,[i+(\frac{n}{2}-1)]_n}(R_{i+1,i+(\frac{n}{2}-1)}+S_{i+1,i+(\frac{n}{2}-1)}-T_{i+1,i+(\frac{n}{2}-1)})}{(\sum_{k=i+1}^{i+(\frac{n}{2}-2)}\Delta_{[k]_n})^2} \\
&+ \frac{c_{[i+1]_n,[i+\frac{n}{2}]_n}(R_{i+1,i+\frac{n}{2}}-T_{i+1,i+\frac{n}{2}})}{(\sum_{k=i+1}^{i+(\frac{n}{2}-1)}\Delta_{[k]_n})^2} \\
&- \frac{c_{i,[i+(\frac{n}{2}-1)]_n}(R_{i,i+(\frac{n}{2}-1)}-T_{i,i+(\frac{n}{2}-1)})}{(\sum_{k=i}^{i+(\frac{n}{2}-2)}\Delta_{[k]_n})^2}\Bigg)
\end{aligned}
$$

$$
\begin{aligned}
\frac{\partial \Delta_i'}{\partial \Delta_{i+(\frac{n}{2}-1)}} &= KT\left(\frac{c_{[i+1]_n,[i+\frac{n}{2}]_n}(R_{i+1,i+\frac{n}{2}} - T_{i+1,i+\frac{n}{2}})}{(\sum_{k=i+1}^{i+(\frac{n}{2}-1)} \Delta_{[k]_n})^2}\right) \\
\frac{\partial \Delta_i'}{\partial \Delta_{[i+\frac{n}{2}]_n}} &= 0 \\
\frac{\partial \Delta_i'}{\partial \Delta_{[i+(\frac{n}{2}+1)]_n}} &= KT\left(\frac{c_{i,[i+(\frac{n}{2}+1)]_n}(R_{i,i+(\frac{n}{2}+1)} - T_{i,i+(\frac{n}{2}+1)})}{(\sum_{k=i+(\frac{n}{2}+1)}^{i+(n-1)} \Delta_{[k]_n})^2}\right) \\
\frac{\partial \Delta_i'}{\partial \Delta_{i+(\frac{n}{2}+2)}} &= KT\Bigg(-\frac{c_{[i+1]_n,[i+(\frac{n}{2}+2)]_n}(R_{i+1,i+(\frac{n}{2}+2)} - T_{i+1,i+(\frac{n}{2}+2)})}{(\sum_{k=i+(\frac{n}{2}+2)}^{i+n} \Delta_{[k]_n})^2} \\
&\quad + \frac{c_{i,[i+(\frac{n}{2}+2)]_n}(R_{i,i+(\frac{n}{2}+2)} + S_{i,i+(\frac{n}{2}+2)} - T_{i,i+(\frac{n}{2}+2)})}{(\sum_{k=i+(\frac{n}{2}+2)}^{i+(n-1)} \Delta_{[k]_n})^2} \\
&\quad + \frac{c_{i,[i+(\frac{n}{2}+1)]_n}(R_{i,i+(\frac{n}{2}+1)} - T_{i,i+(\frac{n}{2}+1)})}{(\sum_{k=i+(\frac{n}{2}+1)}^{i+(n-1)} \Delta_{[k]_n})^2}\Bigg) \\
\frac{\partial \Delta_i'}{\partial \Delta_{[m]_n}} &= KT\Bigg(-\sum_{j=i+(\frac{n}{2}+3)}^{m} \frac{c_{[i+1]_n,[j]_n}(R_{i+1,j} + S_{i+1,j} - T_{i+1,j})}{(\sum_{k=j}^{i} \Delta_{[k]_n})^2} \\
&\quad - \frac{c_{[i+1]_n,[i+(\frac{n}{2}+2)]_n}(R_{i+1,i+(\frac{n}{2}+2)} - T_{i+1,i+(\frac{n}{2}+2)})}{(\sum_{k=i+(\frac{n}{2}+2)}^{i+n} \Delta_{[k]_n})^2} \\
&\quad + \sum_{j=i+(\frac{n}{2}+2)}^{m} \frac{c_{i,[j]_n}(R_{i,j} + S_{i,j} - T_{i,j})}{(\sum_{k=j}^{i+(n-1)} \Delta_{[k]_n})^2} \\
&\quad + \frac{c_{i,[i+(\frac{n}{2}+1)]_n}(R_{i,i+(\frac{n}{2}+1)} - T_{i,i+(\frac{n}{2}+1)})}{(\sum_{k=i+(\frac{n}{2}+1)}^{i+(n-1)} \Delta_{[k]_n})^2}\Bigg), \\
&\quad \text{for } m = i + (\frac{n}{2}+3), i + (\frac{n}{2}+4), \cdots, i + (n-2) \\
\frac{\partial \Delta_i'}{\partial \Delta_{[i+(n-1)]_n}} &= KT\Bigg(-\sum_{j=i+(\frac{n}{2}+3)}^{i+(n-1)} \frac{c_{[i+1]_n,[j]_n}(R_{i+1,j} + S_{i+1,j} - T_{i+1,j})}{(\sum_{k=j}^{i} \Delta_{[k]_n})^2} \\
&\quad - \frac{c_{[i+1]_n,[i+(\frac{n}{2}+2)]_n}(R_{i+1,i+(\frac{n}{2}+2)} - T_{i+1,i+(\frac{n}{2}+2)})}{(\sum_{k=i+(\frac{n}{2}+2)}^{i+n} \Delta_{[k]_n})^2} \\
&\quad + \sum_{j=i+(\frac{n}{2}+2)}^{i+(n-2)} \frac{c_{i,[j]_n}(R_{i,j} + S_{i,j} - T_{i,j})}{(\sum_{k=j}^{i+(n-1)} \Delta_{[k]_n})^2} \\
&\quad + \frac{c_{i,[i+(\frac{n}{2}+1)]_n}(R_{i,i+(\frac{n}{2}+1)} - T_{i,i+(\frac{n}{2}+1)})}{(\sum_{k=i+(\frac{n}{2}+1)}^{i+(n-1)} \Delta_{[k]_n})^2} \\
&\quad + \frac{c_{i,[i+(n-1)]_n}(R_{i,i+(n-1)} + S_{i,i+(n-1)})}{(\Delta_{[i+(n-1)]_n})^2}\Bigg).
\end{aligned} \tag{6.21}
$$

At this point, we already get the general form of each row of the Jacobian matrix.

To locally approximate at the equilibrium, we have to substitute $c_{i,j}, R_{i,j}, S_{i,j}, T_{i,j}$, and Δ_i for all $i, j \in 0, 1, \cdots, n-1$ where $j \neq i$ with the value at the equilibrium state. Then, we have find the maximum value of n that bounds the eigenvalues within a unit circle to guarantee the stability. However, such values depend on the topology. For example, the connectivity $c_{i,j}$ depends on whether node i can perceive the presence of node j or not. If node i and j are within two-hop communication, this value is 1, otherwise, this value is 0.

In this dissertation, we prove the stability of the multi-hop star topology as an example because this topology is less complicated to prove and may be the easiest example for the reader to follow the proof. For other topologies, we conjecture that the local stability can also be assured as well.

For the multi-hop star topology, the time interval between arbitrary two consecutive nodes is T/n at the equilibrium. Therefore, each row of the Jacobian matrix from Equation 6.21 is changed by substituting all Δ_k with T/n and re-indexing the summation as follows,

$$
\begin{aligned}
\frac{\partial \Delta_i'}{\partial \Delta_i} = 1 + \frac{Kn^2}{T}\Bigg(& - \frac{c_{[i+1]_n,[i+(\frac{n}{2}+2)]_n}(R_{i+1,i+(\frac{n}{2}+2)} - T_{i+1,i+(\frac{n}{2}+2)})}{(\frac{n}{2}-1)^2} \\
& - \frac{c_{[i+1]_n,[i]_n}(R_{i+1,i} + S_{i+1,i})}{1^2} \\
& - \sum_{j=2}^{\frac{n}{2}-2} \frac{c_{[i+1]_n,[i+(n+1-j)]_n}(R_{i+1,i+(n+1-j)} + S_{i+1,i+(n+1-j)} - T_{i+1,i+(n+1-j)})}{j^2} \\
& - \sum_{j=2}^{\frac{n}{2}-2} \frac{c_{i,[i+j]_n}(R_{i,i+j} + S_{i,i+j} - T_{i,i+j})}{j^2} \\
& - \frac{c_{i,[i+(\frac{n}{2}-1)]_n}(R_{i,i+(\frac{n}{2}-1)} - T_{i,i+(\frac{n}{2}-1)})}{(\frac{n}{2}-1)^2} \\
& - \frac{c_{i,[i+1]_n}(R_{i,i+1} + S_{i,i+1})}{1^2}\Bigg)
\end{aligned}
$$

$$
\begin{aligned}
\frac{\partial \Delta_i'}{\partial \Delta_{[i+1]_n}} = \frac{Kn^2}{T}\Bigg(& \sum_{j=2}^{\frac{n}{2}-2} \frac{c_{[i+1]_n,[i+1+j]_n}(R_{i+1,i+1+j} + S_{i+1,i+1+j} - T_{i+1,i+1+j})}{j^2} \\
& + \frac{c_{[i+1]_n,[i+\frac{n}{2}]_n}(R_{i+1,i+\frac{n}{2}} - T_{i+1,i+\frac{n}{2}})}{(\frac{n}{2}-1)^2}
\end{aligned}
$$

$$
\begin{aligned}
&+\frac{c_{[i+1]_n,[i+2]_n}(R_{i+1,i+2}+S_{i+1,i+2})}{1^2}\\
&-\sum_{j=2}^{\frac{n}{2}-2}\frac{c_{i,[i+j]_n}(R_{i,i+j}+S_{i,i+j}-T_{i,i+j})}{j^2}\\
&-\frac{c_{i,[i+(\frac{n}{2}-1)]_n}(R_{i,i+(\frac{n}{2}-1)}-T_{i,i+(\frac{n}{2}-1)})}{(\frac{n}{2}-1)^2}\Bigg)\\
\frac{\partial\Delta_i'}{\partial\Delta_{[m]_n}}=&\frac{Kn^2}{T}\Bigg(\sum_{j=m-i}^{\frac{n}{2}-2}\frac{c_{[i+1]_n,[i+1+j]_n}(R_{i+1,i+1+j}+S_{i+1,i+1+j}-T_{i+1,i+1+j})}{j^2}\\
&+\frac{c_{[i+1]_n,[i+\frac{n}{2}]_n}(R_{i+1,i+\frac{n}{2}}-T_{i+1,i+\frac{n}{2}})}{(\frac{n}{2}-1)^2}\\
&-\sum_{j=m-i+1}^{\frac{n}{2}-2}\frac{c_{i,[i+j]_n}(R_{i,i+j}+S_{i,i+j}-T_{i,i+j})}{j^2}\\
&-\frac{c_{i,[i+(\frac{n}{2}-1)]_n}(R_{i,i+(\frac{n}{2}-1)}-T_{i,i+(\frac{n}{2}-1)})}{(\frac{n}{2}-1)^2}\Bigg)\\
&\text{for } m=i+2,i+3,\cdots,i+(\frac{n}{2}-3)\\
\frac{\partial\Delta_i'}{\partial\Delta_{[i+(\frac{n}{2}-2)]_n}}=&\frac{Kn^2}{T}\Bigg(\frac{c_{[i+1]_n,[i+(\frac{n}{2}-1)]_n}(R_{i+1,i+(\frac{n}{2}-1)}+S_{i+1,i+(\frac{n}{2}-1)}-T_{i+1,i+(\frac{n}{2}-1)})}{(\frac{n}{2}-2)^2}\\
&+\frac{c_{[i+1]_n,[i+\frac{n}{2}]_n}(R_{i+1,i+\frac{n}{2}}-T_{i+1,i+\frac{n}{2}})}{(\frac{n}{2}-1)^2}\\
&-\frac{c_{i,[i+(\frac{n}{2}-1)]_n}(R_{i,i+(\frac{n}{2}-1)}-T_{i,i+(\frac{n}{2}-1)})}{(\frac{n}{2}-1)^2}\Bigg)\\
\frac{\partial\Delta_i'}{\partial\Delta_{[i+(\frac{n}{2}-1)]_n}}=&\frac{Kn^2}{T}\Bigg(\frac{c_{[i+1]_n,[i+\frac{n}{2}]_n}(R_{i+1,i+\frac{n}{2}}-T_{i+1,i+\frac{n}{2}})}{(\frac{n}{2}-1)^2}\Bigg)\\
\frac{\partial\Delta_i'}{\partial\Delta_{[i+\frac{n}{2}]_n}}=&0\\
\frac{\partial\Delta_i'}{\partial\Delta_{[i+(\frac{n}{2}+1)]_n}}=&\frac{Kn^2}{T}\Bigg(\frac{c_{i,[i+(\frac{n}{2}+1)]_n}(R_{i,i+(\frac{n}{2}+1)}-T_{i,i+(\frac{n}{2}+1)})}{(\frac{n}{2}-1)^2}\Bigg)\\
\frac{\partial\Delta_i'}{\partial\Delta_{[i+(\frac{n}{2}+2)]_n}}=&\frac{Kn^2}{T}\Bigg(-\frac{c_{[i+1]_n,[i+(\frac{n}{2}+2)]_n}(R_{i+1,i+(\frac{n}{2}+2)}-T_{i+1,i+(\frac{n}{2}+2)})}{(\frac{n}{2}-1)^2}\\
&+\frac{c_{i,[i+(\frac{n}{2}+2)]_n}(R_{i,i+(\frac{n}{2}+2)}+S_{i,i+(\frac{n}{2}+2)}-T_{i,i+(\frac{n}{2}+2)})}{(\frac{n}{2}-2)^2}\\
&+\frac{c_{i,[i+(\frac{n}{2}+1)]_n}(R_{i,i+(\frac{n}{2}+1)}-T_{i,i+(\frac{n}{2}+1)})}{(\frac{n}{2}-1)^2}\Bigg)\\
\frac{\partial\Delta_i'}{\partial\Delta_{[m]_n}}=&\frac{Kn^2}{T}\Bigg(-\frac{c_{[i+1]_n,[i+(\frac{n}{2}+2)]_n}(R_{i+1,i+(\frac{n}{2}+2)}-T_{i+1,i+(\frac{n}{2}+2)})}{(\frac{n}{2}-1)^2}
\end{aligned}
$$

$$
\begin{aligned}
&- \sum_{j=i+n-m+1}^{\frac{n}{2}-2} \frac{c_{[i+1]_n,[j-\frac{n}{2}+2+m]_n}(R_{i+1,j-\frac{n}{2}+2+m} + S_{i+1,j-\frac{n}{2}+2+m} - T_{i+1,j-\frac{n}{2}+2+m})}{j^2} \\
&+ \sum_{j=i+n-m}^{\frac{n}{2}-2} \frac{c_{i,[j-\frac{n}{2}+2+m]_n}(R_{i,j-\frac{n}{2}+2+m} + S_{i,j-\frac{n}{2}+2+m} - T_{i,j-\frac{n}{2}+2+m})}{j^2} \\
&+ \frac{c_{i,[i+(\frac{n}{2}+1)]_n}(R_{i,i+(\frac{n}{2}+1)} - T_{i,i+(\frac{n}{2}+1)})}{(\frac{n}{2}-1)^2}\Bigg), \\
&\text{for } m = i+(\frac{n}{2}+3), i+(\frac{n}{2}+4), \cdots, i+(n-2)
\end{aligned}
$$

$$
\begin{aligned}
\frac{\partial \Delta_i'}{\partial \Delta_{[i+(n-1)]_n}} = \frac{Kn^2}{T}\Bigg(&- \frac{c_{[i+1]_n,[i+(\frac{n}{2}+2)]_n}(R_{i+1,i+(\frac{n}{2}+2)} - T_{i+1,i+(\frac{n}{2}+2)})}{(\frac{n}{2}-1)^2} \\
&- \sum_{j=2}^{\frac{n}{2}-2} \frac{c_{[i+1]_n,[i+\frac{n}{2}+1+j]_n}(R_{i+1,i+\frac{n}{2}+1+j} + S_{i+1,i+\frac{n}{2}+1+j} - T_{i+1,i+\frac{n}{2}+1+j})}{j^2} \\
&+ \sum_{j=2}^{\frac{n}{2}-2} \frac{c_{i,[i+\frac{n}{2}+j]_n}(R_{i,i+\frac{n}{2}+j} + S_{i,i+\frac{n}{2}+j} - T_{i,i+\frac{n}{2}+j})}{j^2} \\
&+ \frac{c_{i,[i+(\frac{n}{2}+1)]_n}(R_{i,i+(\frac{n}{2}+1)} - T_{i,i+(\frac{n}{2}+1)})}{(\frac{n}{2}-1)^2} \\
&+ \frac{c_{i,[i+(n-1)]_n}(R_{i,i+(n-1)} + S_{i,i+(n-1)})}{1^2}\Bigg).
\end{aligned}
$$

Then, for the star topology, nodes perceive the presence of all two-hop neighbors. Therefore, all terms $c_{i,j}, R_{i,j}, S_{i,j}$, and $T_{i,j}$ are 1. Consequently, the row of the Jacobian matrix at the equilibrium is the following:

$$
\begin{aligned}
\frac{\partial \Delta_i'}{\partial \Delta_i} &= 1 + \frac{Kn^2}{T}\Bigg(- \sum_{j=2}^{\frac{n}{2}-2} \frac{1}{j^2} - 0 - \frac{2}{1^2} - \sum_{j=2}^{\frac{n}{2}-2} \frac{1}{j^2} - 0 - \frac{2}{1^2}\Bigg) \\
&= 1 - \frac{2Kn^2}{T}\Bigg(1 + \sum_{j=1}^{n-2} \frac{1}{j^2}\Bigg) \\
\frac{\partial \Delta_i'}{\partial \Delta_{[i+1]_n}} &= \frac{Kn^2}{T}\Bigg(\sum_{j=2}^{\frac{n}{2}-2} \frac{1}{j^2} + 0 + 2 - \sum_{j=2}^{\frac{n}{2}-2} \frac{1}{j^2} - 0\Bigg) = \frac{2Kn^2}{T} \\
\frac{\partial \Delta_i'}{\partial \Delta_{[m]_n}} &= \frac{Kn^2}{T}\Bigg(\sum_{j=m-i}^{\frac{n}{2}-2} \frac{1}{j^2} + 0 - \sum_{j=m-i+1}^{\frac{n}{2}-2} \frac{1}{j^2} - 0\Bigg) = \frac{Kn^2}{T(m-i)^2} \\
&\text{for } m = i+2, i+3, \cdots, i+(\frac{n}{2}-3)
\end{aligned}
$$

$$\frac{\partial \Delta_i'}{\partial \Delta_{[i+(\frac{n}{2}-2)]_n}} = \frac{Kn^2}{T}\left(\frac{1}{(\frac{n}{2}-2)^2}+0-0\right) = \frac{Kn^2}{T(\frac{n}{2}-2)^2}$$

$$\frac{\partial \Delta_i'}{\partial \Delta_{[i+(\frac{n}{2}-1)]_n}} = 0$$

$$\frac{\partial \Delta_i'}{\partial \Delta_{[i+\frac{n}{2}]_n}} = 0$$

$$\frac{\partial \Delta_i'}{\partial \Delta_{[i+(\frac{n}{2}+1)]_n}} = 0$$

$$\frac{\partial \Delta_i'}{\partial \Delta_{[i+(\frac{n}{2}+2)]_n}} = \frac{Kn^2}{T}\left(-0+\frac{1}{(\frac{n}{2}-2)^2}+0\right) = \frac{Kn^2}{T(\frac{n}{2}-2)^2}$$

$$\frac{\partial \Delta_i'}{\partial \Delta_{[m]_n}} = \frac{Kn^2}{T}\left(-\sum_{j=i+n-m+1}^{\frac{n}{2}-2}\frac{1}{j^2}-0+\sum_{j=i+n-m}^{\frac{n}{2}-2}\frac{1}{j^2}+0\right) = \frac{Kn^2}{T(i+n-m)^2},$$

$$\text{for } m = i+(\frac{n}{2}+3), i+(\frac{n}{2}+4), \cdots, i+(n-2)$$

$$\frac{\partial \Delta_i'}{\partial \Delta_{[i+(n-1)]_n}} = \frac{Kn^2}{T}\left(-\sum_{j=2}^{\frac{n}{2}-2}\frac{1}{j^2}-0+\sum_{j=2}^{\frac{n}{2}-2}\frac{1}{j^2}+0+\frac{2}{1^2}\right) = \frac{2Kn^2}{T}. \tag{6.22}$$

The result of the Jacobian matrix at the equilibrium is the circulant matrix as shown below:

$$\begin{pmatrix}
D_0 & 2A & \cdots & \frac{A}{(\frac{n}{2}-2)^2} & 0 & 0 & 0 & \frac{A}{(\frac{n}{2}-2)^2} & \cdots & \frac{A}{2^2} & 2A \\
2A & D_0 & \cdots & \frac{A}{(\frac{n}{2}-3)^2} & \frac{A}{(\frac{n}{2}-2)^2} & 0 & 0 & 0 & \cdots & \frac{A}{3^2} & \frac{A}{2^2} \\
\vdots & \vdots & \ddots & \vdots & \vdots & \vdots & \vdots & \vdots & \ddots & \vdots & \vdots \\
\frac{A}{(\frac{n}{2}-2)^2} & \frac{A}{(\frac{n}{2}-3)^2} & \cdots & D_0 & 2A & \frac{A}{2^2} & \frac{A}{3^2} & \frac{A}{4^2} & \cdots & 0 & 0 \\
0 & \frac{A}{(\frac{n}{2}-2)^2} & \cdots & 2A & D_0 & 2A & \frac{A}{2^2} & \frac{A}{3^2} & \cdots & 0 & 0 \\
0 & 0 & \cdots & \frac{A}{2^2} & 2A & D_0 & 2A & \frac{A}{2^2} & \cdots & \frac{A}{(\frac{n}{2}-2)^2} & 0 \\
0 & 0 & \cdots & \frac{A}{3^2} & \frac{A}{2^2} & 2A & D_0 & 2A & \cdots & \frac{A}{(\frac{n}{2}-3)^2} & \frac{A}{(\frac{n}{2}-2)^2} \\
\frac{A}{(\frac{n}{2}-2)^2} & 0 & \cdots & \frac{A}{4^2} & \frac{A}{3^2} & \frac{A}{2^2} & 2A & D_0 & \cdots & \frac{A}{(\frac{n}{2}-4)^2} & \frac{A}{(\frac{n}{2}-3)^2} \\
\vdots & \vdots & \ddots & \vdots & \vdots & \vdots & \vdots & \vdots & \ddots & \vdots & \vdots \\
\frac{A}{2^2} & \frac{A}{3^2} & \cdots & 0 & 0 & \frac{A}{(\frac{n}{2}-2)^2} & \frac{A}{(\frac{n}{2}-3)^2} & \frac{A}{(\frac{n}{2}-3)^2} & \cdots & D_0 & 2A \\
2A & \frac{A}{2^2} & \cdots & 0 & 0 & 0 & \frac{A}{(\frac{n}{2}-2)^2} & \frac{A}{(\frac{n}{2}-3)^2} & \cdots & 2A & D_0
\end{pmatrix}, \tag{6.23}$$

where the diagonal entry $D_0 = 1 - 2A\left(1 + \sum_{j=1}^{n-2} 1/j^2\right)$ and $A = Kn^2/T$.

We can find each eigenvalue of a circulant matrix with a general solution presented in Gray (2001). However, we only need to guarantee that all eigenvalues lay on a unit circle. Therefore, we find the bound of eigenvalues instead.

6.3.2 The Bound of Eigenvalues

To find the bound of an $n \times n$ matrix, we use the Gershgorin's Circle Theorem (Brakken-Thal (2007); Gershgorin (1931)).

Theorem 6.1 (Gershgorin's Theorem Round 1) *Every eigenvalue λ of $n \times n$ matrix A satisfies:*

$$|\lambda - A_{i,i}| \leq \sum_{j \neq i} |A_{i,j}|, \ i \in 0, 1, \cdots, n-1$$

In other words, every eigenvalue lies within at least one of Gershgorin discs centered at $A_{i,i}$ with radius $\sum_{j \neq i} |A_{i,j}|$, where $A_{i,i}$ is the diagonal entry of a matrix.

In our circulant matrix, all diagonal entries and the sums of elements in each row and each column are the same. Therefore, in our matrix, all Gershgorin's discs are centered at $D_0 = 1 - 2A(1 + \sum_{j=1}^{n-2} 1/j^2)$ with radius $r = 2A(1 + \sum_{j=1}^{\frac{n}{2}-2} 1/j^2)$, where $A = Kn^2/T$.

Then, we find the maximum number of nodes n that guarantees the Gershgorin' discs are in a unit circle.

Let $\vec{D}$ be a vector drawn from the origin $(0, 0)$ to the center of the Gershgorin's disc $(1 - 2A(1 + \sum_{j=1}^{n-2} 1/j^2), 0)$. Due to the imaginary part of $\vec{D}$ is zero, the magnitude $|\vec{D}|$ is $|1 - 2A(1 + \sum_{j=1}^{n-2} 1/j^2|$. Therefore, we derive the following to guarantee the Gershgorin's discs are in a unit circle:

$$
\begin{aligned}
|\vec{D}| + r &\leq 1 \\
\left|1 - 2A\left(1 + \sum_{j=1}^{n-2} \frac{1}{j^2}\right)\right| + 2A\left(1 + \sum_{j=1}^{\frac{n}{2}-2} \frac{1}{j^2}\right) &\leq 1 \\
\left|1 - \frac{2Kn^2}{T}\left(1 + \sum_{j=1}^{n-2} \frac{1}{j^2}\right)\right| + \frac{2Kn^2}{T}\left(1 + \sum_{j=1}^{\frac{n}{2}-2} \frac{1}{j^2}\right) &\leq 1. \qquad (6.24)
\end{aligned}
$$

From the M-DWARF algorithm, we substitute K with $38.597 \times n^{-1.874} \times T/1000$. Additionally, when n is large, the value of $\sum_{j=1}^{n-2} 1/j^2$ and $\sum_{j=1}^{\frac{n}{2}-2} 1/j^2$ converge to the Reimann zeta function $\zeta(2) = \sum_{i=1}^{\infty} 1/i^2 = \pi^2/6 \approx 1.645$. From Equation 6.24, we get the following:

$$
\begin{aligned}
\left|1 - 0.077194n^{0.126}(1 + 1.645)\right| + 0.077194n^{0.126}(1 + 1.645) &\leq 1 \\
\left|1 - 0.20417813n^{0.126}\right| + 0.20417813n^{0.126} &\leq 1 \\
-(1 - 0.20417813n^{0.126}) \leq 1 - 0.20417813n^{0.126} &\leq 1 - 0.20417813n^{0.126} \qquad (6.25)
\end{aligned}
$$

The condition $1-0.20417813n^{0.126} \leq 1-0.20417813n^{0.126}$ is always true regardless of the number of nodes n. Then, we consider the following condition:

$$
\begin{aligned}
-(1 - 0.20417813n^{0.126}) &\leq 1 - 0.20417813n^{0.126} \\
2(0.20417813n^{0.126} - 1) &\leq 0 \\
n^{0.126} &\leq \frac{1}{0.20417813} \\
n &\leq 299,307 \qquad (6.26)
\end{aligned}
$$

Therefore, if the number of nodes is less than 2.99×10^5 nodes, every eigenvalue is guaranteed to lay in a unit circle. In other words, the non-linear dynamic system for the

multi-hop star topology is locally stable at the equilibrium. If there is a small perturbation around the equilibrium, the system is able to converge back to the equilibrium.

To prove the stability of other topologies, we can substitute Δ_i and $c_{i,j}$ in the Jacobian matrix with the value at the equilibrium of each topology. Then, finding the eigenvalues of the substituted Jacobian matrix. If we can bound that every eigenvalue lies in a unit circle, the algorithm is locally stable for such topologies. We conjecture that the proof of other topologies is similar to the proof of the star topology with the similar procedure.

6.4 Summary

In this chapter, we analyse the stability of M-DWARF, a multi-hop physicomimetics desynchronization algorithm. We transform the system into a dynamic system and locally analyse at the equilibrium. However, to find eigenvalues to guarantee stability depends on connectivity and topology. In this dissertation, we derive the Jacobian to be used for a general topology and provide an in-depth stability proof by bounding eigenvalues for multi-hop star topology as an instance. We conjecture that, with a similar proof, the proposed algorithm is also stable for other multi-hop topologies at the equilibrium as well.

CHAPTER VII

CONCLUSION

7.1 Dissertation Summary

In the beginning of this dissertation, we study and analyse the desynchronization problem. Desynchronization is useful for scheduling nodes to perform tasks at different time. This property is desirable for resource sharing, TDMA scheduling, and collision avoiding. However, to desynchronize nodes in wireless sensor networks is difficult due to several limitations. This dissertation focuses on wireless sensor networks that sensor nodes lack of global time knowledge (*i.e.*, clocks are not synchronized). Without global time knowledge, nodes perceive different local times. The beginning of time slots and the exact number of time slots are difficult to determine. In addition, due to the hidden terminal problem, a node cannot sense a transmission signal from two-hop neighboring nodes. If two nodes transmit messages simultaneously, two messages collide at a middle receiver node.

To solve such problems, this dissertation proposes a novel physicomimetics desynchronization algorithm. Inspired by robotic circular formation and Physics principle, the proposed algorithm creates an artificial force field for wireless sensor nodes. Nodes with closer time phases have stronger forces to repel each other in the time domain. Each node adjusts its time phase proportionally to the total amount of received forces. Once the received forces are balanced, nodes are desynchronized. The proposed algorithm has several benefits. First, the algorithm runs distributedly on each sensor node. No central master node is required. Second, the algorithm works even nodes are not synchronized and do not realize global time. Third, the algorithm is able to work for both single-hop and multi-hop networks. In addition, the algorithm is lightweight, simple, and practical. The size of a compiled binary is less than 30 kilobytes. The required memory is less than 2 kilobytes. This property is desirable to implement, extend, and apply for resource-limited wireless sensor nodes. We also demonstrate that the algorithm is runnable on both simulation and real hardware. Furthermore, the algorithm requires only local 2-hop information and scales well with network size.

We also mathematically analyse the convexity and stability of the proposed physicomimetics algorithm. The analysis reveals that the force function used in the algorithm is a convex function in the case of single-hop networks. Therefore, there is only global minima and no local minima. The analysis also proves that the algorithm is stable under small perturbation at the equilibrium which is also another desirable property of desynchronization.

7.2 Discussion on Limitations and Future Works

Despite of several benefits, there are limitations that should be mentioned.

First, the proposed algorithm does not always lead to perfect desynchronization on multi-hop networks even if the algorithm performs very well on single-hop networks and outperforms previous works on both single-hop and multi-hop networks. On multi-hop networks, to achieve the perfect desynchrony state depends on topology and initial network configuration.

Second, even, in single-hop networks, the proposed algorithm does not incur any message overhead, the multi-hop algorithm incurs overhead because it includes one-hop neighbors' relative phases in firing messages. We present the optimization scheme that reduces the frequency to include relative phases in firing messages. However, there is a trade-off between message overhead and convergence speed. There is room for further optimization. One feasible approach is that each node is not necessary to include all relative phases of one-hop neighbors because this dissertation shows that the algorithm tolerates to packet loss. With this approach, the multi-hop algorithm is not limited to a small number of neighbors.

Third, in stability analysis, this dissertation analyses the stability of the dynamic system only at the equilibrium. This is due to the fact that the dynamic system of our approach is non-linear dynamic and the standard linear dynamic system analysis does not suffice. We conjecture that the full proof of stability can be achieved with the advance mathematical analysis based on the Lyapunov stability theorem.

In addition, the proper value of step size K that is used in this dissertation is derived from the empirical experiments on the simulation environment. This value works

very well on both simulator and real devices in our investigated scenarios. However, it should be tuned for a proper value for each actual operating environment to maximize the performance of a system.

Last but not least, this dissertation provides a fundamental mechanism to desynchronize nodes. Future works on application development based on our mechanism are viable. Developing an application could lead to new ideas to improve the proposed algorithm.

7.3 Concluding Remark

To the best of our knowledge, this dissertation is the first to introduce a physicomimetics desynchronization protocol for wireless sensor networks that is based on the concept of electromagnetic fields, a foundation of physics. We believe that this dissertation could be a primer for further studies in physicomimetics approaches for wireless networks and could be extended to support several applications.

References

Kittipat Apicharttrisorn, Supasate Choochaisri, and Chalermek Intanagonwiwat. 2010. Energy-Efficient Gradient Time Synchronization for Wireless Sensor Networks. In Computational Intelligence, Communication Systems and Networks (CICSyN), 2010 Second International Conference on, pp. 124–129.

N Boonpinon and A Sudsang. 2006. Heterogeneity Driven Circular Formation. In Robotics and Biomimetics, 2006. ROBIO '06. IEEE International Conference on, pp. 971–976.

Sean Brakken-Thal. 2007, Gershgorin's theorem for estimating eigenvalues. URL http://buzzard.ups.edu/courses/2007spring/projects/brakkenthal-paper.pdf .

Supasate Choochaisri, Vit Niennarttrakul, Sarun Jenjaturong, Chalermek Intanagonwiwat, and Chotirat Ann Rattanamahattana. 2010. SENVM: a Server Environment Monitoring and Controlling System for a Small Data Center Using Wireless Sensor Network. In 2010 International Computer Science and Engineering Conference.

Reuven Cohen and David Peleg. 2008. Local spreading algorithms for autonomous robot systems. Theor. Comput. Sci. 399,1-2:71–82. ISSN 0304-3975.

J Degesys and R Nagpal. 2008. Towards Desynchronization of Multi-hop Topologies. In Self-Adaptive and Self-Organizing Systems, 2008. SASO '08. Second IEEE International Conference on, pp. 129–138.

J Degesys, I Rose, A Patel, and R Nagpal. 2007. DESYNC: Self-Organizing Desynchronization and TDMA on Wireless Sensor Networks. In Information Processing in Sensor Networks, 2007. IPSN 2007. 6th International Symposium on, pp. 11–20.

Samitha W. Ekanayake and Pubudu N. Pathirana. 2010. Formations of robotic swarm: An artificial force based approach. International Journal of Advanced Robotic Systems . ISSN 1729-8806.

William M Faucette. 1996. A geometric interpretation of the solution of the general quartic polynomial. American Mathematical Monthly 103,1:51.

Paola Flocchini, Giuseppe Prencipe, and Nicola Santoro. 2008. Self-deployment of mobile sensors on a ring. Theor. Comput. Sci. 402,1:67–80. ISSN 0304-3975.

Saurabh Ganeriwal, Ram Kumar, and Mani B Srivastava. 2003. Timing-sync protocol for sensor networks. In Proceedings of the 1st international conference on Embedded networked sensor systems, SenSys '03, pp. 138–149, New York, NY, USA. ACM. ISBN 1-58113-707-9.

Semyon Aranovich Gershgorin. 1931. Uber die abgrenzung der eigenwerte einer matrix. Bulletin de l'Académie des Sciences de l'URSS. Classe des sciences mathématiques et na 6:749–754.

Shyamnath Gollakota and Dina Katabi. 2008. Zigzag decoding: combating hidden terminals in wireless networks. In Proceedings of the ACM SIGCOMM 2008 conference on Data communication, SIGCOMM '08, pp. 159–170, New York, NY, USA. ACM. ISBN 978-1-60558-175-0.

Haigang Gong, Ming Liu, Guihai Chen, and Xue Zhang. 2010. A study on event-driven tdma protocol for wireless sensor networks. EURASIP J. Wirel. Commun. Netw. 2010:9:1–9:12. ISSN 1687-1472. doi: http://dx.doi.org/10.1155/2010/169132. URL http://dx.doi.org/10.1155/2010/169132 .

Robert M. Gray. 2001. Toeplitz and circulant matrices: A review. Technical report.

Chao Gui and Prasant Mohapatra. 2004. Power conservation and quality of surveillance in target tracking sensor networks. In Proceedings of the 10th annual international conference on Mobile computing and networking, MobiCom '04, pp. 129–143, New York, NY, USA. ACM. ISBN 1-58113-868-7.

Tian He, Sudha Krishnamurthy, John A. Stankovic, Tarek Abdelzaher, Liqian Luo, Radu Stoleru, Ting Yan, Lin Gu, Jonathan Hui, and Bruce Krogh. 2004. Energy-efficient surveillance system using wireless sensor networks. In Proceedings of the 2nd international conference on Mobile systems, applications, and services, MobiSys '04, pp. 270–283, New York, NY, USA. ACM. ISBN 1-58113-793-1.

Ted Herman and Sébastien Tixeuil. 2004. A distributed tdma slot assignment algorithm for wireless sensor networks. In Sotiris Nikoletseas and José Rolim, editors, Algorithmic Aspects of Wireless Sensor Networks, volume 3121 of Lecture Notes

in Computer Science, pp. 45–58. Springer Berlin / Heidelberg. ISBN 978-3-540-22476-1.

Holly P. Hirst and Wade T. Macey. 1997. Bounding the roots of polynomials. The College Mathematics Journal 28,4:pp. 292–295. ISSN 07468342.

Hui Kang and J.L. Wong. 2009. A localized multi-hop desynchronization algorithm for wireless sensor networks. In INFOCOM 2009, IEEE, pp. 2906 –2910.

Philip Levis, Nelson Lee, Matt Welsh, and David Culler. 2003. Tossim: accurate and scalable simulation of entire tinyos applications. In SenSys '03: Proceedings of the 1st international conference on Embedded networked sensor systems, pp. 126–137, New York, NY, USA. ACM. ISBN 1-58113-707-9.

Philip Levis, Sam Madden, Joseph Polastre, Robert Szewczyk, Alec Woo, David Gay, Jason Hill, Matt Welsh, Eric Brewer, and David Culler. 2004. Tinyos: An operating system for sensor networks. In in Ambient Intelligence. Springer Verlag.

Alan Mainwaring, David Culler, Joseph Polastre, Robert Szewczyk, and John Anderson. 2002. Wireless sensor networks for habitat monitoring. In Proceedings of the 1st ACM international workshop on Wireless sensor networks and applications, WSNA '02, pp. 88–97, New York, NY, USA. ACM. ISBN 1-58113-589-0.

Miklós Maróti, Branislav Kusy, Gyula Simon, and Ákos Lédeczi. 2004. The flooding time synchronization protocol. In Proceedings of the 2nd international conference on Embedded networked sensor systems, SenSys '04, pp. 39–49, New York, NY, USA. ACM. ISBN 1-58113-879-2.

Renato E. Mirollo and Steven H. Strogatz. 1990. Synchronization of pulse-coupled biological oscillators. SIAM J. Appl. Math. 50:1645–1662. ISSN 0036-1399.

A Motskin, T Roughgarden, P Skraba, and L Guibas. 2009. Lightweight Coloring and Desynchronization for Networks. In INFOCOM 2009, IEEE, pp. 2383–2391.

Clemens Mühlberger and Reiner Kolla. 2009. Extended desynchronization for multi-hop topologies. Technical Report 460, Institut für Informatik, Universität Würzburg.

Victor Y. Pan. 1997. Solving a polynomial equation: Some history and recent progress. SIAM Rev. 39,2:187–220. ISSN 0036-1445.

Srinivasan Parthasarathy and Rajiv Gandhi. 2005. Distributed algorithms for coloring and domination in wireless ad hoc networks. In Kamal Lodaya and Meena Mahajan, editors, FSTTCS 2004: Foundations of Software Technology and Theoretical Computer Science, volume 3328 of Lecture Notes in Computer Science, pp. 447–459. Springer Berlin / Heidelberg. ISBN 978-3-540-24058-7.

A Patel, J Degesys, and R Nagpal. 2007. Desynchronization: The Theory of Self-Organizing Algorithms for Round-Robin Scheduling. In Self-Adaptive and Self-Organizing Systems, 2007. SASO '07. First International Conference on, pp. 87–96.

Venkatesh Rajendran, Katia Obraczka, and J. J. Garcia-Luna-Aceves. 2006. Energy-efficient, collision-free medium access control for wireless sensor networks. Wirel. Netw. 12:63–78. ISSN 1022-0038.

Tossaphol Settawatcharawanit, Supasate Choochaisri, Chalermek Intanagonwiwat, and Kultida Rojviboonchai. 2012. V-desync: Desynchronization for beacon broadcasting in vehicular networks. In Proceedings of IEEE 75th Vehicular Technology Conference, VTC2012-Spring. ISBN 978-1-60558-175-0.

P Sommer and R Wattenhofer. 2009. Gradient clock synchronization in wireless sensor networks. In Information Processing in Sensor Networks, 2009. IPSN 2009. International Conference on, pp. 37–48.

Samia Souissi, Xavier Défago, and Takuya Katayama. 2004. Convergence of a uniform circle formation algorithm for distributed autonomous mobile robots. In Proceedings of the Joint Japan-Tunisia Workshop on Computer Systems and Information Technology, JT-CSIT'04. ISBN 978-1-60558-175-0.

William M. Spears, Diana F. Spears, Rodney Heil, Wesley Kerr, and Suranga Hettiarachchi. 2005. An overview of physicomimetics. In Lecture Notes in Computer Science – State of the Art Series.

W.M. Spears and D.F. Gordon. 1999. Using artificial physics to control agents. In Information Intelligence and Systems, 1999. Proceedings. 1999 International Conference on, pp. 281 –288.

Ichiro Suzuki and Masafumi Yamashita. 1996. Distributed anonymous mobile robots-formation and agreement problems. In Proceedings of the

3rd International Colloquium on Structural Information and Communication Complexity, SIROCCO '96, pp. 313–330. ISBN 978-1-60558-175-0.

Ichiro Suzuki and Masafumi Yamashita. 1999. Distributed anonymous mobile robots: Formation of geometric patterns. SIAM J. Comput. 28,4:1347–1363. ISSN 0097-5397.

Pongpakdi Taechalertpaisarn, Supasate Choochaisri, and Chalermek Intanagonwiwat. 2011. An orthodontics-inspired desynchronization algorithm for wireless sensor networks. In Proceedings of the 13th IEEE International Conference on Communication Technology. ISBN 978-1-60558-175-0.

Yan Wang, Jian-chao Zeng, and Ying Tan. 2010. An artificial physics optimization algorithm for multi-objective problems based on virtual force sorting proceedings. In Bijaya Panigrahi, Swagatam Das, Ponnuthurai Suganthan, and Subhransu Dash, editors, Swarm, Evolutionary, and Memetic Computing, volume 6466 of Lecture Notes in Computer Science, pp. 615–622. Springer Berlin / Heidelberg. ISBN 978-3-642-17562-6.

Geoffrey Werner-Allen, Geetika Tewari, Ankit Patel, Matt Welsh, and Radhika Nagpal. 2005. Firefly-inspired sensor network synchronicity with realistic radio effects. In Proceedings of the 3rd international conference on Embedded networked sensor systems, SenSys '05, pp. 142–153, New York, NY, USA. ACM. ISBN 1-59593-054-X.

Ning Xu, Sumit Rangwala, Krishna Kant Chintalapudi, Deepak Ganesan, Alan Broad, Ramesh Govindan, and Deborah Estrin. 2004. A wireless sensor network for structural monitoring. In Proceedings of the 2nd international conference on Embedded networked sensor systems, SenSys '04, pp. 13–24, New York, NY, USA. ACM. ISBN 1-58113-879-2.

APPENDICES

APPENDIX A

PUBLICATION

During my Ph.D. study, I have published several papers as follows.

International Journal Publications

1. Supasate Choochaisri, Kittipat Apicharttrisorn, Kittiporn Korprasertthaworn, Pongpakdi Taechalertpaisarn, and Chalermek Intanagonwiwat, "Desynchronization with an Artificial Force Field for Wireless Networks", ACM SIGCOMM Computer Communication Review, Vol.42, No.2, 2012.4, pages(s):7-15.

2. Supasate Choochaisri, Nuttanart Pornprasitsakul, and Chalermek Intanagonwiwat, "Logic Macroprogramming for Wireless Sensor Networks", International Journal of Distributed Sensor Networks, Vol.2012, Article ID 171838, 2012, page(s):1-12.

3. Supasate Choochaisri and Chalermek Intanagonwiwat, "An Analysis of Deductive-Query Processing Approaches for Logic Macroprograms in Wireless Sensor Networks", Engineering Journal, Vol.16, No.4, 2012.7.

4. Phannaphatr Savetpanuvong, Uthai Tanlamai, Chidchanok Lursinsap, Pairote Leelaphattarakij, Wisit Kunarittipol, and Supasate Choochaisri, "Technology Adoption of InnovViz 2.0 : A Study of Mixed-Reality Visualization and Simulation System for Innovation Strategy with UTAUT Model", Journal of Information Technology Applications & Management Vol.18, No.3, 2011.9, page(s): 1-110.

International Conference Publications

1. Utai Tanlamai, Phannaphatr Savetpanuvong, Pairote Leelaphattaraki, and Supasate Choochaisri, "Usefulness of Mixed Reality Visuals in the Learning and Assessment of Financial Data", in Proceedings of the 2012 International Conference on Business and Information (BAI), Sapporo, Japan, July 3-5, 2012.

2. Supasate Choochaisri, Siam Aurburananont, Akekanat Saowwapak-adisak, and Chalermek Intanagonwiwat, “DeVise: a Tool for Visualizing and Validating Desynchronization Protocols for Multi-hop Wireless Sensor Networks”, in Proceedings of 9th International Conference on Electrical Engineering/Electronics, Computer, Telecommunications and Information Technology(ECTI-CON), Hua Hin, Thailand, May 16-18, 2012.

3. Tossaphol Settawatcharawanit, Supasate Choochaisri, Chalermek Intanagonwiwat, and Kultida Rojviboonchai, “V-DESYNC: Desynchronization for Beacon Broadcasting on Vehicular Networks”, in Proceedings of the 75th IEEE Vehicular Technology Conference (IEEE VTC), Yokohama, Japan, May 6-9, 2012.

4. Prateep Puttrapornpisut, Supasate Choochaisri, Kwanjira Narkdej, Chalermek Intanagonwiwat, and Kultida Rojviboonchai, “2PMP: A Push-Pull with Buffer-Map Prediction Algorithm for Peer to Peer Live Streaming”, in Proceedings of the 19th IEEE International Symposium on Intelligent Signal Processing and Communication Systems (IEEE ISPACS), Chiang Mai, Thailand, December 7-9, 2011.

5. Pongpakdi Taechalertpaisarn, Supasate Choochaisri, and Chalermek Intanagonwiwat, “An Orthodontics-Inspired Desynchronization Algorithm for Wireless Sensor Networks”, in Proceedings of the 13th IEEE International Conference on Communication Technology (IEEE ICCT), Jinan, China, September 25-28, 2011.

6. Phuri Nicrovanachumrus, Supasate Choochaisri, and Chalermek Intanagonwiwat, “Efficiency and Speed Improvement for Network Coded File Distribution with Adaptive Request”, in Proceedings of the 13th IEEE International Conference on Communication Technology (IEEE ICCT), Jinan, China, September 25-28, 2011.

7. Kwanjira Narkdej, Supasate Choochaisri, and Chalermek Intanagonwiwat, “A Reinforcement-Based Push-Pull Approach for Peer-to-Peer Live Streaming”, in Proceedings of the 7th IEEE International Conference on Wireless Communications, Networking, and Mobile Computing (IEEE WiCOM), Wuhan, China, September 23-25, 2011.

8. Phannaphatr Savetpanuvong, Uthai Tanlamai, Chidchanok Lursinsap, Pairote Leelaphattarakij, Wisit Kunarittipol, and Supasate Choochaisri, ”Technology Adoption of InnovViz 2.0 : A Study of Mixed-Reality Visualization and Simulation System for

Innovation Strategy with UTAUT Model", in Proceedings of the 6th International Conference on Information Technology Applications and Management (ITAM-6): Smart Technology in Tourism and Culture, Jeju, Korea, 23-24 June, 2011. (Best Paper Award)

9. Supasate Choochaisri, Vit Niennattrakul, Saran Jenjaturong, Chalermek Intanagonwiwat, and Chotirat Ann Ratanamahatana, "SENVM: Server Environment Monitoring and Controlling System for a Small Data Center Using Wireless Sensor Networks", in Proceedings of the International Computer Science and Engineering Conference (ICSEC 2010), Chiang Mai, Thailand, November 17-19, 2010.

10. Kittipat Apicharttrisorn, Supasate Choochaisri, and Chalermek Intanagonwiwat, "Energy-Efficient Gradient Time Synchronization for Wireless Sensor Networks", in Proceedings of the Second IEEE International Conference on Computational Intelligence, Communication Systems, and Networks (IEEE CICSyN), Liverpool, UK, July 28-30, 2010.

APPENDIX B

EXTENDED ACKNOWLEDGEMENT

The regulation limits the front acknowledgement section not to be longer than one page. However, there are so many people that they deserve to be acknowledged. I would be regret if I cannot express my gratitude to them. Therefore, I use this space acknowledge them.

For UbiNET research group members, I thank Asst. Prof. Dr. Chalermek Intanagontwiwat, Asst. Prof. Dr. Kultida Rojviboonchai, Tanapoom Danmanee, Kittipat Apicharttrisorn, Jirawat Sirilar, Saran Jenjaturong, Wanchai Ngiwlay, Kulit Na Nakorn, Pongpakdi Taechalertpaisarn, Tossaphol Settawatcharawanit, Kwanjira Narkdej, Phuri Nicro-vanachumrus , Prateep Puttrapornpisut, Vittawus Prueksasri, Chayanin Thaina, Wipawee Viriyapongsukit, Nattavit Kamoltham, Kiattikun Kawila, Nuttanart Pornprasitsakul, Siam Aurburananont, and Akekanat Saowwapak-adisak.

For DMDE research group members, I thank Vit Niennattrakul, Haemwaan Sivaraks, Sura Rodpongpun, Pawan Nunthanid, Pongsakorn Ruengronghirunya, Poat Sajjipanon, Angkana Chanrungutai, Thanapong Intharah, Waiyawuth Euachongprasit, Warissara Mee-srikamolkul, Dechawut Wanichsan, and Dararat Srisai.

I thank all my current and past teachers at Chulalongkorn University, Suankularb Wittayalai Nonthaburi School, and Ampornpaisarn School. They have educated me not only for academic matter but also for life. Without them, I would not be here.

I also thank my friends at LarnGear Technology Co., Ltd. including Arnupharp Viratanapanu, Wisit Kunarittipol, and Singhapong Sukuntho.

Last but not least, I thank everyone who always supports and helps me in every aspect in my life. I really appretiate their flowing hearts.

Biography

Supasate Choochaisri was born in Bangkok, Thailand, on April, 1984. He graduated from Suankularb Wittayalai Nonthaburi school in 2002. While in high school, he was elected as a student president. Then, he received B.Eng. and M.Eng., both in Computer Engineering, from Chulalongkorn University, Thailand, in 2006 and 2009, respectively. His bachelor degree has been supervised by Assoc. Prof. Dr. Wiwat Vatanawood. His master and doctorate have been under the supervision of Asst. Prof. Dr. Chalermek Intanagonwiwat. Since 2009, he has received a grant from the Department of Computer Engineering, Chulalongkorn University through the CP CU Academic Excellence Scholarship (Ad-cha-ri-ya-kuen-rang Scholarship). He is also a co-founder of Larngear Technology Co., Ltd. His company has won several regional and international awards and has been listed in Software Park's Hall of Fame. His field of interest includes various topics in ubiquitous computing and computer networks with emphasis on wireless sensor networks, wireless adhoc networks, mobile computing, and distributed algorithms.